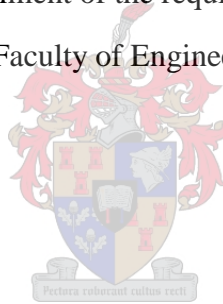


The effect of macro-synthetic fibres on the drying shrinkage cracking behaviour of concrete slabs on grade.

By:

Louise du Plessis

Thesis presented in fulfilment of the requirements for the degree of
Masters in Engineering in the Faculty of Engineering at Stellenbosch University



Supervisor: Prof WP Boshoff

Faculty of Engineering

December 2015

DECLARATION

By submitting this thesis electronically, I declare that the entirety of the work contained therein is my own, original work, that I am the copyright owner thereof (unless to the extent explicitly otherwise stated) and that I have not previously in its entirety or in part submitted it for obtaining any qualification

Signature: _____

Date: _____

ACKNOWLEDGEMENTS

I would like to thank my supervisor, Prof. W.P. Boshoff, for his guidance. I thank God for the ability to learn and understand and I want to thank Him for the opportunity to be able to improve myself in life. I want to thank my husband, Gerhard du Plessis, for all the moral support and help with my experiments. I want to thank my parents for their moral and financial support. Sincere thanks to the laboratory personnel for all their physical help as well as their help with my experiments. Lastly I want to thank NRF for funding my studies over the last two years and, making it possible for me to complete my masters degree.

ABSTRACT

Slabs on grade are the most commonly used floors for the ground floor of structures without basements. These slabs are made from the generally used construction material called concrete. Concrete is known for its relatively high compressive strength, but because of its comparatively low tensile capacity the concrete cracks easily under tensile forces. Cracks in the concrete slabs on grade reduce the serviceability and durability of the floor. The use of synthetic fibre reinforced concrete (SynFRC) in slabs on grade has shown major advantages particularly in controlling the extent and size of cracks that are formed due to drying shrinkage.

An investigation is done to determine the effect of locally produced macro-synthetic fibres on the drying shrinkage cracks in slabs on grade. This is done through a large scale test that compared the drying shrinkage cracking of polypropylene fibre reinforced concrete (PPFRC) with that of conventional concrete. The results of the large scale tests are then compared with that of a mathematical finite element method (FEM) model created in a finite element program called Diana. The different material properties of the PPFRC that are needed for the FEM analyses are obtained through flexural three point beam tests, wedge splitting tests, compression tests and shrinkage tests.

The effect of the fibres are tested in terms of the different spacings between saw cut joint, the different fibre dosages, the slab thickness and the degree of friction between the concrete and the sub-base under the concrete. It is found that the use of macro-synthetic fibres results in an increase in the number of cracks between the saw cut joints, especially if the joint spacing is increased. Although there is an increase in the number of cracks, the use of fibres does consequently lead to a decrease in the crack widths. The use of macro polypropylene fibres in slabs on grade will thus result in an increase in the number of cracks, but with smaller crack widths, especially with an increase in spacings between the joints.

OPSOMMING

Grond ondersteunde vloere is die mees gewilde tipe vloer vir die grondvloer van strukture sonder kelders. Hierdie vloere word van beton gemaak wat 'n bekende konstruksie materiaal is. Beton het die kapasiteit om 'n relatiewe hoë drukspanning te kan weerstaan, maar as gevolg van beton se relatiewe lae trekspanning, kraak die beton maklik onder as dit bloodgestel word aan trek kragte. Kraake in die beton vloere wat deur laagwerk en direk deur die grond ondersteun word, verminder die diensbaarheid en duursaamheid van die vloer. Die gebruik van sintetiese vesel gewapende beton in grond ondersteunde vloere, het bewys dat dit groot voordele het veral in die beheer oor die aantal en die grootte van kraake wat vorm as gevolg van droog krimpings.

'n Ondersoek is gedoen om die effek van plaaslik vervaardigde makro-sintetiese vesels op die droog krimpings kraake in grond ondersteunde vloere te bepaal. Dit word gedoen deur gebruik te maak van 'n groot-skaalse toets wat die droog krimpings kraake van polipropileen vesel gewapende beton (PPFRC) te vergelyk met dié van konvensionele beton. Die resultate van die groot-skaalse toetse word dan vergelyk met dié van 'n eindige element metode (EEM) model. Die verskillende materiaal eienskappe van die PPFRC wat nodig is vir die EEM ontledings, word verkry deur drie-punt balk buigtoetse, wig splyttoetse, druktoetse en materiaal krimpings toetse.

Die effek van die vesels word getoets in terme van die verskillende spasiërings tussen die gesnyde voeë, die verskillende vesel volumes, die blad dikte en die graad van wrywing tussen die beton en die sub-basis onder die beton. Daar is gevind dat die gebruik van makro-sintetiese vesels lei tot 'n toename in die getal kraake tussen die gesnyde voeë. Alhoewel daar 'n toename in die aantal kraake is, dra die vesels in die beton by tot 'n afname in die kraak wydtes. Die gebruik van SynFRC in grond geondersteunde vloere sal dus lei tot 'n toename in die aantal kraake, maar met kleiner kraak wydtes, soos die spasiërings tussen die gesnyde voeë toeneem.

TABLE OF CONTENTS

Declaration.....	ii
Acknowledgements.....	iii
Abstract.....	iv
Opsomming.....	v
Table of contents.....	vi
List of tables.....	xi
List of Figures.....	xii
Symbols and Abbreviations	xvii
1. Chapter 1: Introduction	1
2. Chapter 2: Conventional and polypropylene fibre reinforced concrete.....	4
2.1. The behaviour of conventional concrete	4
2.1.1. The fracture energy properties of concrete	5
2.1.2. The development of tensile strength and elasticity modulus	9
2.1.3. Shrinkage of concrete.....	10
2.1.4. Prediction models for drying shrinkage of concrete	17
2.2. Fibre reinforced concrete	23
2.2.1. Steel fibres.....	25
2.2.2. Glass fibres.....	26
2.2.3. Natural fibres.....	26
2.2.4. Synthetic fibres.....	26
2.3. Macro synthetic polypropylene fibre reinforced concrete	27
2.3.1. Flexural strength and flexural toughness of PPFRC	29
2.3.2. Tensile strength of PPFRC.....	31
2.3.3. Compressive Strength of PPFRC	31
2.3.4. Cracking of FRC	31
2.3.5. Shrinkage of FRC.....	32

2.4.	Concluding summary	33
3.	Chapter 3: Concrete floors on grade: Construction and modelling	35
3.1.	Construction methods.....	36
3.2.	Subgrade and sub-base	37
3.3.	Friction between the soil and the concrete	38
3.4.	Joints.....	42
3.4.1.	Restrained movement joint.....	42
3.4.2.	Tied joint	43
3.4.3.	Isolation joint.....	44
3.4.4.	Free movement joint/Construction joint	44
3.5.	Modelling of concrete slabs on grade	47
3.5.1.	Modelling of hardened concrete.....	47
3.5.2.	Multi-directional fixed crack model.....	49
3.5.3.	Modelling the interface between the soil and the concrete.	53
3.6.	Concluding summary	56
4.	Chapter 4: Material characteristic study	57
4.1.	Research design.....	57
4.2.	Test setup.....	59
4.2.1.	Compressive test	59
4.2.2.	Shrinkage test	60
4.2.3.	Flexural test and tensile behaviour.....	61
4.2.4.	Wedge splitting test.....	62
4.2.5.	Sieve analysis	64
4.3.	Results	65
4.3.1.	Compression test	65
4.3.2.	Shrinkage test	66
4.3.3.	Flexural test and tensile behaviour.....	70

4.3.4.	Fracture energy of PPFRC	72
4.3.5.	Sieve analysis	75
4.4.	Discussion	75
4.4.1.	Compression test	75
4.4.2.	Shrinkage test	76
4.4.3.	Flexural and tension test.....	77
4.4.4.	Fracture energy.....	78
4.5.	Concluding summary	78
5.	Chapter 5: Large scale tests of slabs on grade	80
5.1.	Test setup.....	80
5.2.	Testing method.....	85
5.3.	Testing procedure.....	86
5.4.	Results	86
5.5.	Discussion	92
5.5.1.	9 m joint spacing slabs containing different fibre dosages	93
5.5.2.	Slabs containing 5 kg/m ³ fibres.....	94
5.5.3.	Slabs containing different fibre dosages and different saw cut joint spacings 94	
5.6.	Concluding summary	95
6.	Chapter 6: Verification of numerical model	96
6.1.	Testing procedure.....	96
6.2.	Structural analysis design.....	97
6.2.1.	Geometry.....	97
6.2.2.	Mesh.....	98
6.2.3.	The interface.....	98
6.2.4.	Loads	99
6.2.5.	Boundary conditions	99

6.2.6.	Cracks.....	100
6.3.	Material properties	101
6.3.1.	The sand	101
6.3.2.	The conventional concrete and PPFRC material models.....	102
6.4.	Results	104
6.4.1.	Conventional concrete.....	105
6.4.2.	Polypropylene fibre reinforced concrete	107
6.4.3.	Other results	109
6.4.4.	Joint openings.....	112
6.5.	Discussion	113
6.5.1.	Number of cracks formed between joints	113
6.5.2.	The width of the cracks opened.....	114
6.5.3.	The joint openings.....	115
6.5.4.	The average crack opening widths	116
6.6.	Concluding summary	116
7.	Chapter 7: FEM model results	118
7.1.	Results	119
7.1.1.	Different joint spacings	119
7.1.2.	Different fibre dosages	122
7.1.3.	Different slab thicknesses.....	124
7.1.4.	Different friction between soil and concrete	126
7.2.	Discussion	128
7.2.1.	The effect of the size of the spacing between saw cut joints	129
7.2.2.	The effect of the fibre dosage on the crack widths	130
7.2.3.	The effect of the slab thickness on the crack width	130
7.2.4.	The effect of friction on the width of the cracks	131
7.3.	Concluding summary	131

8.	Chapter 8: Conclusion.....	132
8.1.	The parameter study	132
8.2.	Large scale test	133
8.3.	Finite element analysis	133
8.4.	Future Research.....	134
9.	Bibliography	135
	Appendix 1.....	144
	Appendix 2.....	145
	Appendix 3.....	148
	Appendix 4.....	150
	Appendix 5.....	152
	Appendix 6.....	154
	Appendix 7.....	159
	Appendix 8.....	165

LIST OF TABLES

Table 2.1: Table alpha factors used to predict shrinkage for fib 2010 model code.....	21
Table 4.1: The designed concrete mix	58
Table 4.2: Properties of the fibre	59
Table 4.3: The compressive force for different fibre dosages	66
Table 4.4: The Re3 values for the fibre reinforced concrete	71
Table 4.5: The flexural strength of concrete containing different fibre dosages.....	71
Table 4.6: The tensile strength and compressive strength of the different fibre dosages according to BS EN 1992-1-1:2004.....	71
Table 4.7: The fracture energy recorded for selected fibre dosages per volume.....	72
Table 5.1: Summary of the large scale tests	86
Table 6.1: The tests used for verifications of the FEM model.....	96
Table 6.2: The required parameters for the interface elements	99
Table 7.1: The analyses conducted	118

LIST OF FIGURES

Figure 2.1: a) uncracked, b) micro-cracked, c) macro-cracked (Petersson, 1980)	5
Figure 2.2: a) Force over CMOD for the energy balance approach (Petersson, 1980), b) simplified force over-CMOD for the energy balance approach (Petersson, 1980)	6
Figure 2.3: Stress-crack relationship (Ostergaard, 2003)	8
Figure 2.4: The effect of w/c ratio on shrinkage of concrete for different aggregate contents (Odman, 1968).	14
Figure 2.5: The shrinkage of concrete stored at different levels of relative humidity. Time is from 28 days after wet curing (Troxell et al., 1958).	15
Figure 2.6: Influence of the concrete member's volume/surface ratio on the shrinkage of concrete (Hanson & Mattock, 1966).	16
Figure 2.7: The development of induced tensile stress leading to cracks after relief by creep (Neville & Brooks, 2001).	17
Figure 2.8: The drying shrinkage of normal-density concrete (SANS 10100-1:2000, 2000) .	19
Figure 2.9: Typical stress-strain curve for FRC (Cement & Concrete Institute, 2010).....	25
Figure 2.10: Load-deflection curve for 4.6 to 5.3 kg/m ³ dosage synthetic fibres. (Soutsos et al., 2012)	30
Figure 2.11: The crack patterns of steel reinforced concrete compared to FRC (Brandt, 2008)	32
Figure 2.12: The drying shrinkage for different fibre reinforced concrete (Choi et al., 2011)	33
Figure 3.1: The effect of slab movement and frictional forces on the tensile stresses in concrete slabs (Lee, 2001).	39
Figure 3.2: Sawn restrained movement joint (Technical Report No. 34, 2003).....	43
Figure 3.3: Formed restrained movement joints (Technical Report No. 34, 2003).....	43
Figure 3.4: Tied joint (Technical Report No. 34, 2003)	44
Figure 3.5: Details of typical free movement joints (a) un-dowelled joint, (b) dowelled joint. (Technical Report No. 34, 2003)	45
Figure 3.6: Multi-directional fixed crack model (TNO DIANA material library)	50
Figure 3.7: Tension softening-multi-directional fixed crack model (TNO DIANA material lib, 2012)	52
Figure 3.8: The tension cut-off in two-dimensional principal stress space as used in software (TNO DIANA material lib, 2012)	52

Figure 3.9: Interface elements (TNO DIANA material lib, 2012)	53
Figure 3.10: The coulomb friction criterion. Where c is the cohesion, ϕ is the friction angle and ψ is the dilatancy angle. (TNO DIANA material lib, 2012)	54
Figure 4.1: The strain gauge	60
Figure 4.2: The targets used to measure the shrinkage	60
Figure 4.3: The setup for the three point beam test	61
Figure 4.4: The setup of the LVDT's for the three point beam test.....	62
Figure 4.5: WST setup. (Nordcn, 2005)	63
Figure 4.6: Wedge splitting test setup.....	64
Figure 4.7: The shrinkage test results for open specimens	66
Figure 4.8: The shrinkage test results for the waterproofed beams	67
Figure 4.9: The shrinkage test results for beams tested in a temperature controlled room	67
Figure 4.10: The shrinkage test results for beams containing no fibres	68
Figure 4.11: The shrinkage test results for beams containing 5 kg/m^3 fibres.....	68
Figure 4.12: The shrinkage test results for beams containing 8 kg/m^3 fibres.....	69
Figure 4.13: The temperature fluctuation in the temperature controlled room.....	69
Figure 4.14: The shrinkage strain calculated with fib Model Code 2010 compared to experimental results	70
Figure 4.15: The average flexural behaviour of PPFRC for different fibre dosages.....	70
Figure 4.16: The force versus CMOD graph for different volume fibres.....	72
Figure 4.17: Spatial distribution of fibres for selected fibre dosages	73
Figure 4.18: The average fibre count for four different fibre dosages.....	73
Figure 4.19: The cross sectional physical fibre distribution for a fibre dosage of 2 kg/m^3	74
Figure 4.20: The cross sectional physical fibre distribution for a fibre dosage of 5 kg/m^3	74
Figure 4.21: The cross sectional physical fibre distribution for a fibre dosage of 6 kg/m^3	74
Figure 4.22: The cross sectional physical fibre distribution for a fibre dosage of 8 kg/m^3	74
Figure 4.23: The sieve analysis results for the two batches of sand used.....	75
Figure 5.1: The layout of the large scale test	81
Figure 5.2: Large scale test setup.....	81
Figure 5.3: Concrete strip with 9 m spacing between saw cut joints.....	82
Figure 5.4: Concrete strip with 4.5 m spacing between saw cut joints.....	82
Figure 5.5: Concrete strip with 6 m and 3 m spacing between saw cut joints.....	82
Figure 5.6: The angle section bolting the structure to the floor.....	83
Figure 5.7: The threaded bar restraining the concrete against movement	83

Figure 5.8: The compacted sand layer before casting.....	84
Figure 5.9: Ruler used to measure crack opening width.....	85
Figure 5.10: The number of cracks over time in slab with a 9 m joint spacing containing different fibre dosages.....	87
Figure 5.11: The number of cracks over time for slabs with different joint spacings containing 5 kg/m ³ fibres.....	87
Figure 5.12: The average crack openings for 9 m joint spacing slabs containing different fibre dosages.....	88
Figure 5.13: The average crack openings excluding joints for different saw cut joint spacings containing 5 kg/m ³ fibres.....	88
Figure 5.14: The joint openings for 9 m joint spacing slabs with different fibre dosages.....	89
Figure 5.15: The joint openings of different joint spacings all containing 5 kg/m ³ fibres.....	89
Figure 5.16: The crack at the joint.....	90
Figure 5.17: The total crack opening of a 9 m slab containing different fibre dosages.....	90
Figure 5.18: The shrinkage strain in 9 m joint spacing slabs containing different fibre dosages.....	91
Figure 5.19: The crack pattern of a 9 m joint spacing slab containing 5kg/m ³ fibres.....	91
Figure 5.20: The crack pattern of a 9 m joint spacing slab containing no fibres.....	91
Figure 5.21: The crack pattern of a 9 m joint spacing slab containing 8 kg/m ³ fibres.....	92
Figure 5.22: The crack pattern of a 150 mm thick 9 m joint spacing slab containing 5 kg/m ³ fibres.....	92
Figure 5.23: The crack pattern of a 4.5 m joint spacing slab containing 5 kg/m ³ fibres.....	92
Figure 5.24: The crack pattern of a 6 m joint spacing slab containing 5 kg/m ³ fibres.....	92
Figure 6.1: Basic layout of the model.....	97
Figure 6.2: The constrain representing the steel bar in the concrete.....	100
Figure 6.3: The shrinkage strain used in FEM analysis.....	104
Figure 6.4: The number of cracks excluding joints in 9m joint spacing slab containing no fibres.....	105
Figure 6.5: The crack opening width between joints in a 9m joint spacing slab containing no fibres.....	105
Figure 6.6: The average joint opening in a 9m joint spacing slab containing no fibres.....	106
Figure 6.7: The total crack opening width including joints in a 9 m joint spacing slab containing no fibres.....	106

Figure 6.8: Combined FEM and experimental work results of a 9 m joint spacing slab containing no fibres (9,0,100,s) 107

Figure 6.9: The number of cracks formed in a 9m joint spacing slab containing 5kg/m³ fibres 107

Figure 6.10: The crack opening width excluding joints in a 9 m joint spacing slab containing 5 kg/m³ fibres..... 108

Figure 6.11: The average joint opening in a 9 m joint spacing slab containing 5 kg/m³ fibres 108

Figure 6.12: The total average crack opening in a 9 m joint spacing slab containing 5 kg/m³ fibres 109

Figure 6.13: Combined FEM and experimental work results of a 9 m joint spacing slab containing 5 kg/m³ fibres (9,5,100,s)..... 109

Figure 6.14: Combined FEM and experimental work results of a 9 m joint spacing slab containing 8 kg/m³ fibres (9,8,100,s)..... 110

Figure 6.15: Combined FEM and experimental work results of a 9 m joint spacing slab containing 5 kg/m³ fibres (9,5,150,s)..... 110

Figure 6.16: Combined FEM and experimental work results of a 4.5 m joint spacing slab containing 5 kg/m³ fibres (4.5,5,100,s)..... 111

Figure 6.17: Combined FEM and experimental work results of a 4.5 m joint spacing slab containing no fibres (4.5,0,100,s) 111

Figure 6.18: Combined FEM and experimental work results of a 6 m joint spacing slab containing 5 kg/m³ fibres (6,5,100,s)..... 112

Figure 6.19: The average joint opening of 9 m joint spacing slabs containing 0 kg/m³ and 5 kg/m³ fibres..... 112

Figure 7.1: The crack opening of 4.5 m, 6 m and 9 m joint spacings containing no fibres... 119

Figure 7.2: The crack opening of 4.5 m, 6 m and 9 m joint spacings containing 5 kg/m³ fibres 120

Figure 7.3: The crack opening of 4.5 m and 9 m joint spacings containing 8 kg/m³ fibres... 120

Figure 7.4: The crack opening of 9 m joint spacing slab with a slab thickness of 150 mm containing no fibres or 5 kg/m³ fibres..... 121

Figure 7.5: The crack opening of 4.5 m joint spacing slab with a thickness of 150 mm containing no fibres or 5 kg/m³ fibres..... 121

Figure 7.6: Comparing the crack openings of 9 m joint spacing slabs containing different fibre dosages 122

Figure 7.7: Comparing the crack openings of 4.5 m joint spacing slabs containing different fibre dosages 122

Figure 7.8: Comparing the crack openings of 6 m joint spacing slabs containing different fibre dosages 123

Figure 7.9: The crack distribution in FEM for a 9,0,100,s slab..... 123

Figure 7.10: The crack distribution in FEM for a 9,5,100,s slab..... 123

Figure 7.11: the crack distribution in FEM for a 9,8,100,s slab 124

Figure 7.12: Comparing the crack openings of 100 mm thick 9 m joint spacing slabs with a 150 mm thick 9 m joint spacing slab, both containing no fibres 124

figure 7.13: comparing the crack openings of 100 mm thick 9 m joint spacing slabs with a 150 mm thick 9 m joint spacing slab, both containing 5 kg/m³..... 125

Figure 7.14: Comparing the crack openings of 100 mm thick 4.5 m joint spacing slabs with a 150 mm thick 4.5 m joint spacing slab, both containing no fibres 125

Figure 7.15: Comparing the crack openings of 100 mm thick 4.5 m joint spacing slabs with a 150 mm thick 4.5 m joint spacing slab, both containing 5 kg/m³..... 126

Figure 7.16: Comparing the crack openings of 100 mm thick, 9 m joint spacing slab resting on either soil or plastic, both containing 5 kg/m³ 127

Figure 7.17: Comparing the crack openings of 100 mm thick, 9 m joint spacing slab resting on either soil or plastic, both containing no fibres..... 127

Figure 7.18: Comparing the crack openings of 100 mm thick, 4.5 m joint spacing slab resting on either soil or plastic, both containing no fibres..... 128

Figure 7.19: Comparing the crack openings of 100mm thick, 4.5 m joint spacing slab resting on either soil or plastic, both containing 5 kg/m³ 128

SYMBOLS AND ABBREVIATIONS

A	a reduction factor to make the interface weaker and more flexible than the soil (range from 0.5 to 1)
A_c	the cross-sectional area of the specimen on which the compressive force acts (mm^2)
A_{lid}	the crack area equal to the length of the crack, times the width of the specimen in m^2
A_1	the total area of an element
a	mass of the original test sample (g)
b	mass of the sample after washing (g)
b_1	the width of the specimen (mm)
c	mass of the material that passed the 75 μm sieve
c'	the cohesion of the interface
c_{soil}	the cohesion of the soil
D	the material stiffness matrix
D_I^{cr}	the Mode I stiffness modulus of a crack
D_{II}^{cr}	the Mode II stiffness modulus of a crack
d	the depth of the specimen (mm)
E	Young's modulus
$E_{\text{cm}}(t)$	Young's modulus at a specific time (GPa)
E_{cm}	Young's modulus at 28 days (GPa)
E_{soil}	Young's modulus of the sand
F	the maximum load at failure (N)

F_s	the shearing force
F_{sp}	the splitting force (N)
F_v	the vertical force applied on the specimen (N)
f	the crack material stiffness matrix
f_{cc}/f_c	the compressive strength (MPa)
f_{cf}	the flexural stress (MPa)
f_{cm}	the mean compressive strength at the age of 28 days (MPa)
$f_{cm}(t)$	the mean compressive strength at a specific time (MPa)
f_t	the tensile strength in MPa
$f_t(t)$	tensile strength at specific time (MPa)
f_a	the multiplication factor (ranging from 10 to 100)
G_f	fracture energy (N/m)
h	the size of the member
h_1	the crack bandwidth
k	modulus of subgrade reaction
k_n	the normal stiffness
k_s	the shear stiffness
L_i	the length at a specific time between the two targets (mm)
L_0	the initial length between the two targets (mm)
l	the distance between supporting rollers (mm)
l_x	transformation vector to convert x coordinate of local axis to global axis
l_y	transformation vector to convert y coordinate of local axis to global axis
M_{Pt}	mass of the total test sample after sieving

m_x	transformation vector to convert x coordinate of local axis to global axis
m_y	transformation vector to convert y coordinate of local axis to global axis
N	transformation matrix
$\{n_1\}$	local coordinate system of first crack to indicate orientation of crack formed
$\{n_2\}$	local coordinate system of second crack to indicate orientation of crack formed
Re_3	Equivalent flexural strength
s	coefficient that depends on the type of cement in concrete
s^{cr}	the crack stress
t	the time at which shrinkage must be calculated (in days)
t_1	the concrete age in days
t_{inter}	the thickness of the interface
t_n	x-direction indicator of the friction in a concrete section
t_t	y-direction indicator of the friction in a concrete section
t_s	the concrete age at the start of drying in days
$\{t_1\}$	local coordinate system of first crack to indicate orientation of crack formed
$\{t_2\}$	local coordinate system of second crack to indicate orientation of crack formed
u	the perimeters of the member that is in contact with the atmosphere in mm.
v	Poisson's ratio
v_{soil}	the Poisson's ratio of the sand
W	crack opening in m
W_0	the work done by the applied force in the process of splitting the concrete (N•m)

α	the constant for a given member size and range between 0.9 to 1.1
α_1	the wedge angle in degrees
α_{as}	a coefficient, dependent on the type of cement (see Table 2.1)
β	reduction factor
$\beta_{as}(t)$	a coefficient, to determine autogenous shrinkage at a specific age
$\beta_{cc}(t)$	a coefficient that depends on the age of the concrete
$\beta_{ds}(t-t_s)$	defines the time development
$\beta_{RH}(RH)$	takes the relative humidity into account
$\beta_{s1}(f_{cm})$	a coefficient, to determine the drying shrinkage for a specific concrete strength.
$\beta_{ds}(t-t_s)$	a coefficient, to determine drying shrinkage for a specific concrete age
ε	the total strain
ε^e	the elastic strain
ε^{cr}	the crack strain
$\varepsilon_c(t)$	the total shrinkage strain
ε_{cas}	the autogenous shrinkage
$\varepsilon_{cas0}(f_{cm})$	the ultimate autogenous shrinkage strain for concrete with a specific strength
ε_{cds}	the drying shrinkage
$\varepsilon_{cds0}(f_{cm})$	the nominal shrinkage coefficient
$\varepsilon_{cc}(t)$	the creep strain in the concrete
$\varepsilon_{ci}(t_0)$	the initial strain of the concrete
$\varepsilon_{cs}(t)$	the shrinkage strain made up out of drying shrinkage strain, autogenous shrinkage strain and carbonation shrinkage strain

$\epsilon_{cT}(t)$	the movement in the concrete due to temperature changes
$\epsilon_{sh}(t)$	the shrinkage strain at a specific time (m/m)
$(\epsilon_{sh})_u$	the ultimate shrinkage strain
μ	the friction coefficient of the rollers
σ	the tensile stress in the concrete member (Pa)
σ_1	stress in x direction
σ_2	stress in y direction
σ_n	normal stress
τ	shear stress
ϕ	the friction angle of shear resistance
ϕ_{soil}	the friction angle of the soil
ψ	the dilatancy angle
Δ_n	the displacement normal to interface
Δ_s	the displacement along the interface
CMOD	crack mouth opening displacement in m
PPFRC	polypropylene fibre reinforced concrete
SFRC	steel fibre reinforced concrete
RH	the ambient relative humidity in %
WST	wedge splitting test
SCM	smearred crack model
FEM	finite element method
LVDT	linear variable differential transformer
COV	coefficient of variance

DSB direct shear box

CHAPTER 1: INTRODUCTION

One of the key structural elements of buildings is the ground floor. For structures without basements the ground floor is generally constructed out of slabs on grade, using concrete which is one of the more popular construction materials. Worldwide concrete is a commonly used building material, because of its high compressive strength and its ability to be moulded into almost any shape. However, concrete has the disadvantage of having a relatively poor tensile strength, and when introduced to tensile stresses exceeding its tensile capacity, cracks will form.

One of the main initiators of high tensile stresses in concrete floors is shrinkage that already occurs at the mixing stage. Different stages of shrinkage occur over the life span of the structure. In concrete floors one of the main types of shrinkage causing early age cracking, is called drying shrinkage. Cracks form when the shrinkage is restrained, resulting in an increase in the tensile stresses. This restraint against movement is due to the boundary conditions of the floor as well as the friction between the concrete and the soil or supporting layers (sub-base).

Crack formation in concrete can typically be controlled with one of two solutions of which adding reinforcement is one. Steel reinforcement with a high tensile strength is the most commonly used material, but due to its high price and its labour intensity, a more economical, uncomplicated method to mitigate drying shrinkage cracking, is needed. The use of macro polypropylene fibres has proved to be the answer for replacing reinforcing steel (Banthia & Gupta, 2006).

Another way to mitigate the cracks formed through shrinkage induced tensile stresses in a slab is by using saw cut joints. The use of saw cut joints generates a point of weakness in the slab, creating a desirable location for cracks to form. These cracks can then easily be covered at a later stage. The joints are typically spaced 4.5 m or 30 times the slab thickness, whichever is the lesser (Marais & Perrie, 2000). Joint cutting is time consuming, resulting in

more man hours and higher construction costs. Joints also require higher quality control on site due to them being dependent on a strict cutting timeframe.

The purpose of this project is to estimate to what extent the use of locally produced macro polypropylene fibres in concrete slabs on grade can mitigate the effects of drying shrinkage cracks, and as a result allow an increase in the spacing between the saw cut joints. If the joint spacings can be enlarged but still provide the same result, it will have a positive economic value for the construction industry.

The research methodology of the study consists of experimental work and finite element analyses. The experimental work starts off with a parameter study of the macro polypropylene fibre reinforced concrete compared to that of conventional concrete, and secondly, a large scale test to evaluate the material behaviour in a more realistic application. The experimental work is then compared to the analyses to verify the accuracy of the analyses. The results of the analyses can then be used to determine the influence of the fibres on the different joint spacings.

The study hypothesis is that the use of polypropylene fibres in slabs on grade has a positive effect in mitigating macro cracks created by drying shrinkage in the concrete, which could result in an increase of the spacing between the saw cut joints in the slab.

There are three main aims in this study. Firstly, an investigation of the properties of macro polypropylene fibre reinforced concrete is done to evaluate the impact of the fibres on the concrete. This is done with a shrinkage test, a large scale test and comparing the fracture energy of the reinforced concrete containing different fibre dosages. Secondly, a large scale test is done to determine if the spacing between saw cut joints can be increased when fibres are added to the concrete. Lastly, a finite element model is created to replicate the effect of the different fibre dosages on the spacings between saw cut joints of slabs on grade. The size and magnitude of the macro drying shrinkage cracks is then compared with the effect of slab thickness, fibre content and joint spacings of different slabs.

The layout of the report is as follows. Chapter 2 gives a literature review of the behaviour of conventional concrete compared to that of polypropylene fibre reinforced concrete. Chapter 3 gives a literature review of the construction of concrete slabs on grade and how the slabs can be modelled in a finite element analysis. A full property characterisation of the reinforced concrete is given in Chapter 4. Chapter 5 explains the setup of the large scale test

and provides the results. Chapter 6 shows the setup of the finite element model and compares the results of the large scale test in Chapter 5 with the results of the model to verify accuracy. The model is then used in Chapter 7 to determine the effect of different geometry, fibre dosages and sub-base layers of the slabs on grade. Chapter 8 concludes all of the findings and proposes suggestions for future studies.

CHAPTER 2: CONVENTIONAL AND POLYPROPYLENE FIBRE REINFORCED CONCRETE

The first use of polypropylene fibres in concrete dates back to 1965 where it was used as an impact resistant material for a blast-resistant building in the U.S. (Singh, 2010). Since then it was determined that the ductility, toughness and impact resistance of concrete can be improved when combined with polypropylene fibres (Alhozaimy et al., 1996). The use of polypropylene fibres in concrete has also proved to be useful in limiting the width of cracks in slab on grade by preventing micro-cracks, known as small hair-line cracks, to become large, aesthetically unacceptable cracks called macro-cracks (Labib & Eden, 2004). Apart from discussing the behaviour of polypropylene fibre reinforced concrete, this chapter will also examine the behaviour of conventional concrete as well as the mechanical properties of the polypropylene fibres.

2.1. THE BEHAVIOUR OF CONVENTIONAL CONCRETE

Concrete by itself is a relatively brittle material due to its poor tensile strength, but because of concrete's ability to withstand high compressive forces and also its desirable capability to take on complicated shapes in the casting process, concrete is the preferred material in the construction industry. To overcome the relatively low tensile strength of concrete, it can be reinforced with materials such as steel bars or, to some extent, fibres.

Two material properties of concrete that are improved with the use of fibres are the fracture properties and the shrinkage abilities (Banthia & Gupta, 2006). A brief overview of these properties, before fibres are added, is given in the following section. The development of strength in concrete is also discussed.

2.1.1. THE FRACTURE ENERGY PROPERTIES OF CONCRETE

The fracture energy of concrete (G_f) is a parameter which can be used to quantify the behaviour of the concrete structural component under tensile loading. These properties can be expressed with a value called fracture energy, nominated by G_f , referring to the energy required to propagate a tensile crack over a unit area (Hillerborg et al., 1976).

Fracture energy has been examined in numerous publications like Hillerborg et al. (1976), Ostergaard, (2003) and Lofgren et al., (2013). Petersson (1980) found that the fracture energy of the concrete increases up to an age of 91 days after which the fracture energy reduces with a further increase of age. He also looked at a suitable method to calculate the fracture energy of concrete and stated that when a concrete member is loaded in tension, there is a stress concentration at the tip of the weakest point. This point can be a joint, an existing crack or the position in the member where the stress would be at its highest, as seen in Figure 2.1a. When the tensile stress in the concrete reaches the tensile strength of the concrete itself, a micro-cracked zone is formed as seen in Figure 2.1b. This micro-cracked zone will continue to grow as long as the load is increased. This will occur until the micro-cracked zone interlinks and a macro-crack forms as seen in Figure 2.1c.

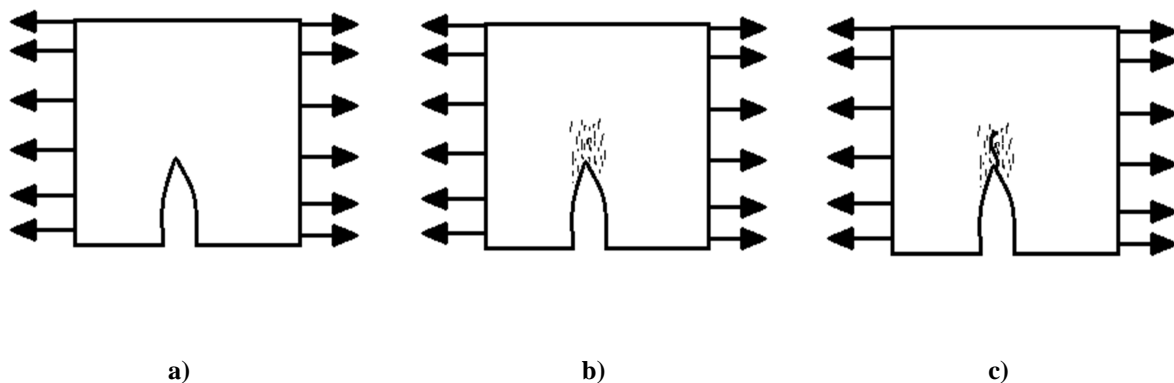


Figure 2.1: a) uncracked, b) micro-cracked, c) macro-cracked (Petersson, 1980)

Stresses can be transferred in the micro-cracked zone, with the magnitude of the stress transfer being dependent on the amount of micro-cracks, i.e. the more cracks the less the stress transfer. These stresses can be represented graphically by the force over crack mouth opening displacement (CMOD) seen in Figure 2.2 (Petersson, 1980). The duration of the crack formation is dependent on the fracture ligament that refers to the area over which the crack must form before the concrete breaks apart.

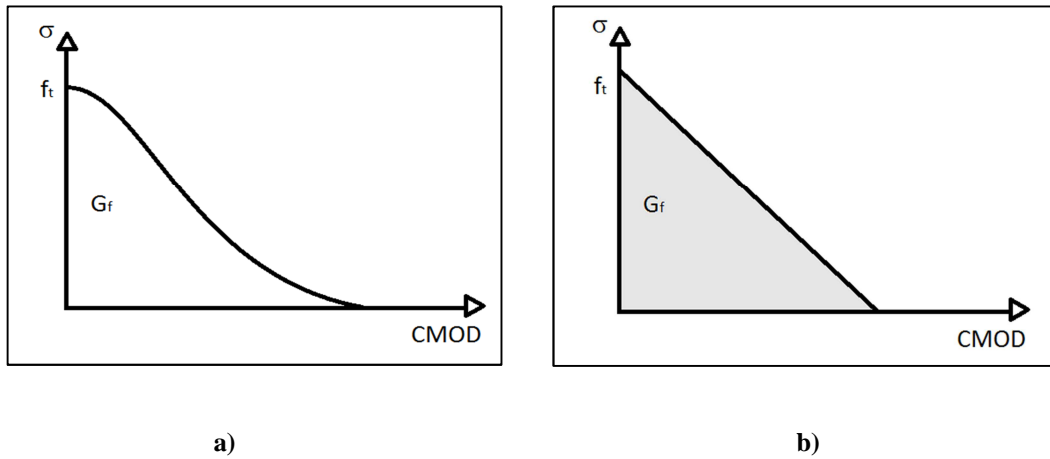


Figure 2.2: a) Force over CMOD for the energy balance approach (Petersson, 1980), b) simplified force over-CMOD for the energy balance approach (Petersson, 1980)

Hillerborg et al. (1976) developed a model to define the fracture energy that is based on the energy balance approach. The model assumes that when a crack forms, a certain amount of energy is released. This could only take place if the released energy is greater than the absorbed energy required for a crack to form (Hillerborg et al., 1976). This means that micro-cracks will form as soon as the stress at a point in the concrete is larger than the tensile strength, (f_t), of the concrete. When a crack starts to open, the stress at that point does not fall to zero, but instead decreases with the increase of the crack opening, (W), as shown in Figure 2.2a. For conventional concrete this line can be simplified with a straight line, as seen in Figure 2.2b. The graphs in Figure 2.2 show the energy absorbed per unit crack area that is used to open the crack from the point where the crack opening is equal to zero, to where the total crack opening is equal to the CMOD of the crack (Hillerborg et al. 1976). The fracture energy of the concrete that is equal to the area under the curve in Figure 2.2a can be calculated as follows:

$$G_f = \int_0^W \sigma dw \quad (2.1)$$

where G_f is the fracture energy in (N/m), W is the crack opening in (m) and σ is the tensile stress in the concrete member in (Pa).

From Figure 2.2b the simplified fracture energy can be determined using:

$$\int_0^W \sigma dw = \frac{f_t \text{CMOD}}{2} \quad (2.2)$$

The reverse of Equation 2.2 can be used if the CMOD is required using:

$$\text{CMOD} = \frac{2G_f}{f_t} \quad (2.3)$$

where CMOD is the crack mouth opening displacement in (m), f_t is the tensile strength in (Pa) and w , σ and G_f are as defined above.

The assumption must be made that the concrete is linear elastic until f_t is reached. For conventional concrete the CMOD is in the order of 0.01 – 0.02 mm, making it easy to calculate the fracture energy using Equation 2.2 if the tensile strength is known (Hillerborg et al., 1976).

When designing with conventional concrete from here on referring to concrete containing no reinforcement the main aspects of fracture design are the tensile strength (f_t), the fracture energy (G_f), and the shape of the softening curve as indicated by Hillerborg et al. (1976). The shape of the curve refers to either a linear or exponential decrease in tensile strength over time. When using fibre reinforced concrete (FRC) in construction, the fracture energy is a key value in the design stage because of FRC's energy absorption capabilities (Hillerborg et al., 1976). Löfgren (2004) explained that when FRC is used in a design the fracture energy and softening curve become more complex and less predictable.

The energy balance approach does not specifically refer to FRC, but the basic formulation of calculating the fracture energy as the area under the stress over CMOD graph seen in Figure 2.2a, can still be used. Löfgren (2004) stated that all the required parameters as given above by Hillerborg et al. (1976) and Hillerborg (1980) are more complicated when using FRC, referring to the shape of the softening curve that varies depending on the volume and type of fibres used, and the quality of the concrete (Löfgren, 2004).

There is more than one way to obtain the fracture energy by using different test methods and calculations. Two popular test methods that are used to determine the fracture properties of concrete is the three point beam test and the wedge splitting test. From both these tests the splitting force over CMOD graph is obtained.

The splitting work (W_o), is equal to the area under the graph and the fracture energy can then be calculated using:

$$G_f = \frac{W_o}{A_{lid}} \quad (2.4)$$

where A_{lid} is the crack area equal to the length of the crack times the width of the specimen in m^2 .

Although the three point beam test is the most commonly used test, it should be noted that the test requires sophisticated test equipment, it is time consuming, and it requires uncomfortably large test samples. The test is also not suitable for testing existing structural material properties. (Löfgren et al., 2013)

The wedge splitting tests on the other hand are easy to conduct: The test setup is easy and can be done by a single person; the test samples are small in size; the test can easily be completed in a short time frame. The test was first proposed by Linsbauer et al. in 1986 and later developed by Brühwiler et al. (1990). The test has been used for normal concrete, lightweight aggregate concrete and steel or synthetic fibre reinforced concrete (Löfgren, 2004)

If required the stress-crack relationship can be calculated through inverse analysis of the data collected from the force over CMOD graph. This is a useful tool to describe the pre-crack behaviour of the concrete. Wittmann et al. (1990) investigated this development of the stress-crack relationship with the use of three point bending tests, assuming that the pre-crack behaviour of the concrete is linear-elastic. After cracks have formed due to the tensile stress being reached as seen in Figure 2.3a, the concrete follows a bilinear stress-crack relationship. This can be seen in Figure 2.3b.

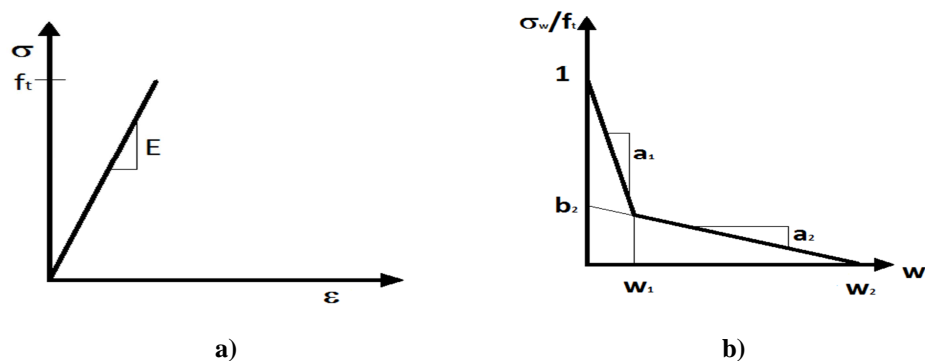


Figure 2.3: Stress-crack relationship (Ostergaard, 2003)

2.1.2. THE DEVELOPMENT OF TENSILE STRENGTH AND ELASTICITY MODULUS

As concrete hardens, its material properties such as compressive strength, tensile strength and the elasticity modulus increase until the ultimate strengths of the concrete are reached (Cement & Concrete Institute, 2009). The drying shrinkage discussed in Section 2.1.3 also increases over time. When examining the drying shrinkage cracks over time, it is important to take the changing material properties into consideration. These changes can be determined through experimental tests or by simplified formulas in model codes that only require the 28 day material properties of the concrete.

To calculate the tensile and elasticity modulus development used for the analysis in Chapter 6 the Eurocode (EN 1992-1-1:2004) is used. In this model the development of the tensile strength and the elasticity modulus is dependent on the 28 day compression strength of the concrete that can easily be obtained through cube tests. This compressive strength is referred to as the mean concrete compressive strength (f_{cm}) of the concrete. The concrete compressive strength at a specific time, $f_{cm}(t)$, can be calculated using:

$$f_{cm}(t) = \beta_{cc}(t) \cdot f_{cm} \quad (2.5)$$

where f_{cm} is the mean compressive strength at 28 days (Pa), $f_{cm}(t)$ is the mean compressive strength at a specific time (Pa) and $\beta_{cc}(t)$ is a coefficient that is dependent on the age of the concrete and can be calculated by using:

$$\beta_{cc}(t) = \exp \left\{ s \left[1 - \left(\frac{28}{t_1} \right)^{1/2} \right] \right\} \quad (2.6)$$

where t_1 is the age of the concrete (days) and s is a coefficient that is dependent on the type of cement:

= 0.2 for CEM 42.5 R, CEM 52.5 N and CEM 52.5 R

= 0.25 for CEM 32.5 R and CEM 42.5 N (Class N)

= 0.38 for CEM 32.5 N (Class S)

The tensile strength of the concrete refers to the highest stress reached under concentric tensile loading. The development of the tensile strength is greatly time dependent and it is influenced by the curing and drying conditions of the member. The geometry of the structure

can also influence the tensile strength development in terms of the surface area versus the sections dimensions due to different rates of drying (Cement & Concrete Institute, 2009). The following equation can be used to calculate the development of the tensile strength in the concrete, but for more accurate results tensile tests can be performed:

$$f_t(t) = (\beta_{cc}(t))^\alpha \cdot f_t \quad (2.7)$$

where $f_t(t)$ is the tensile strength at a specific time, f_t is the tensile strength at 28 days measured in (Pa), $\beta_{cc}(t)$ is a coefficient that is dependent on the age of the concrete and can be calculated with Equation 2.6 and $\alpha = 1$ for $t < 28$ days or $\alpha = 2/3$ for $t \geq 28$ days.

The elastic deformation is mainly depended on the composition of the concrete, referring to the aggregates used in the concrete. The development of the modulus of elasticity with time can be calculated using:

$$E_{cm}(t) = \left(\frac{f_{cm}(t)}{f_{cm}} \right)^{0.3} \cdot E_{cm} \quad (2.8)$$

where $E_{cm}(t)$ is the modulus of elasticity at a specific time in (GPa), E_{cm} is the modulus of elasticity at 28 days in (GPa), $f_{cm}(t)$ is the mean compressive strength at a specific time and f_{cm} is the mean compressive strength at 28 days.

All these parameters can then be calculated at specific ages and used in the modelling of the concrete behaviour over time for the analysis part of this work. The specific ages are relevant to the ages used to calculate the drying shrinkage in concrete that is discussed in the following section.

2.1.3. SHRINKAGE OF CONCRETE

Shrinkage is the result of a volume reduction in concrete due to the movement of moisture in the concrete matrix. It is a physical action that takes place in the concrete and it is generally caused by a change in humidity or temperature, or in the movement of agents such as water in the concrete. Shrinkage occurs without the influence of stresses acting externally on the concrete and is expressed as a dimensionless strain (ACI Committee 360, 2006).

In water to cement ratios the water requirement of concrete to be workable is almost twice that of the water content needed for the cement to be hydrated. This high water content results in higher shrinkage in a concrete member. The water content of concrete plays a direct part in the extent of shrinkage in the concrete. Concrete with a low slump of 76 - 100 mm will shrink less than a mix with a slump of 150 – 180 mm (ACI Committee 360, 2006). It should be noted that the slump test is not a reliable testing method to determine the degree of shrinkage. Other tests, as specified in the fib Model Code (2010), will give more accurate results. When adding water-reducing admixtures, care must be taken as some admixtures increase shrinkage even if it does reduce the water content and lowers the slump value (ACI Committee 360, 2006).

Looking at the shrinkage of concrete slabs in particular, the water that was not absorbed by the concrete in the hydration process primarily evaporated out of the slab from the open surface. This results in faster drying of the exposed or top surface in comparison to the bottom surface, which is constrained by the ground. This creates a moisture gradient between the upper and lower part of the slab resulting in curling at the top surface (ACI Committee 360, 2006). Curling is the result of the difference in shrinkage between the top and the bottom of the slab on grade. Stresses in the slab are generated due to the curling as well as movement, and Walker and Holland (1999) found that these stresses can easily range from 1.4 MPa to 3.1 MPa. This is higher than typical tensile strength of concrete that are used for slabs on grade.

The total shrinkage strain in a concrete member consists of different types of shrinkage that take place over its lifespan. Apart from shrinkage the concrete also undergoes strain due to temperature changes and creep. Creep is known as the time-dependent increase in the internal strain of a concrete member that is placed under a constant or controlled stress (Cement & Concrete Institute, 2009). The total strain over time in a concrete member can be calculated by using:

$$\varepsilon_c(t) = \varepsilon_{ci}(t_0) + \varepsilon_{cc}(t) + \varepsilon_{cs}(t) + \varepsilon_{cT}(t) \quad (2.9)$$

where $\varepsilon_c(t)$ is the total strain, $\varepsilon_{ci}(t_0)$ is the initial strain at loading, $\varepsilon_{cc}(t)$ is the creep strain in the concrete, $\varepsilon_{cs}(t)$ is the total shrinkage strain made up out of drying shrinkage strain, autogenous shrinkage strain and carbonation shrinkage strain and $\varepsilon_{cT}(t)$ is the thermal strain. A short discussion of these types of shrinkage follows.

AUTOGENOUS SHRINKAGE

The autogenous shrinkage in concrete refers to the shrinkage caused by the hydration of the cement. This deformation of the concrete usually takes place at a constant temperature and no moisture is exchanged with the environment (Barcelo et al., 2005). As the hydration process of concrete progresses, its volume decreases. Autogenous shrinkage can be divided into two parts, namely autogenous plastic shrinkage that takes place as the cement is exposed to water, and self-desiccation shrinkage that takes place after the concrete has set (Barcelo et al., 2001). Barcelo et al. (2001) explained that the autogenous plastic shrinkage ends at the point of transition from suspension to solid form. The self-desiccation shrinkage follows with regards to the autogenous swelling phenomenon as shown by Barcelo et al. (2005).

Although autogenous shrinkage takes place in the first few days after casting, its role in terms of tensile stress development leading to tensile failure in restrained structures, should not be underestimated. In a study done by Igarashi et al. (2000) it was explained that the restrained autogenous shrinkage can cause cracking especially in high strength concrete due to the stress increases in the concrete. Fibre reinforced concrete has shown to mitigate the cracking of concrete due to autogenous shrinkage. Autogenous shrinkage is negligible for conventional strength concrete which is typically used for concrete slabs on grade.

PLASTIC SHRINKAGE

The plastic shrinkage results in small cracks forming on the surface of concrete soon after casting. At this stage the concrete is still in a plastic state and the shrinkage is caused by high evaporation rates that result in the concrete surface drying out before setting. Apart from the fact that small cracks that are formed due to plastic shrinkage, create an unsightly surface, it has no real threat to the strength or durability of the concrete itself. The effect of plastic shrinkage cracks can be mitigated with the use of proper measures in the casting, curing and finishing processes (National Ready Mixed Concrete Association, 1998). Adding synthetic fibres to the concrete can influence the effect of the plastic shrinkage cracks according to a study done by Boshoff et al. (2013). They stated that the use of short micro polypropylene fibres does have a positive effect in restricting the crack formation due to plastic shrinkage.

CARBONATION SHRINKAGE

Carbonation shrinkage is the carbonation of cement hydration products in the presence of CO₂ (carbon dioxide). Carbonation refers to the chemical process of the reaction of calcium hydroxide with carbon dioxide resulting in the formation of calcium carbonate and water. (RILEM, 1976). One of the largest problems with carbonation shrinkage is the pH reduction in the concrete, causing breakdown of the passivation layer that protects the reinforcement steel from corrosion (Saetta et al., 1993). Polypropylene fibres are immune to corrosion and can resist most chemicals due to its chemical inertness (Hannant, 1978) and thus they will not be affected by the carbonation shrinkage.

DRYING SHRINKAGE

The drying shrinkage of concrete is due to the movement of moisture in the concrete over time (Jianyong & Yan, 2001). This is caused by the evaporation of water in the concrete as it is exposed to an environment with a lower relative humidity than the concrete's own pore system. This results in the moisture migrating out of the concrete, followed by a volume reduction of the pores (Idiart, 2009). The drying shrinkage starts occurring at the end of the curing process and it continues to take place over the concrete's lifetime.

The volume change in the concrete can be explained using four mechanisms. These mechanisms are capillary tension, surface tension, disjoining pressure, and movement of interlayer water. All these mechanisms are dependent on the relative humidity (RH) gradient that exists between the concrete and surrounding environment (Newman & Choo, 2003). The capillary tension in hardened concrete is due to a meniscus that is formed in the capillaries of the cement paste when subjected to drying. This causes tensile stresses in the capillary water that is balanced with compressive stresses in the solids, resulting in an elastic shrinkage strain (Idiart, 2009).

Surface tension occurs when the non-symmetrical surface molecules of solid material result in a un-equilibrium in the acting forces, causing contractions in the molecules which act like a stretched elastic skin that creates a tension on the surface (Idiart, 2009). These forces induce compression stresses resulting in elastic deformation. This phenomenon is dependent

on the water content of the concrete as well as the water layer on the surface of the material. The water layer will decrease the compression stresses resulting in less deformation and less tensile stresses.

The thickness of the water layer mentioned above is determined by the RH. With an increase in RH the water layer thickness will increase (Idiart, 2009). Disjoining pressure will occur where different surfaces are close to each other resulting in hindered absorption that take place when a layer could not develop fully under surrounding RH. This pressure can separate the two surfaces causing swelling in the material (Idiart, 2009). The reverse will occur in the case of drying, resulting in a decrease of pressure and shrinkage in the material.

The shrinkage in concrete is affected by multiple factors such as the aggregate, w/c ratio, RH, the ambient temperature and the size of the concrete member (Newman & Choo, 2003). The aggregate acts as a restraint in the concrete, resulting in lower shrinkage with an increase of the aggregate volume. This is due to the aggregate not being subject to drying because of its low permeability (Idiart, 2009). The stiffness of the aggregate also impacts the shrinkage, with a high stiffness resulting in a lower shrinkage in a concrete member. This has a direct impact on the w/c ratio of the concrete. With a constant aggregate volume, the increase in the w/c ratio will lead to an increase in the shrinkage as seen in Figure 2.4 (Newman & Choo, 2003)

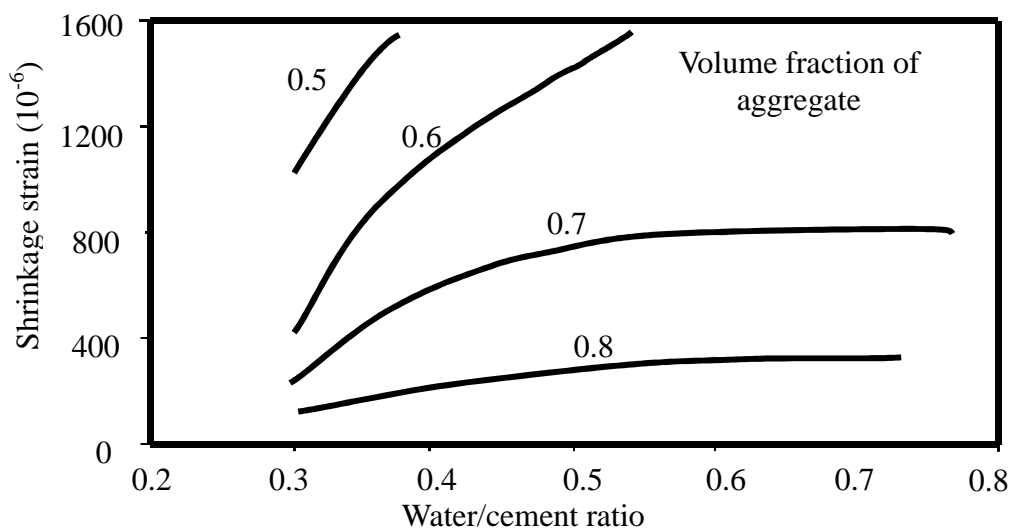


Figure 2.4: The effect of w/c ratio on shrinkage of concrete for different aggregate contents (Odman, 1968).

A greater shrinkage will be found with a lower RH due to the higher RH gradient between the concrete and the environment (Newman & Choo, 2003). This means that the environmental conditions can have a large impact on the extent of the shrinkage. Idiart (2009) stated that the effect of elevated temperatures and high wind velocities will also increase the shrinkage but not to the same extent as a low RH. Figure 2.5 illustrates the effect of a low RH on the shrinkage. It also shows the effect of concrete being stored in water, resulting in a swelling effect rather than shrinkage and it is compared to concrete being free to dry.

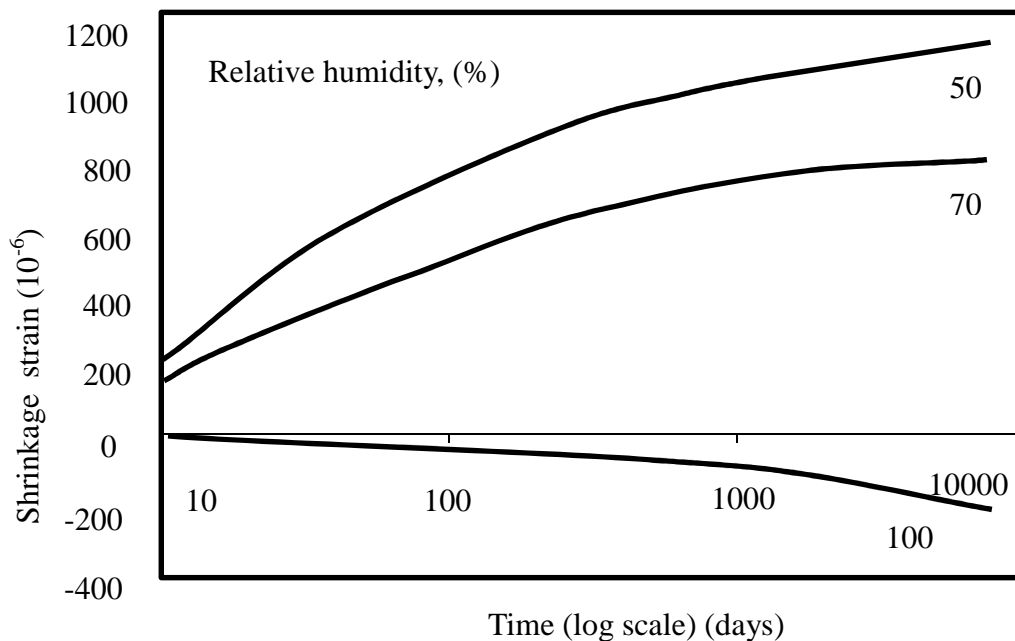


Figure 2.5: The shrinkage of concrete stored at different levels of relative humidity. Time is from 28 days after wet curing (Troxell et al., 1958).

The shrinkage in concrete changes over time with a typical proportion of shrinkage in concrete over 20 years being 20 per cent in the first 2 weeks, 60 per cent in the first 3 months, and 75 per cent in the first year. The shrinkage has a high initial rate that decreases rapidly over the lifespan of the concrete (Newman & Choo, 2003).

The size of the concrete member affects the shrinkage since the shrinkage is due to the moisture evaporation from the surface. Members with a large cross section will undergo less shrinkage than those with smaller cross sections. This is because it is difficult for water to escape with a larger cross section and can be expressed with the volume/surface ratio (V/S)

which is the average drying path length (Newman & Choo, 2003). Figure 2.6 shows the effects of the size of the cross section.

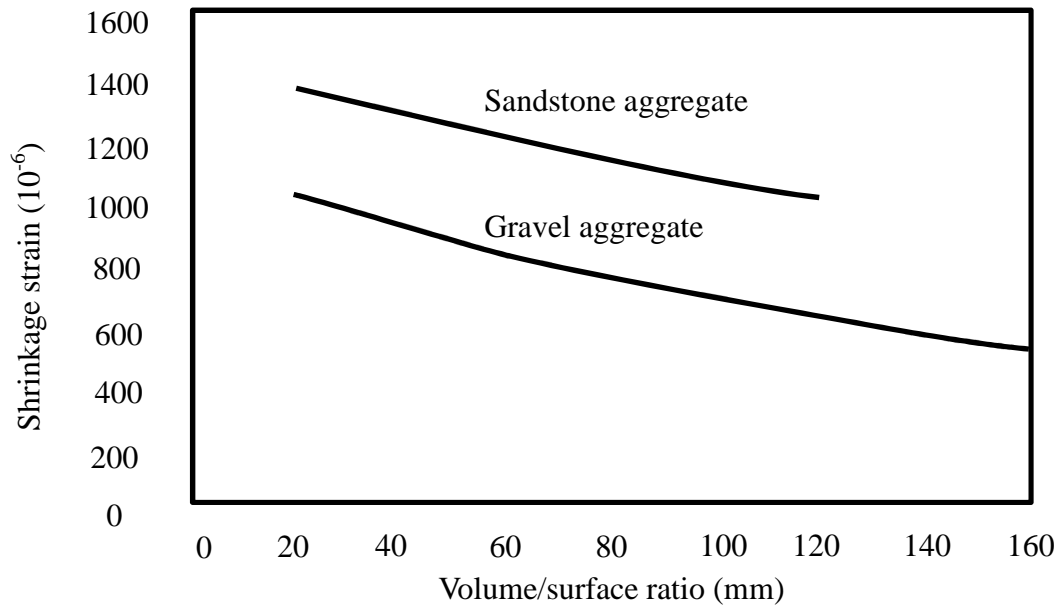


Figure 2.6: Influence of the concrete member's volume/surface ratio on the shrinkage of concrete (Hanson & Mattock, 1966).

When drying shrinkage in conventional concrete is restrained, it can cause cracks. This is due to the drying shrinkage being higher than the tension failure strain of the concrete (Newman & Choo, 2003). These restraints can be internal (reinforcement) or external (surface restraints such as foundation). The actual tensile stress that can develop is not only dependent on the shrinkage but also on the creep (see Figure 2.7). The creep relieves some of the elastic stress in the concrete.

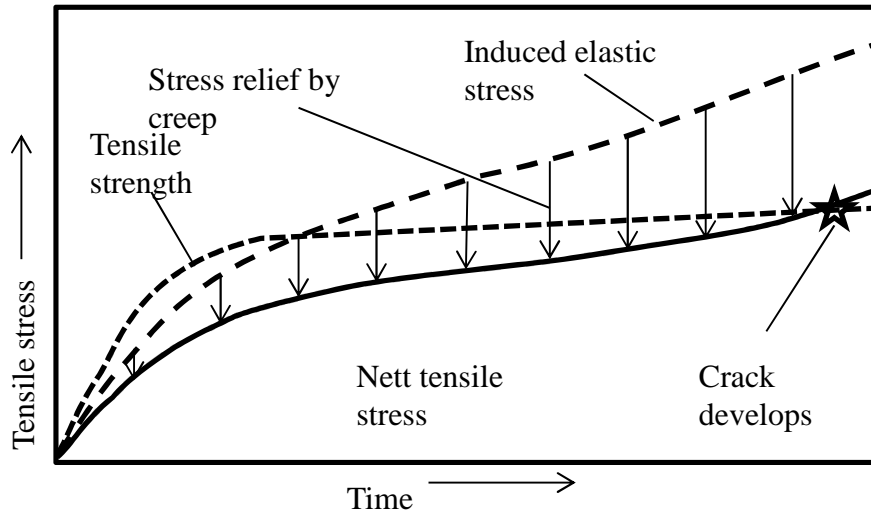


Figure 2.7: The development of induced tensile stress leading to cracks after relief by creep (Neville & Brooks, 2001).

Shrinkage can cause a loss in pre-stress in pre-stressed concrete as well as an increase in the deflection in asymmetrically reinforced concrete (Newman & Choo, 2003). The shrinkage in a slab on grade can be controlled in the design process by taking care when studying the mix design, type and location of the reinforcement, the effect that the sub-grade has on the slab in terms of friction and moisture, the slab thickness, the shrinkage restraints and the location of the saw cut joints in the slab. The following section examines prediction models that can be used to predict the shrinkage in concrete depending on the above mentioned parameters influencing the drying shrinkage.

2.1.4. PREDICTION MODELS FOR DRYING SHRINKAGE OF CONCRETE

The shrinkage and creep of concrete is a complex mechanism consisting of multiple factors, therefore, there is yet a theory to be developed that explains the behaviour of shrinkage and creep in full. Prediction models, based on experimental data, have been designed to help with the design of creep and shrinkage sensitive structures. The various analytical models as stated by Goel et al. (2007) include: The effective modulus method by McMillan in 1916; the Double power law of creep by Bazant and Osman in 1976; ACI 209-R82 by ACI in 1982; fib model code 1990 and the modified CEB-FIP 2010 by fib Special Activity Group 5; B3 model

by RILEM in 1995; Muller model and GL2000 model by Gardner and Lockman 2001. Some of the more common models are discussed in the following sections.

ACI 209R -92

The American Concrete Institute gave a prediction for the creep, shrinkage and temperature effects on concrete in the ACI 209R-92 report in 1997. The ACI 209R is a simplified method to predict the time-dependent material response and the service performance of a concrete structure. The potential for shrinkage in a concrete mix, according to the ACI 209R-92, is dependent on the water-cement ratio, the elastic stiffness of the coarse aggregate and the relative volume fractions of the cement paste and the aggregate. The shrinkage strain calculated can be anything between 400×10^{-6} and 1100×10^{-6} m/m for unrestrained concrete. ACI Committee 209 reports that the shrinkage strain is dependent on the duration of the initial curing period, the elapsed time after wet curing, the ambient relative humidity and the volume-to-surface ratio (Carino & Clifton, 1995).

The unrestrained shrinkage, $\epsilon_{sh}(t)$, can be calculated by using:

$$\epsilon_{sh}(t) = \frac{t_1^\alpha}{t+t_1^\alpha} \epsilon_{sh,u} \quad (2.10)$$

Where $\epsilon_{sh}(t)$ is the unrestrained shrinkage strain at a specific time in (m/m), t is the time at which shrinkage must be calculated (in days), α is the constant for a given member size and range between 0.9 to 1.1, $(\epsilon_{sh})_u$ is the ultimate shrinkage strain and t_1 is the time after loading.

The model gets more complex at this point, taking into account stress relaxation, types of curing, member thickness, reinforcement, and time and temperature changes. The model is best used to determine the shrinkage and creep for pre-stressed members and can give a high percentage of error due to the large amount of parameters required for accurate calculations.

SABS 0100-1:2000

The SANS 0100-1:2000 gives a guideline for calculating the shrinkage strains that can be used for determining the pre-stressed losses. It also gives a graph that was modified from the BS 8110-1997, which can be used to obtain a rough estimate of the shrinkage strain at 6 months and at 30 years. The information required to use this method is the relative humidity and the effective section thickness. Figure 2.8 shows the graph that can be used to obtain the drying shrinkage for normal-density concrete made without admixtures, containing 190l/m³ water.

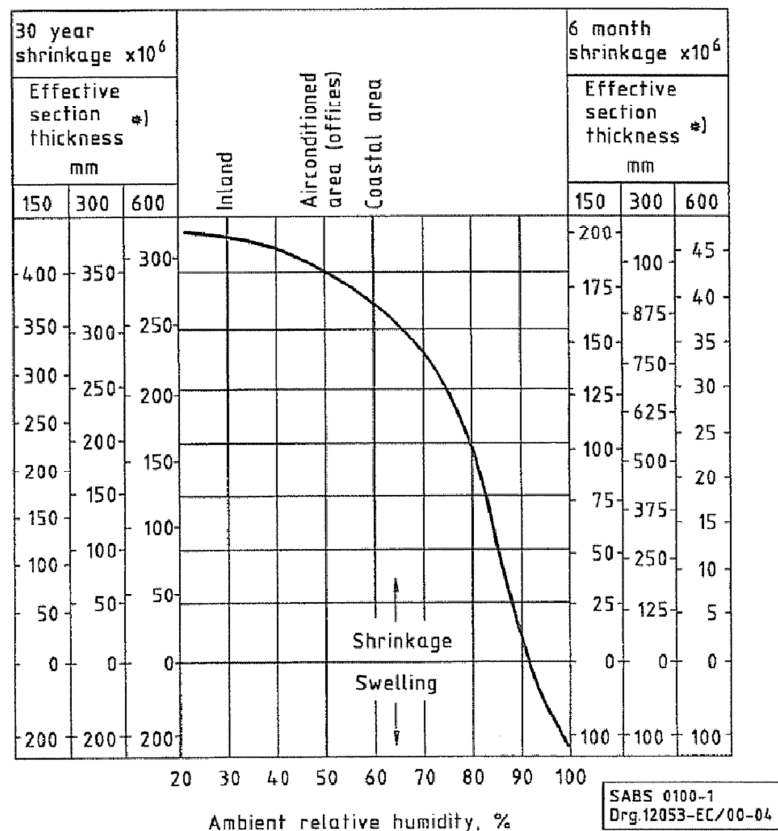


Figure 2.8: The drying shrinkage of normal-density concrete (SANS 10100-1:2000, 2000)

Although the method is simple to use, some important parameters like the drying time, the temperature and aggregate stiffness is not taken into consideration during the calculations. The accuracy of the method is solely dependent on the graph with little reference of where the graph originated from.

RILEM B3 MODEL

The Model B3 is an improvement of the ACI 209R-92, with lower percentages of error. The model was derived by Bazant and Baweja in 2000. The model is based on the compliance function reducing the level of errors created by inaccurate values of elastic modulus. It takes into account the age of the concrete as the drying process starts, the age of loading, the aggregate size and volume, the cement content and type, the curing method, the relative humidity, the shape and surface volume of the member, and w/c ratio of the concrete (ACI Committee 209, 2008). Although the model incorporates a large number of parameters that leads to a more accurate result, the model was designed to be applied to structures that will undergo large deflection such as long-span pre-stressed box girders. Due to its complicity it is seldom used for structures with a lower sensitivity level (Bazant & Baweja, 2000).

FIB MODEL CODE 2010

The fib Model 2010 is a modification of the popularly used CEB-FIP Model 1990 that has been adopted by concrete codes worldwide. The code can be used for any concrete mix with an average 28 day compressive strength between 20 MPa and 90 MPa. The relative humidity should be between 40 per cent and 100 per cent with an environmental temperature between 5 and 30 degrees Celsius. This model is also used in the modelling software that is used in Chapter 6, making it the most suitable model for the shrinkage prediction of this report.

The fib Model splits the total shrinkage, (ϵ_{cs}) into two parts, namely: the autogenous shrinkage and the drying shrinkage by using:

$$\epsilon_{cs}(t, t_s) = \epsilon_{cas}(t) + \epsilon_{cds}(t, t_s) \quad (2.11)$$

where ϵ_{cas} is the autogenous shrinkage and ϵ_{cds} is the drying shrinkage, calculated with Equation 2.16.

The autogenous shrinkage of the concrete can be calculated by using:

$$\epsilon_{cas}(t) = \epsilon_{cas0}(f_{cm}) \cdot \beta_{as}(t) \quad (2.12)$$

where $\varepsilon_{cas0}(f_{cm})$ is ultimate autogenous shrinkage strain for concrete with a specific strength, calculated with an alpha factor from Table 2.1 and the mean design concrete strength by using:

$$\varepsilon_{cas0}(f_{cm}) = -\alpha_{as} \left(\frac{f_{cm}/10}{6+f_{cm}/10} \right)^{2.5} \cdot 10^{-6} \quad (2.13)$$

where α_{as} is a coefficient, dependent on the type of cement (see Table 2.1), f_{cm} is the mean compressive strength at the age of 28 days in MPa.

Table 2.1: Table alpha factors used to predict shrinkage for fib 2010 model code

Strength class of the cement	α_{as}	α_{ds1}	α_{ds2}
32.5 N	800	3	0.013
32.5 R, 42.5 N	700	4	0.012
42.5 R, 52.5 N, 52.5 R	600	6	0.012

The beta factor is a function of the concrete age and can be calculated by using Equation 2.14:

$$\beta_{as}(t) = 1 - \exp(-0.2 \cdot \sqrt{t}) \quad (2.14)$$

where $\beta_{as}(t)$ is a coefficient used to determine autogenous shrinkage at a specific age and t is the concrete age in days.

The drying shrinkage is determined by using Equation 2.15 that is dependent on the concrete strength, cement type, cement strength, relative humidity and the effective section thickness.

$$\varepsilon_{cds}(t_1, t_s) = \varepsilon_{cds0}(f_{cm}) \cdot \beta_{RH}(RH) \cdot \beta_{ds}(t_1 - t_s) \quad (2.15)$$

where t_1 is the concrete age in days, t_s is the concrete age at the start of drying in days, $\varepsilon_{cds0}(f_{cm})$ is the nominal shrinkage coefficient, $\beta_{RH}(RH)$ takes the relative humidity into account and $\beta_{ds}(t-t_s)$ defines the time development.

All the factors that are given in Equation 2.16 to 2.19 are in line with regards to fib Model code (2010).

The nominal drying shrinkage coefficient can be calculated by using:

$$\epsilon_{cds0}(f_{cm}) = [(220 + 110 \cdot \alpha_{ds1}) \cdot \exp(-\alpha_{ds2} \cdot f_{cm})] \cdot 10^{-6} \quad (2.16)$$

where α_{ds1} and α_{ds2} are coefficients that are dependent on the type of cement as seen in Table 2.1

The two beta factors are calculated by using:

$$\beta_{RH}(RH) = \begin{cases} -1.55 \cdot \left[1 - \left(\frac{RH}{100}\right)^3\right] & \text{for } 40\% \leq RH < 99\% \cdot \beta_{s1} \\ 0.25 & \text{for } RH \geq 99\% \cdot \beta_{s1} \end{cases} \quad (2.17)$$

with

$$\beta_{s1}(f_{cm}) = \left(\frac{35}{f_{cm}}\right)^{0.1} \leq 1.0 \quad (2.18)$$

where $\beta_{s1}(f_{cm})$ is a coefficient that are used to determine the drying shrinkage for a specific concrete strength and RH is the ambient relative humidity in percent.

The second beta factor in Equation 2.15 is dependent on the change in time and the effective section thickness and can be calculated by using:

$$\beta_{ds}(t_1 - t_s) = \left(\frac{(t_1 - t_s)}{0.035 \cdot h^2 + (t_1 - t_s)}\right)^{0.5} \quad (2.19)$$

where $\beta_{ds}(t-t_s)$ is a coefficient, to determine drying shrinkage for a specific concrete age, t_s is equal to the concrete age as drying starts measured in days and h is the size of the member under discussion and can be calculated by using:

$$h = \frac{2A_c}{u} \quad (2.20)$$

where A_c is the cross-section of the concrete member in mm^2 and u is the parameters of the member that is in contact with the atmosphere in mm.

The importance of a realistic model of creep and shrinkage is significant when using a finite element analysis, because an unrealistic representation of the creep and shrinkage will result in inaccurate results. This model was chosen to be used for the analyses as part of this study.

2.2. FIBRE REINFORCED CONCRETE

On its own concrete has a relatively poor tensile strength and acts brittle under tensile stresses and impact loads. Apart from this, concrete perform significantly better than most materials under compression stress which is a desired characteristic in the construction industry. In order to overcome the relatively poor tensile strength of concrete, it is reinforced with steel bars that have a high tensile capacity. The steel reinforcement can partially be substituted with fibres (Banthia, 2004). This idea dates back almost 3500 years when natural fibres, namely straw, was used to reinforce clay bricks to build the hill of Aqar Quf near Baghdad. This was followed by the use of fibres such as horsehair and asbestos, and in the 1960s new fibres were designed for the use of reinforcing cement products (Labib & Eden, 2004).

One of the disadvantages of FRC is the lack of knowledge of the performance improvement and of the economic value of FRC (Banthia, 2004). In terms of designing with FRC, the current codes and standards restrict engineers to the point that fibre reinforced concrete can only be used for non-structural, non-load bearing elements. These limits are due to a lack of design and of performance knowledge (Manolis et al., 1997). One of the advantages of using FRC includes mitigating crack formation in the concrete through added tensile strength (Kakooei et al., 2011). FRC also has the potential for easier construction; weight reduction of the structure; and adds ductility, strength and toughness to the concrete (Manolis et al., 1997).

A concrete mix containing fibres consists of a mixture of hydraulic cement, fine aggregate, coarse aggregate, water and the fibres (Manolis et al., 1997). When working with fibres there are some design aspects that have to be considered such as the workability required and the available equipment. Mixing the fibres into concrete has no effect on the water to cement ratio of the concrete since the polypropylene fibres is of a hydrophobic nature (Kakooei et al. 2011). The fibres are usually mixed in near the end of the mixing process as the fibres tend to shred if they are left too long in the mixer. Mixing can take place with a tumbler or with mixing lorries, as long as the fibres are only added in a few minutes before casting the concrete. The workability is partly dependant on the length and dosage of the fibres. Normal testing methods like the slump test used for conventional concrete are not applicable to FRC, since the accuracy is influenced by the fibres (Hannant, 1978). The TR 65 gives a range of test methods that can be used for FRC (Concrete Society Technical Report No. 65, 2007)

When designing concrete reinforced with polypropylene fibres, the anchorage and the staple length of the fibres that best suit the aggregate must be used. The dosage of fibres added to the concrete is dependent on the spacing factor. This can be influenced by the size of the aggregate used in the concrete matrix, with a courser aggregate resulting in a low spacing factor. A large spacing factor can be found for small aggregate due to the fibres that are able to position themselves between the aggregate stones instead of around one solid piece of aggregate (Hannant, 1978).

There are five standardised tests used to determine the properties of FRC. Firstly there is the Three Point Beam test as given by EN 14651 (2007), determining the limit of proportionality, residual flexural tensile strengths or the equivalent flexural tensile strength and ratios. The Four Point Beam Bending tests documented by ASTM C78 (2010) can be used to determine the equivalent flexural tensile strength ratio, the residual flexural tensile strengths or toughness of the FRC. The Four Point Beam Bending test gives the same type of results as the Three Point Beam test, but the results have lower values (SANS 5864, 2006). Another test is the Round Determinate Panel test standardised in ASTM C1550. It was designed to overcome the large scatter in results obtained with the beam tests (Odendaal, 2015). The EFNARC Panel test developed by EFNARC in 1996 consists of a square panel and is used to measure the energy absorption capacity of the FRC (Odendaal, 2015). Lastly, the Wedge Splitting test by NT Build 511 (2005) determines the crack mouth opening displacement (CMOD) over the applied load and can be used to calculate the fracture energy and the residual tensile stresses in the concrete.

The effect of fibres is best described with a stress-strain diagram obtained through typical load to deflections tests. When fibres are added to concrete, the curve typically shows a strain softening behaviour (linear increase in stress with a slow decrease after the first crack). The opposite effect, called strain hardening, is where higher loads can be supported after the first crack occurs. This can be seen for high volume fibres and occurs because of the high crack bridging effects of the fibres. This effect typically does not take place for conventional FRC, but rather in high performance fibre reinforced concrete composites (HPFRCC) (Brandt, 2008). Figure 2.9 shows a typical load to deformation curve used by the Cement and Concrete Institute in 2010 to describe the effect of FRC.

As previously discussed, it is commonly known that conventional concrete is a brittle material which fails once the designed tensile strength is reached, as seen in Figure 2.9. The

fibres in the concrete will only start working after the concrete reaches its tensile strength, and from that point on the fibres withstand stresses at much larger deflections than that of conventional concrete.

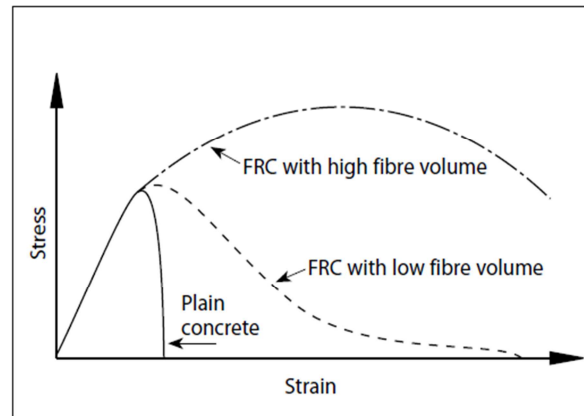


Figure 2.9: Typical stress-strain curve for FRC
(Cement & Concrete Institute, 2010)

The effects of the fibres are dependent on the type and volume of fibres used in the matrix. These types of fibres can be categorised into four groups, namely steel fibres, glass fibres, natural fibres and synthetic fibres.

2.2.1. STEEL FIBRES

The use of steel fibres dates back to the early 1900s. Early fibres were round and smooth but modern fibres are made with rough surfaces and hooked edges for better grip when added to concrete. Modern fibres are manufactured from drawn steel wire, slit steel or through the melt-extraction process, with carbon steels being the commonly used material. Stainless steel or corrosion-resistant alloys have also been used to make fibres. Steel fibres come in lengths from 7 to 75 mm with diameters ranging between 0.15 to 2 mm. Steel fibres have a high tensile strength between 0.5 and 5 GPa and a modulus of elasticity of 200 GPa. It also has relatively low creep and ductile stress-strain characteristics (Cement & Concrete Institute, 2010). The use of steel fibres has a wide range of applications such as in conventional concrete and shotcrete with dosages of anything between 0.25 per cent and 2.0 per cent of the concrete volume. Greater substantial impact resistance, higher ductility of failure in

compression, and flexure and torsion have been obtained with steel fibre reinforced concrete (Cement & Concrete Institute, 2010).

2.2.2. GLASS FIBRES

Glass fibres that are used for glass-reinforced cement products are made from an alkali-resistant glass and dates back to the 1960s. Glass fibres come in a length of up to 35 mm and are mainly used in spray applications but shorter fibres can be used in premix applications. Although glass fibres have a high tensile strength of between 2 and 4 GPa and an elastic modulus between 70 and 80 GPa, it undergoes brittle stress-strain behaviour and has a low creep tolerance at room temperature. It also has a loss in strength and ductility when exposed to outdoor environments resulting in the use of glass fibre reinforced concrete being confined to non-structural uses such as various precast products and small containers (The Concrete Institute, 2013).

2.2.3. NATURAL FIBRES

Natural fibres include coconut, sisal and bagasse fibres. It comes in two categories namely, processed and unprocessed fibres. The properties of the fibres are specific to each material and most of the fibres are specific to its origin. Natural fibres can be of low cost and is of interest as a concrete reinforcement in less developed regions where conventional building materials are scarce. Fibres like sisal have been used to produce roof tiles, pipes and silos and elephant-grass-reinforced mortar has been used in low-cost housing projects (Cement & Concrete Institute, 2010).

2.2.4. SYNTHETIC FIBRES

Since 1965 the use of this man-made fibre has grown due to it being relatively inexpensive and abundantly available. Many types of fibres that are used in concrete today are made of a

variety of organic polymers such as acrylic, carbon, nylon, polyester, polyethylene and polypropylene. The fibres come in two physical forms namely, monofilament fibres and fibres produced from fibrillated tape. Fibres are typically added to concrete in either low-volumes (0.1 – 0.3 per cent by volume) or high-volumes (0.4 – 0.8 per cent by volume) (Cement & Concrete Institute, 2010). Similar to the natural fibres the fibre characteristics are dependent on the material used. For the purpose of this work only the polypropylene fibre will be discussed in the following section.

2.3. MACRO SYNTHETIC POLYPROPYLENE FIBRE REINFORCED CONCRETE

Over the past 30 years numerous studies have been done on the use of polypropylene fibres to enhance the properties of concrete. Some of the more recent literature is discussed here.

Initially there were only two forms of polypropylene fibres, namely monofilament fibres and film fibres. Currently the Technical Report No. 65 (Concrete Society Technical Report No. 65, 2007) divides fibres into three groups:

Class I (a): Micro fibres < 0.3 mm in diameter, mono-filaments

Class I (b): Micro fibres < 0.3 mm in diameter, fibrillated

Class II: Macro > 0.3 mm in diameter

The micro fibres are used to increase the plastic properties of the concrete, where the macro fibres increase the residual flexural strength of concrete. (Concrete Society Technical Report No. 65, 2007). Figure 2.10 shows typical polypropylene fibres used in South Africa.



Figure 2.10: Polypropylene fibres used in South Africa (Bothma, 2013)

The raw material of polypropylene is a pure hydrocarbon polymer with a methyl group attached that alternates carbon atoms on to the chain. Polypropylene is a thermoplastic with a linear structure based on the monomer C_nH_2N and the manufacturing process depends on propylene gas and a catalyst, like titanium chloride (Hannant, 1978).

Hannant (1978) explained that polypropylene fibres are desirable because of the following properties: Polypropylene is an isotactic because of its composition of isotactic macromolecules and has a relatively high melting point ($165^{\circ}C$). The fibres are resistant to most chemicals due to its chemical inertness that results in a structure less vulnerable to corrosion. The fibres added to a mix, typically do not have any water demand at low volumes and the fibres have a high stretching potential, and a relatively high tensile strength.

The bond between the fibres and the concrete matrix is mainly controlled by the physical properties of the fibres. Two physical properties in particular can be used to define the fibres. The first aspect is the elongation of the fibres. The elongation at break point can be two or three orders larger than that of the strain required by the concrete matrix to fail. This means that in theory the matrix will crack long before the fibres fail (Beaudoin, 1990). The fibres can have a tensile stress between 100 and 650 MPa that is usually specified by the manufacturers (Concrete Society Technical Report No. 65, 2007).

Secondly, the modulus of elasticity of the fibres is important and range typically between 2 and 10 GPa. This is five times less than the concrete matrix's modulus of elasticity, making the impact of the fibres on the modulus of elasticity of the matrix relatively insignificant (Beaudoin, 1990).

All fibres can be divided into two categories: the first is fibres that have a low modulus of elasticity and high elongation, and the second type refers to fibres with a high modulus of elasticity but low elongation. The first type is fibres made from cellulose, nylon and polypropylene and the second is fibres such as glass, steel, carbon and asbestos. Since polypropylene fibres fall under the first category with a low modulus of elasticity and high elongation, it can be subject to relatively high creep, resulting in large elongations under high stresses in cracked composites (Manolis et al., 1997). The large Poisson's ratio of the polypropylene fibres means that the polypropylene fibres contract in the transverse direction to a larger extent than other fibres when under stress.

The fibres have two failure modes, namely breakage and pull-out. At times the fibre can withstand the high tensile stresses in the cracking matrix, but the high tensile stresses at the interface between the fibre and the matrix result in debond and pull out. Fibre pull out is dependent on the interfacial bond strength and the frictional bond stress between the fibres and the matrix (Beaudoin, 1990). The pull-out can be disregarded to an extent, with the shape of the fibre resulting in better bond stress. The main function of adding the polypropylene fibres to the concrete is to modify the properties of the concrete in an agreeable way as discussed below.

2.3.1. FLEXURAL STRENGTH AND FLEXURAL TOUGHNESS OF PPFRC

The use of polypropylene fibres does not significantly improve the flexural strength of concrete since the load capacity of PPFRC is similar to conventional concrete at first crack. Three or four point beam tests can be used to obtain the load-deflection curve from which the equivalent flexural strength, R_{e3} , value can be calculated. The equivalent flexural strength is defined as the average load applied for the 450 mm span beam to deflect to 3 mm. This is expressed as a ratio of the load compared to the load at first crack (Soutsos et al., 2012). Panel tests can also be used to test the flexural strength but they give less variation in results compared to the beam test (Concrete Society Technical Report No. 65, 2007).

Four point beam tests done by Soutsos et al. (2012) showed that the use of a synthetic fibre, made from a mixture of polypropylene and polyethylene, at dosages ranging from 4.5 to 5.3

kg/m^3 , only increased the flexural strength of the conventional concrete by 0.2 to 0.25 N/mm^2 from its original value of 4.2 MPa (Soutsos et al., 2012).

The increase in the flexural toughness, known as the energy absorbing ability of concrete, of the PPFRC is the main benefit in using fibres to reinforce concrete. This can be seen with the load-deflection curve in Figure 2.9, showing results from the study done by Soutsos et al. (2012).

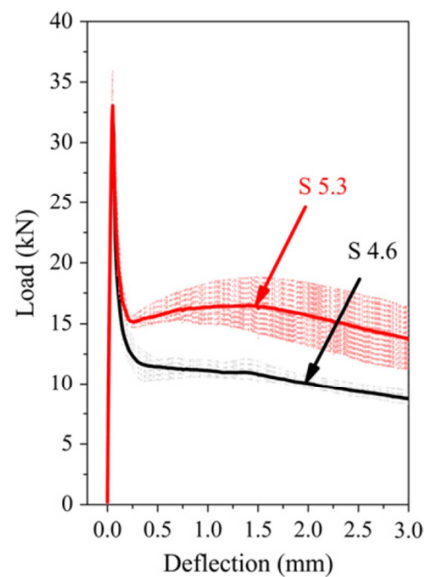


Figure 2.10: Load-deflection curve for 4.6 to 5.3 kg/m^3 dosage synthetic fibres. (Soutsos et al., 2012)

The solid lines represent the average of all the test specimens, whereas the shaded part indicates the range of results obtained. Here the effect of the dosage of fibres is clear as the higher dosage of 5.3 kg/m^3 retains a much higher load over 3 mm deflection than that of a lower dosage. Soutsos et al. (2012) found that the use of synthetic fibres increased the flexural toughness by an average of 40 J, similar to that of steel fibres at low dosages of 30 kg/m^3 . This increase of the equivalent flexural strength ratio of the concrete can be used in the design of the thickness of slabs on grade.

A similar study, done by Alhozaimy et al. (1996), shows the different effects of polypropylene fibres at different dosages. The study proved that the use of these fibres

increased the flexural toughness of the concrete, and to a slight extent, the first crack resistance (Alhozaimy et al., 1996).

2.3.2. TENSILE STRENGTH OF PPFRC

When polypropylene fibres are added to concrete they will not significantly affect the elastic response of the concrete and they only start giving the concrete structural support at the point of cracking. From there the fibres improve the tensile strength as well as the impact strength and toughness (Manolis et al., 1997). This could be attributing to the reduced crack formation and development, providing post-crack strength (Tapcu & Canbaz, 2007).

To test the tensile strength of the SFRC a uniaxial tension test can be used but this test is difficult to carry out. Some standard methods are available that focus on the required strain control for FRC. The RILEM uniaxial tension test method has a standard test procedure for SFRC (Concrete Society Technical Report No. 65, 2007).

2.3.3. COMPRESSIVE STRENGTH OF PPFRC

Some studies done by Kakooei et al. (2011); Nagarkar et al. (1987); Zhang et al. (2009) and Soutsos et al. (2012) have shown that the use of polypropylene fibres increases the compressive strength of the concrete, but not significantly enough to promote the use of fibres for this purpose. The general use for fibres is not to help increase the compressive strength, but rather to help with the brittle effect of concrete under tension.

2.3.4. CRACKING OF FRC

The fracture and cracking properties of conventional concrete is explained in Section 2.1.1, but when polypropylene fibres are added to the concrete, the micro-cracks in the concrete are bridged by the fibres, constraining the formation of macro-cracks (Brandt, 2008) (see Figure

2.10). The fibres transfer the stresses across the cracks and in this way confine the crack tip from expanding to form a macro-crack. This enhances the durability of the structure.

The size and length of the fibre plays an important role in the method of crack bridging. Micro-fibres are densely distributed in the concrete matrix where macro-fibres with larger lengths can bridge larger cracks.

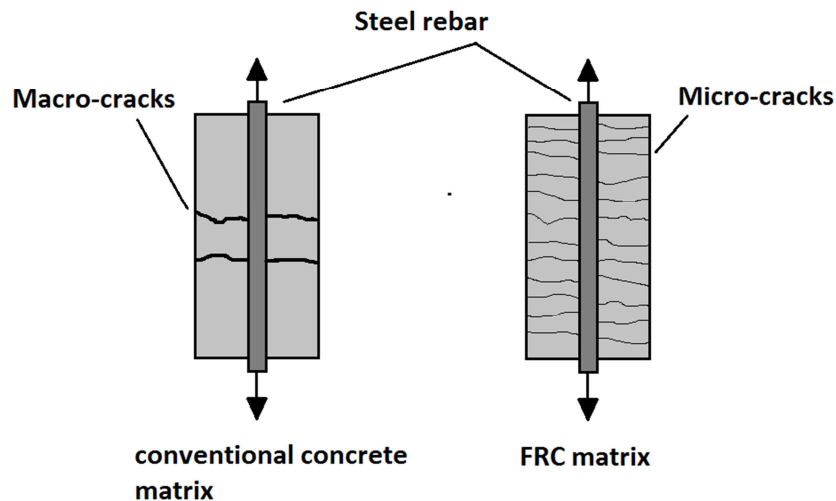


Figure 2.11: The crack patterns of steel reinforced concrete compared to FRC (Brandt, 2008)

It is important to remember that the use of fibres does not prevent cracks but it helps control them (Manolis et al, 1997).

2.3.5. SHRINKAGE OF FRC

There is a vast amount of literature available that states that the effect of plastic and drying shrinkage can be minimised with the use of low dosages of polypropylene fibre (Dahl (1985), Padron et al. (1990), Monolis (1997)). These authors used rectangular slab specimens to prove that the cracks can be controlled by means of fibres, where Grzybowski et al. (1989) used a ring test setup showing that the use of fibres reduced the average crack width significantly (ACI Committee 544, 2002). Banthia et al. (2006) also showed that the plastic and drying shrinkage in the concrete can be controlled by the use of fibres. They also looked at the influence of different lengths and widths of the fibres on the shrinkage (Banthia &

Gupta, 2006). This is done by increasing the homogeneity of the mix, which means it stabilises the movement of the solid particles and blocks the bleeding water channels. The advantage of this is that it helps to slow down the bleeding rate of the concrete that reduces the plastic settlement (Labib et al., 2004).

The drying shrinkage found by Choi et al. (2011) for different fibre reinforced concretes is shown in Figure 2.11. All the mixes contained 0.2 per cent fibres by volume of the same macro fibres. The nylon fibre (NY) refers to a micro fibre while the rest of the fibres were all macro fibres made from either polypropylene (PP) or polyvinyl (PV). The results showed that the use of fibres, and more specifically, the use of polypropylene fibres, helped to decrease the effect of drying shrinkage in concrete (Choi et al. 2011). A study done by Kayali et al. (1999) on normal weight, high strength polypropylene fibre reinforced concrete shows a micro shrinkage strain of almost 400×10^{-6} after 100 days which corresponds with the results found by Choi et al. (2011).

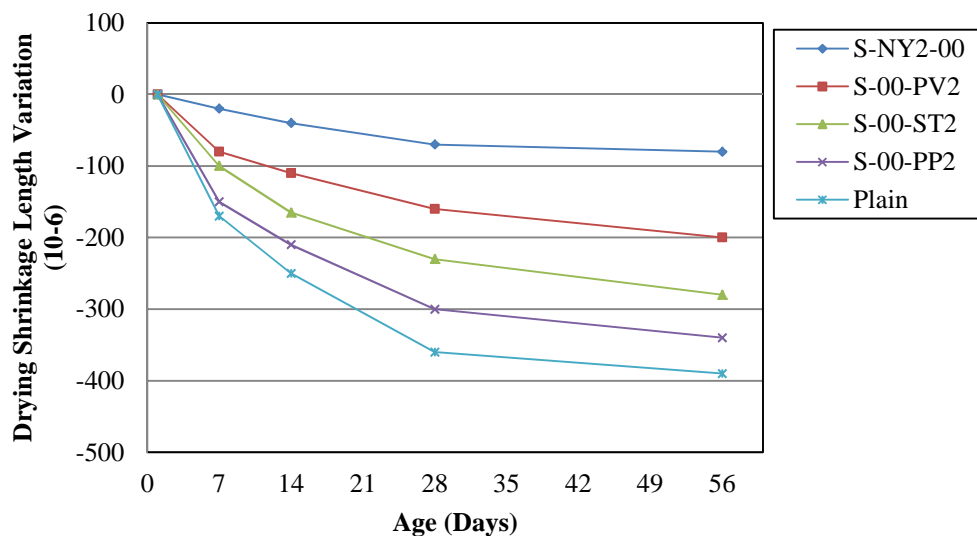


Figure 2.12: The drying shrinkage for different fibre reinforced concrete (Choi et al., 2011)

2.4. CONCLUDING SUMMARY

The discussion in this chapter focussed on the fracture behaviour, development of the tensile strength, elastic modulus and shrinkage of unreinforced concrete. Fibre reinforced concrete was then discussed as a method to enhance the material properties of the concrete. From the

information given in the text above, it is clear that the use of polypropylene fibres can improve the mechanical properties of conventional concrete and help to mitigate the formation of macro-cracks in the concrete. In the following chapters the behaviour of PPFRC used for slabs on grade is investigated.

CHAPTER 3: CONCRETE FLOORS ON GRADE: CONSTRUCTION AND MODELLING

Floor slabs supported by the ground, also known as slabs on grade, consist of different layers of materials namely the subgrade, sub-base, concrete and in some cases a slip membrane. The slab on grade has two main functions: firstly it has to withstand the operational loads applied to the floor, and secondly, it must provide a suitable wearing surface for safe and efficient operations (Labib & Eden, 2004). In the designing stages the thickness, degree of shrinkage, desired use, levelness and the flatness of the slab must be kept under consideration (Marais & Perrie, 1993).

To construct the slabs on grade, different construction methods have been designed. They are based on the construction time, the amount of joints used and cost and purpose of the slab (Marais & Perrie, 2000). In the construction stage, adequate reinforcements must be provided to control the extent and size of cracks. This extent of the reinforcement varies for different slabs on grade depending on the preferred use of the slab (Labib & Eden, 2004). As stated before, the occurrence of cracking in concrete floors is due to the tensile stress in the slab exceeding the tensile strength of the concrete. The high tensile stress is caused by the restraint of the long-term drying shrinkage, as discussed in Chapter 2. These types of cracks have no structural significance, but they do lower the serviceability and aesthetic value of the structure. The dilemma of designing for restrained shrinkage cracking is the vast amount of factors that can influence the extent of the shrinkage. These factors include the w/c ratio, the aggregate size and the curing process of the concrete after casting (Technical Report No. 34, 2003).

Drying shrinkage cracks are found in almost all concrete structures if the formation of these types of cracks is not prevented. To simplify this study, only the drying shrinkage cracking in slabs on grade and the effect of polypropylene fibres on this type of shrinkage are

discussed. This is not an easy task as a specific floor is subject to a unique set of environmental exposures. The subgrade, sub-base and construction methods of the slabs-on-grade must also be taken into consideration to mitigate the effect of drying shrinkage. The listed aspects are discussed in this chapter.

3.1. CONSTRUCTION METHODS

Popularly used slab on grade construction codes specify five well known floor construction methods, namely: large area construction with joints, large area construction without joints, long strip construction, wide bay construction, and two-layer construction.

The large area construction method is the most commonly used method and is specifically used to construct areas which allow free movement of loading traffic for the floor. This method enables large amounts of square meter floor to be laid in a continuous operation. With this method the edges are covered with fixed forms at intervals of 50 m. The concrete is then placed into this area and levelled either manually by using a target staff and a laser level transmitter, or through the direct control of laser-guided spreading machines. After laying and finishing the floor, restrained movement joints are sawn into the slab, dividing the large area into smaller, more controlled areas. The joints help to relieve stress in the concrete that formed due to drying shrinkage. Commonly these areas are a six by six meter grid, but can be changed by the designer. Free movement joints of 5 mm are used at the edges of each area (Technical Report No. 34, 2003).

The large area construction without joints is similar to the large area construction method described above, with the exception that no joints are cut into the slab. In this method, crack control is dependent on reinforcement such as steel bars or fibres that can be used to minimize cracking. However this does not guarantee that cracks will not form (Technical Report No. 34, 2003).

The long strip construction method is similar to large area construction with joints, except that the floor is typically laid in strips of four to six meters wide. The sides of the strips are covered with formwork and the strips are casted in a continuous operation. Joints are sawn diagonally across the strip after the concrete has hardened to help with longitudinal

shrinkage. These 5 mm free movement joints are made, at the widest, 6m apart, similar to that of the large area constructions method (Technical Report No. 34, 2003).

The wide bay construction method is similar to the large area construction method without joints, but instead of a six by six meter grid a twelve to fifteen meter grid can be used. These larger widths allows for ‘bump cutting’ techniques on the surface of the slab (Technical Report No. 34, 2003).

Lastly, the two-layer construction method refers to the use of a secondary layer on top of the hardened slab. These layers are placed between screed rails spaced four meters apart. This construction method is very complex and mostly used for perfectly flat floors as the secondary layer almost acts as a levelling screed (Technical Report No. 34, 2003).

For the purpose of this study only the large area construction method with joints will be used since the study investigates the effect of polypropylene fibre reinforced concrete on the dimensions of saw cut joints.

3.2. SUBGRADE AND SUB-BASE

The layers under the concrete slab are almost as important as the slab itself. The whole weight of the slab, as well as the imposed loads on the slab, is carried by these layers. The subgrade and sub-base is not the focus of the study, but they will be discussed since they have an effect on the shrinkage strain in the concrete slab.

As mentioned before, the friction between the sub-base and the concrete slab must be kept at a minimum, because the magnitude of this friction directly influences the restraint against shrinkage, resulting in cracks. Before this is explained a short overview of the subgrade and sub-base is given.

The subgrade is the natural ground under the slab. The soil of the subgrade should have a specified grading and must be compacted to the degree specified by the designer of the slab on grade. The subgrade differs with each design, with respect to its specific requirements of the slab and the type of soil found in the surrounding areas. The Bates Roads Test demonstrates that the subgrade does not carry high pressure under concentrated loads on the

concrete slab, meaning that the subgrade does not have to be very strong (Marais & Perrie, 2000). The reason for this is because of the rigidity of the concrete slab. What is important is the uniformity of the subgrade. Hard and soft areas must not be present and the upper layer of the subgrade must be of uniform material and density (Marais & Perrie, 2000). For design purposes the strength of the subgrade is given in terms of the modulus of subgrade reaction, k , representing the load per unit area causing unit deflection. This modulus of subgrade reaction is equivalent to stiffness in the normal direction of the subgrade (Technical Report No. 34, 2003).

The sub-base is known as a relatively thin layer between the subgrade and the slab and acts as an interface between these two parts. In normal construction circumstances, a proper classification of the soil can be made according to ASTM D 2487 – 06 showing all the problem areas in the soil (Marais & Perrie, 2000). The main purpose of the sub-base is to provide a platform for the construction activities, provide a level platform for the slab, and to transfer loads to the subgrade. If the subbase is made from granular material it must have a minimum thickness of 150mm. A slip member can also be added between the soil and the concrete to eliminate the friction that can restrain the movement in the slab which could result in cracks (Technical Report No. 34, 2003). The type of material used as a slip member is dependent on the intensity of the friction coefficient of that material. The focus of this study is the friction coefficient between the slab and the sub-base.

3.3. FRICTION BETWEEN THE SOIL AND THE CONCRETE

As stated above, the amount of friction between the top of the sub-base and the slab can influence the extent of the tensile stresses in the concrete, formed by the drying shrinkage. The friction occurs between the soil and concrete, creating restraint in the opposite direction of the movement in the concrete. This can be seen in the top diagram of Figure 3.1.

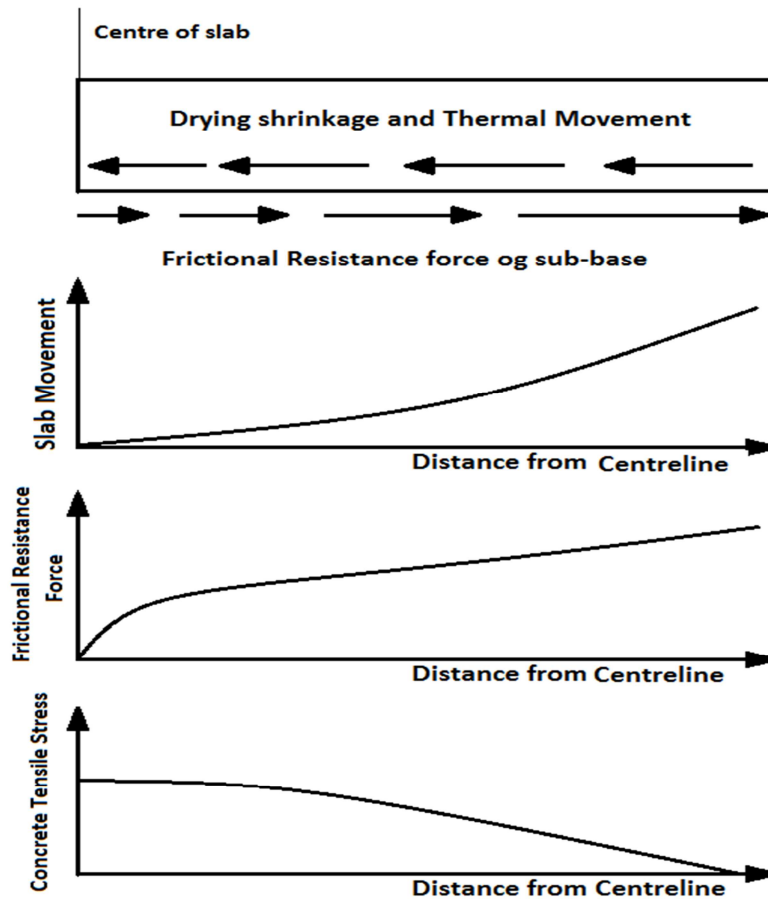


Figure 3.1: The effect of slab movement and frictional forces on the tensile stresses in concrete slabs (Lee, 2001).

Figure 3.1 explains that when shrinkage takes place the movement of the slab is larger at the ends and it gradually decreases towards the centre of the slab. The friction force between the concrete and the soil is created by the movement of the sliding concrete over the soil. This friction is in the opposite direction to the movement of the concrete, and increases from the centre of the slab to the outer edge where the movement is the largest. This results in a high tensile stress at the centre of the slab that decreases to zero at the edges (Lee, 2001). With a higher friction coefficient a large stress development occurs resulting in cracks when the stress is equal or larger than the tensile strength of the concrete.

To define the friction force between the soil and the concrete a thin interface is assumed. This interface only models the shear action (shear stiffness) on the interface. The interface is based on the Coulomb criterion that is used to distinguish between elastic behaviour (small displacements) and plastic behaviour (slip). Equation 3.1 can be used to calculate the shear

stress, τ , at the point of slip on the interface. If the applied shear force is less than the shear stress, τ , then elastic behaviour is assumed and no slip takes place.

$$\tau = c' + \sigma_1 \tan \phi \quad (3.1)$$

Where c' is the cohesion of the interface, σ_1 is the normal stress applied in the vertical direction, ϕ is the friction angle of shear resistance.

The cohesion of friction, c' , is defined as the shearing force, F_s , that is required to initiate the slip between two bodies, divided by the normal force, F_v , between the surfaces of the connecting bodies using (Leonards, 1965):

$$c' = \frac{F_s}{F_v} \quad (3.2)$$

The main influences on the interface behaviour are the interface roughness, the soil density, angularity of the particle and the applied normal stress. The stiffness between rough surfaces can be described as the ratio of the increase in pressure to the decrease in the surface separation. This interfacial stiffness is generated when a pressure load is applied on two connected rough surfaces.

Hu et al. (2004) conducted a Direct Shear box tests to study the mechanical characteristics of the soil-structure interface. The tests showed the two different failure modes of the interface, namely the perfect plastic failure representing a smooth interface and strain localisation representing a rough interface (Hu & Pu, 2004). The roughness between surfaces has a large effect on the type of contact and the friction generated between surfaces. This can be explained with Amontons' law that states that the area, A_0 , of intimate contact between the rough surfaces is a number of orders of magnitudes smaller than that of the apparent surface area A_c . This law explains that the friction between surfaces is independent of A_c , and proportional to the load (Akarapu et al., 2010). The importance of surface roughness has been proven in multiple studies (Hryciw and Irsyam (1993); Nakamura et al. (1999); and Dove and Jarrett (2002)).

Hu et al. (2004) also designed a finite element model to verify the direct shear box tests that can be used to measure the shear strength of an interface. Similar tests were performed by Leonards (1965), raising the question of how much shear can be transferred from the soil before slip between the two surfaces will occur. His study was focused on the dynamic friction (very rapid forces applied to test a sample for a duration of a millisecond or less), but

as a control, Leonards looked at the static friction (force applied over five minutes) between two materials. The friction between the concrete and the soil in slabs on grade is of a static nature, as the force applied by the drying shrinkage takes place over a long period of time. Leonards found an average friction coefficient between a high grade soil and rough mortar to be 0.58.

The most common way of testing the friction on the interface is by using the Direct Shear Box test (DSB) that provides one with the friction angle for designing geotechnical structures. The test was designed to determine the friction between soil-to-soil and soil-to-rock, but has proven to be useful in understanding the behaviour between soil and concrete. The friction behaviour is also useful in determining parameters that are used in modelling the interface response as discussed in Section 3.6.3.

Early shear behaviours between soil and structure materials were tested by Potyondy (1961), Clough & Duncan (1971) and Peterson et al. (1976). All of the above used a modified Direct Shear Box with a half concrete, half soil test sample with the concrete at the bottom. A normal pressure was added to the specimen followed by the shearing of the interface to a maximum displacement of 12.5mm (Gomez et al., 1999).

Gomez et al. (1999) focused on the report by Peterson et al. (1976) that stipulated that the hyperbolic formulation by Clough and Duncan (1971) was accurate for modelling the behaviour under constant normal stress and monotonic shear. A formulation was formed that can derive a set of parameters that can be used in soil-to-structure analyses.

One of the advantages of the Direct Shear box is that it is widely available and has an easy testing procedure. A limitation with the DSB is that the sliding displacement cannot be measured directly as this displacement includes the deformation of the soil due to the shear force applied (Kishida and Uesugi, 1987). Other test methods, like the Direct Simple Shear device and the Large Displacement Shear Box, were designed to overcome these limitations (Uesugi & Kishida, 1987).

3.4. JOINTS

An ideal floor would be free of joints and perfectly flat, but due to the limits on the dimensional accuracy of any construction and imperfect material characteristics, a joint free flat floor is difficult to construct. There is also a limitation on the area of floor that can be constructed within the required time frame. For these reasons joints need to be added to the concrete floor. The joints will help to minimise the formation of cracks, divide construction into parts and help improve quality control on site. Joints can be planned and the expected result can be estimated to some extent before construction.

Joints can be made with two methods namely: sawing or forming with formwork. Sawn joints are more durable and have a smaller joint width than formed joints. The joint width, levelness across joints, stability of joint edges and the joint sealants must be considered when deciding on a type of joint and designing the spacing between the joints. There are a large number of joint types used in slabs on grade namely: free movement joints/construction joints, restrained movement joints, tied joints and isolation joints (Technical Report No. 34, 2003).

3.4.1. RESTRAINED MOVEMENT JOINT

The restrained movement joints are used to allow limited movement to relieve the shrinkage stress with reinforcement across the joints. Restrained joints can be sawn or formed (Technical Report No. 34, 2003). The sawn restrained movement joint is shown in Figure 3.2 and the formed restrained movement joint in Figure 3.3. The type of rebar can be smooth or threaded, depending on the intensity of the restraint required.

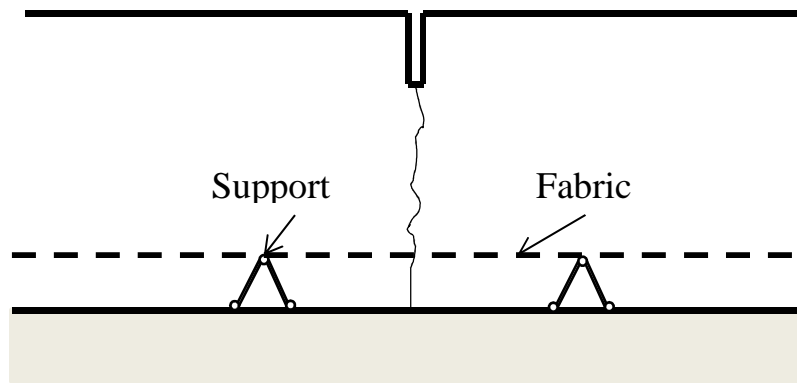


Figure 3.2: Sawn restrained movement joint (Technical Report No. 34, 2003)

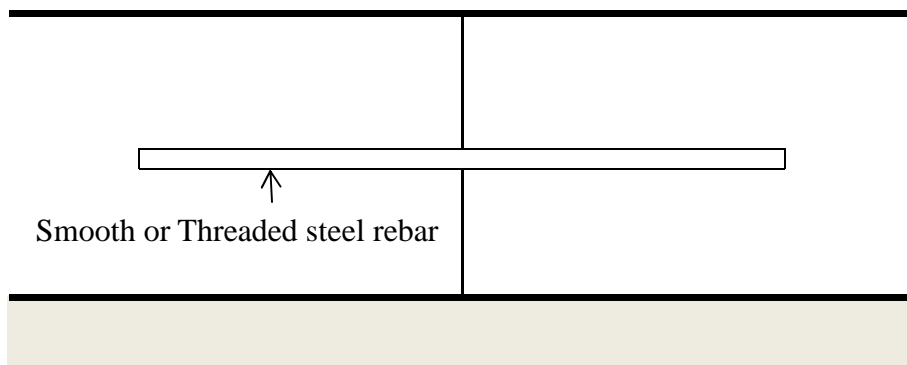


Figure 3.3: Formed restrained movement joints (Technical Report No. 34, 2003)

3.4.2. TIED JOINT

When tied joints are used it is possible to allow for breaks in the construction process. Steel reinforcement with a greater tensile strength than the tensile capacity of the concrete, is placed high over the cross section area to prevent the forming of a joint opening (Technical Report No. 34, 2003). Figure 3.4 shows the tied joint.

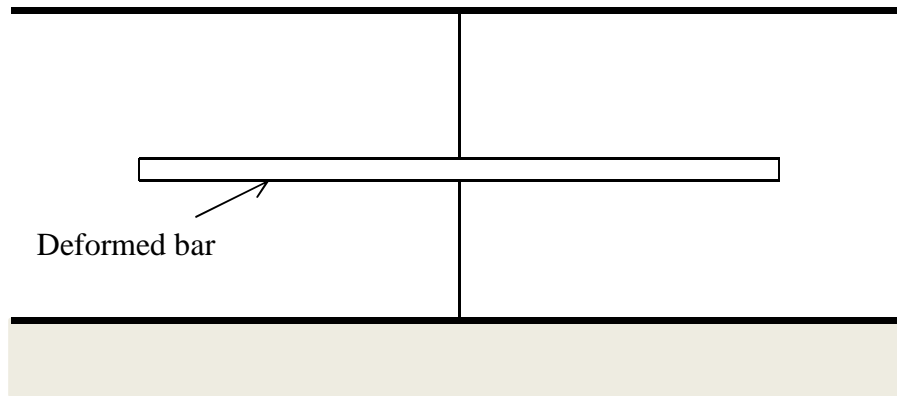


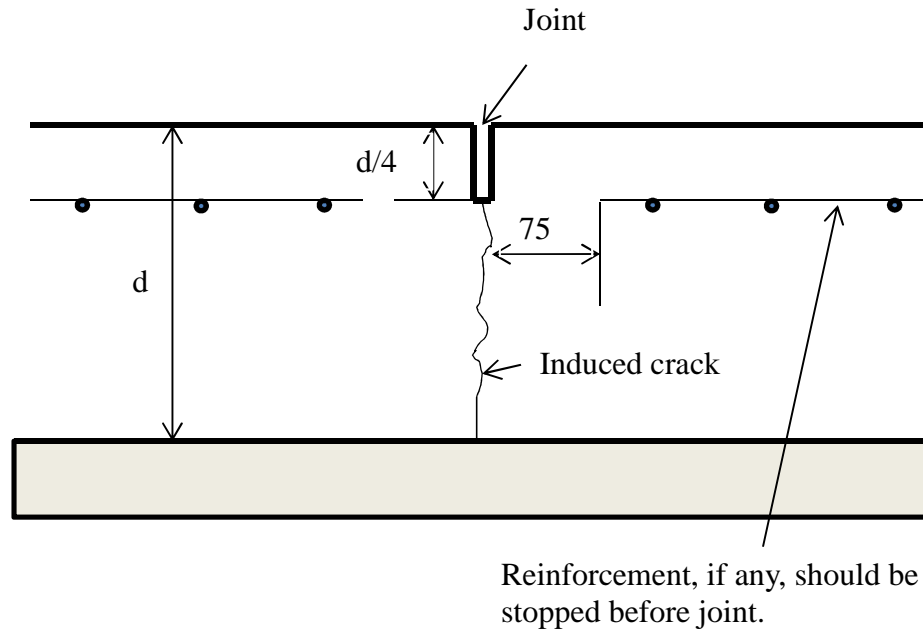
Figure 3.4: Tied joint (Technical Report No. 34, 2003)

3.4.3. ISOLATION JOINT

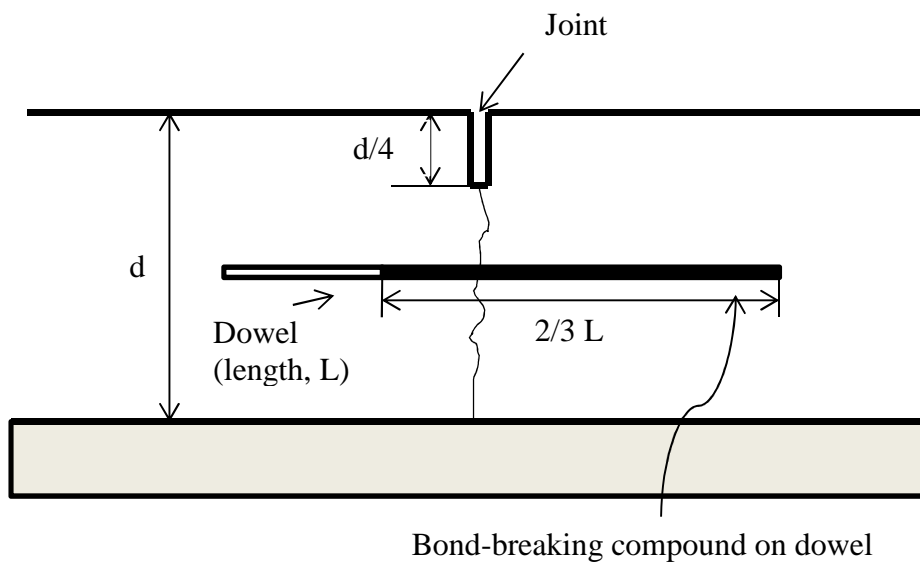
Isolation joints are used to prevent the slab from being restrained by fixed elements such as columns and walls. Compressible filler can be used to prevent the movement of the slab towards a fixed element (Technical Report No. 34, 2003).

3.4.4. FREE MOVEMENT JOINT/CONSTRUCTION JOINT

Free movement joints are designed to have little restraint on horizontal movement caused by drying shrinkage or temperature changes, while restricting the vertical movement in the slab (Marais & Perrie, 2000). In free movement joints there is no reinforcement across the joints and dowels, and dowel-sleeves are designed to minimise the vertical movement and can be used for load transference in the slab. The joint with and without dowels can be seen in Figure 3.5.



a) Undowelled joint



b) Dowelled joint

Figure 3.5: Details of typical free movement joints (a) un-dowelled joint, (b) dowelled joint.

(Technical Report No. 34, 2003)

Free movement joints can be sawn or formed but only sawn joints will be considered from here on. Sawn joints are usually cut with a 3 to 4 mm wide blade. The joints are cut soon after the concrete has hardened, which is usually 24 hours after casting. Earlier cutting is preferable since an increase in hardening time results in an increase in the cut depth. This

causes reduced aggregate interlocking and related load-transfer capacities. After cutting the joint, the open space between slabs is 4 to 5 mm in width and is cut to a depth of at least one quarter of the depth of the slab. This cut will form a line of weakness in the slab, which forces the concrete to first crack below the cut. Load transferring dowels must be set into position in dowel cages before the concrete is casted to prevent steel crossing the joint cut. The dowels should be placed horizontally and perpendicular to the joint line and should not be moved in the casting process. One of the reasons for adding fibres to the concrete is to determine whether it is possible to add fewer joints to a slab, making the construction process easier, and minimizing the quality control needed on site (Technical Report No. 34, 2003).

Contraction joints relieve the stresses responsible for cracking by allowing horizontal movement in the slab. The joints are spaced either 4.5 m or thirty times the thickness of the slab apart, whichever is the least (Marais & Perrie, 2000). The ACI 360 states that the spacing between joints can be up to 5.5 m for unreinforced slabs (ACI Committee 360, 2006).

Kelley (1939) and Walker and Holland (1999) have proven the behaviour where the warping stress in a slab - the stress created in a slab due to the deviation of a slab's surface from its original shape caused mainly by differential shrinkage - only increases up to a certain length, called the critical slab length. The length is measured diagonally from corner to corner and is dependent on the thickness of the slab, the temperature gradient, the modulus of sub-grade reaction and the modulus of elasticity. These sources indicate that the critical length will only slightly change if the modulus of elasticity and the modulus of sub-grade reaction change (ACI Committee 360, 2006).

Although the use of joints reduces the formation of cracks and helps to divide the construction process into controllable parts, it does have the disadvantage of being labour intensive, time consuming and unsightly. The use of macro polypropylene fibres in slabs on grade is investigated in the report to overcome the disadvantages of joints.

3.5. MODELLING OF CONCRETE SLABS ON GRADE

One of the first models used to analyse concrete slabs was based on the Westergaard's approach that was designed to study plain concrete beams and slabs supported on elastic fields such as soil. His approach to designing slabs is based on the elasticity theory. The disadvantage of the Westergaard's approach is that it assumes that the concrete is always in an elastic state, resulting in failure at the point of initial cracking (Barros & Figueiras, 2011). Today the use of Westergaard's approach can be seen in design guides such as *Concrete Industrial Floors on the Ground* by Marais and Perrie (1993). An improved approach is the Yield-Line theory that assumes that concrete cracks do occur. The Yield-line theory assumes plastic deformation which can better describe the behaviour of slabs on grade, particularly if fibres are used to reinforce the concrete. A design guide that uses the Yield-Line theory is the *Concrete Industrial Ground Floors, Technical Report No. 34* (Technical Report No. 34, 2003). In this section, the basic concept of modelling concrete and slabs on grade will be discussed and a Yield-Line theory approach is used. This section also discusses the modelling of hardened concrete referring to the multi-directional fixed crack model that can be used to model the cracking behaviour of the concrete. The modelling of the interface between the concrete and the soil is also discussed.

3.5.1. MODELLING OF HARDENED CONCRETE

The term conventional concrete in this text refers to concrete without reinforcement such as steel or fibres. Conventional, and in some cases reinforced concrete, is known as a brittle or quasi-brittle material. This material can be modelled in terms of tensile cracking and compressive crushing (TNO DIANA Material Lib, 2012). Before the concrete undergoes cracking the concrete is seen as an isotropic linear elastic material (Rots, 1988). This assumption simplifies the modelling of plain uncracked concrete since the only required parameters are the Young's modulus, E , and the Poisson's ratio, ν . Parameters such as the thermal expansion coefficient, α , and the concentration expansion coefficient, γ , can also be added, but to simplify the behaviour of concrete these parameters will not be discussed.

For isotropic linear elastic materials the stress strain relationship can be expressed by using:

$$d\sigma = D * d\varepsilon \quad (3.3)$$

D represents the material stiffness matrix for plane stress:

$$D = \frac{E}{(1-\nu^2)} \begin{bmatrix} 1 & \nu & 0 \\ \nu & 1 & 0 \\ 0 & 0 & \frac{1-\nu}{2} \end{bmatrix} \quad (3.4)$$

Conventional concrete has the tendency to crack when in tension resulting in nonlinear elastic behaviour. The tension is usually due to restrained shrinkage in the concrete. To model this behaviour, more parameters such as the tensile strength, f_t , of the concrete, the Mode-I fracture energy, G_f^I , the Mode-II fracture energy and mean compressive strength, f_{cm} , are required. The behaviour of the concrete after cracking can be indicated with strain softening or hardening curves that can be calculated using the fracture energy. The curves are discussed in the next section.

To replicate the shrinkage in the concrete model an elasticity-based crack model can be used, taking into account the temperature, concentration or the maturity of the concrete. The desired shrinkage strains are manually given as discrete shrinkage functions, based on the age of the element at a time equal to zero and the shrinkage at that age.

When fibres are added to the concrete the behaviour of cracking in the concrete will no longer be brittle, but there is no model that can accurately predict how the FRC will crack since the fibres are distributed at random. When the concrete is reinforced with fibres, the material properties of the concrete change as explained in Chapter 2. To account for these changes certain material properties of the conventional concrete must be changed to that of PPFRC. These parameters are the fracture energy, G_f , of the concrete, the tensile strength, f_t , and the shape and type of strain softening curve that was used.

DIANA has the Total Strain concept that implements a multi-linear softening curve. A total strain crack model will be used to model the crack behaviour, and the tensile behaviour in the concrete that is related to the crack bandwidth is modelled as a Smeared Crack Model, (SCM), will be explained later in this chapter. The SCM will identify the weakest spots in the concrete and will create a crack as soon as the tensile capacity of the concrete at that point is reached. The saw cut joints will act as the first weak spots and cracks are expected to form under these joints. As the joints are placed further apart, the tensile stress will increase to the

centre of the slab and secondary cracks are expected to form. The behaviour of the cracks in a FEM analysis is discussed in the following section.

3.5.2. MULTI-DIRECTIONAL FIXED CRACK MODEL

When using the smeared crack concept, the cracked solid can be seen as a continuum instead of the discrete-crack concept that is geometrically discontinuous (Rots, 1988). The cracking of concrete is modelled with a multi-directional fixed crack model with nonlinear tension softening, shear retention and tension cut-off (TNO DIANA Material Lib, 2012). The concept of smeared cracking was introduced by Litton (1974) and has since been used for crack modelling in hardened concrete.

The fundamental feature of the smeared crack model is the division (break down) of the total strain into the elastic strain increment between the cracks, ε^e , and the strain in the fracture zone of the concrete, ε^{cr} , by using:

$$\varepsilon = \varepsilon^e + \varepsilon^{cr} \quad (3.5)$$

Where ε is the total strain, ε^e is the elastic strain and, ε^{cr} is the crack strain.

This breakdown of the total strain creates the opportunity for combining the decomposed crack model with the plastic behaviour of the concrete. The separating of the crack strain from the elastic strain allows for modelling of a number of cracks simultaneously. With the multi-directional fixed crack concept the stress and strain of the crack is in the local ($n-t$) coordinate system that is aligned with each crack as it occurs (see Figure 3.6) (TNO DIANA Material Lib, 2012).

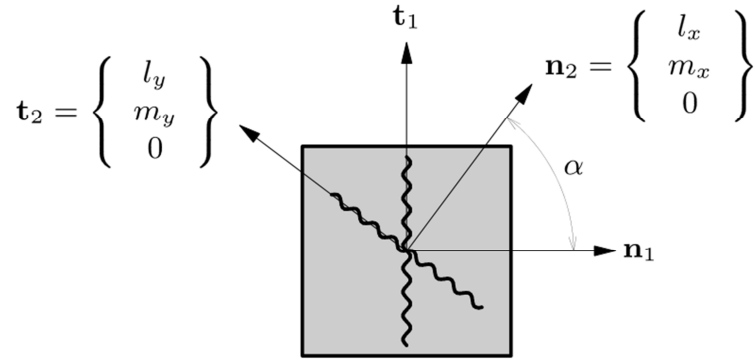


Figure 3.6: Multi-directional fixed crack model (TNO DIANA material library)

All the individual crack strains can then be assembled in a vector denoted by e^{cr} , and this yields

$$e^{cr} = \langle e_1^{cr}, e_2^{cr}, \dots, e_i^{cr}, \dots, e_n^{cr} \rangle^T \quad (3.6)$$

The local vectors of the cracks are then transformed to the global strain

$$\varepsilon^{cr} = N e^{cr} \quad (3.7)$$

where N is the transformation matrix, consisting of all the transformation matrixes of all the occurring cracks given, by using:

$$N = [N_1, N_2, \dots, N_i, \dots, N_n] \quad (3.8)$$

The crack stresses can be transformed in a similar manner and is then given as a function of the crack strain:

$$s^{cr} = f(e^{cr}) \quad (3.9)$$

where s^{cr} is the stress at the crack

As a crack forms, its constitutive model is complete if the relationship in Equation 3.9 is defined. A crack can only form when two conditions are satisfied. Firstly there is the stress cut-off criterion that states that the crack can only form if the principle tensile stress exceeds the maximum stress in the concrete. Secondly, the angle between a present crack and the principal tensile stress should be greater than the threshold angle α_{TD} . Both these conditions must be satisfied before a crack is successfully simulated.

The f in Equation 3.9 represents the crack material stiffness matrix in the following form:

$$f = \begin{bmatrix} D_I^{cr} & 0 \\ 0 & D_{II}^{cr} \end{bmatrix} \quad (3.10)$$

where D_I^{cr} is the Mode I stiffness modulus and D_{II}^{cr} the Mode II stiffness modulus of a crack (TNO DIANA Material Lib, 2012).

D_I^{cr} is characterized by the four fracture parameters of the concrete: the tensile stress, f_t , the fracture energy, G_f , the shape of the softening branch, and the crack bandwidth, h_1 (Barros J. , 1999).

There are a few tension softening models that can be used to define the behaviour of concrete. Firstly there is the brittle tension behaviour (see Figure 3.7(a)) illustrating the behaviour of a clean break without any residual tension after cracking. Figure 3.7(b) shows the linear tension softening and Figure 3.7(d) and 3.7(e) illustrates an exponential nonlinear decrease in tension after cracking. Barros (1999) shows that the bilinear tension softening model (see Figure 3.7(c)) represents the tensile behaviour of steel fibre reinforced concrete (SFRC) the best. In Figure 3.7 ϵ_n refers to the strain in the concrete. Similar shapes have been found for the tensile behaviour of polypropylene fibre reinforced concrete in research done by Van der Westhuizen (2013). The ultimate strain, ϵ_u^{cr} , seen in Figure 3.4(c), representing the bilinear behaviour, is calculated by using:

$$\epsilon_u^{cr} = \frac{2G_f}{f_t h_1} \quad (3.11)$$

where G_f is the fracture energy, h_1 is the crack bandwidth (square root of the area of the element), f_t the tensile strength of the concrete.

The crack bandwidth for two dimensional elements is equal to:

$$h = \sqrt{A_1} \quad (3.12)$$

where A_1 is the total area of the element

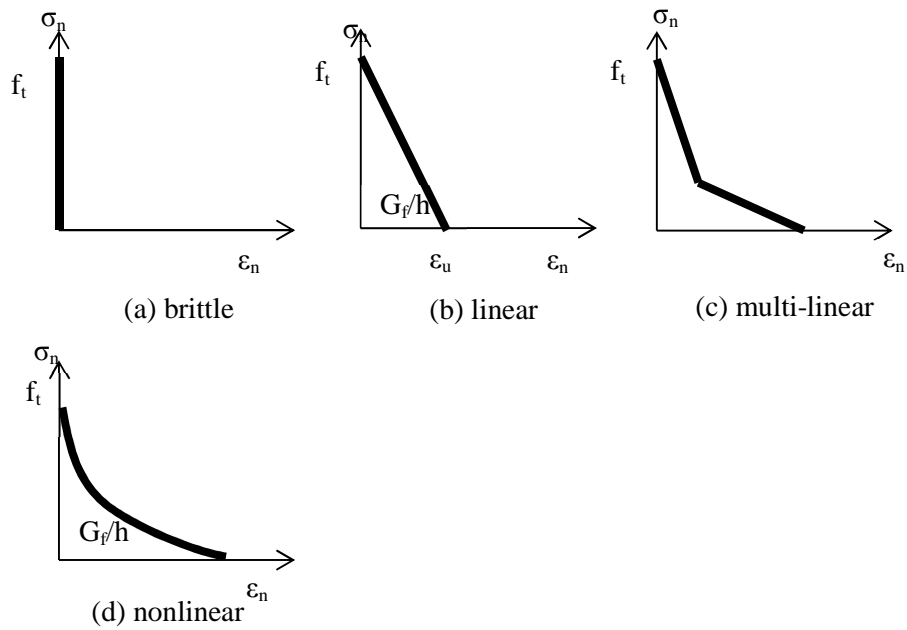


Figure 3.7: Tension softening-multi-directional fixed crack model (TNO DIANA material lib, 2012)

Two forms of tension cut-off are available in DIANA. Firstly, there is constant tension cut-off, which refers to when a crack forms if the major principal tensile stress is exceeded (see Figure 3.8(a)). Secondly, linear tension cut-off which refers to the crack forms when the minimum of the tensile force or $f_t(1+\sigma_{lateral}/f_c)$ is exceeded as seen in Figure 3.8(b) (TNO DIANA Material Lib, 2012). The f_c refers to the compression strength of the concrete and the f_t refers to the tensile strength of the concrete. The σ_1 and σ_2 is the stress in the concrete in the x and the y direction.

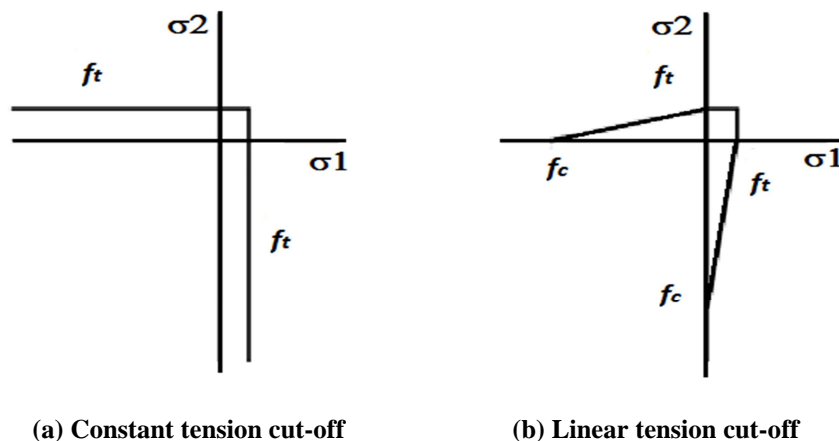


Figure 3.8: The tension cut-off in two-dimensional principal stress space as used in software (TNO DIANA material lib, 2012)

The shear retention of the crack can be either full retention or constant retention. In full shear retention the shear modulus, G , is not reduced which implies that the secant crack shear stiffness, $D_{\text{secant}}^{\text{II}}$, is infinite. In the constant shear retention the shear modulus is reduced by a β factor using: (TNO DIANA Material Lib, 2012)

$$D_{\text{secant}}^{\text{II}} = \frac{\beta}{1-\beta} G \quad (3.13)$$

where β is a reduction factor.

3.5.3. MODELLING THE INTERFACE BETWEEN THE SOIL AND THE CONCRETE.

In the interaction between soil and structure, relative movement of the structure on the soil can be expected. To model this movement an interface is used between the two materials and it consists of interface elements seen in Figure 3.9. This interface can allow differential movement like slip and gap openings to be formed. A method of using zero-thickness interface elements is used (TNO DIANA, 2012).

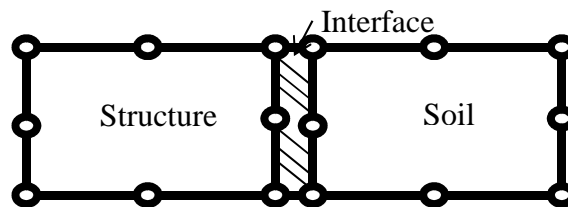


Figure 3.9: Interface elements (TNO DIANA material lib, 2012)

The interface yield stress is determined by the Mohr-Coulomb criterion (Duncan & Clough, 1971) as discussed in Section 3.4, explaining the interface strength. To model the interface between the soil and the concrete, Mohr-Coulomb Friction criteria is used. The interface is defined by the normal end shear displacement across the interface given in Equation 3.14 with the elasticity matrix in Equation 3.15:

$$t = (t_n, t_t)^T \quad (3.14)$$

$$D_{el} = \begin{bmatrix} K_n & 0 \\ 0 & K_t \end{bmatrix} \quad (3.15)$$

The interface between the soil and the concrete undergoes an elastic shearing response with a no-tension state in n and t directions indicated with t_n and t_t . Figure 3.10 illustrates the Coulomb friction criterion.

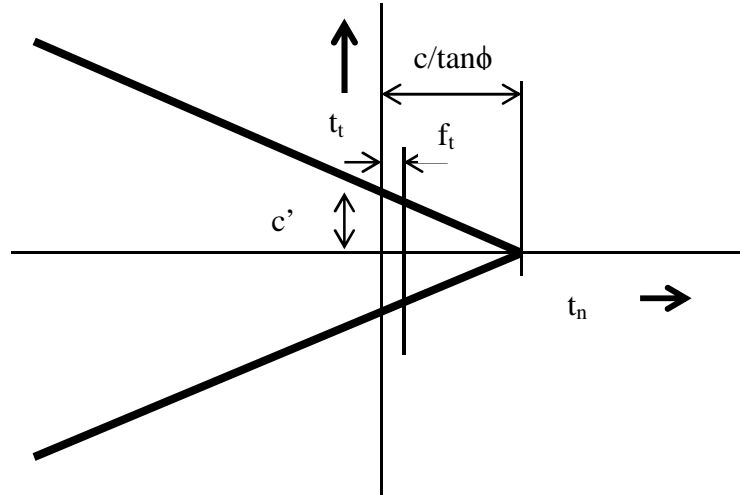


Figure 3.10: The Coulomb friction criterion. Where c is the cohesion, ϕ is the friction angle and ψ is the dilatancy angle. (TNO DIANA material lib, 2012)

The surface between the soil and the concrete can be seen as fully bonded (rough interface) and this influences the friction between the surfaces. To model the roughness a value for the strength reduction factor of the interface is required. This value is dependent on the interface strength and the soil strength which is determined by using the friction angle and the cohesion that can be determined by using the Direct Shear Box test (Arslan, 2005).

The interface element can be seen as zero-thickness element consisting of four-nodes. The constitutive law for interface elements consists of the shear stiffness, and the normal stiffness. These stiffness's are used in the elasticity matrix in Equation 3.15 and can be calculated by using:

$$k_n = \frac{\sigma_n}{\Delta_n} \quad (3.16)$$

$$k_s = \frac{\tau}{\Delta_s} \quad (3.17)$$

where k_n is the normal stiffness, Δ_n is displacement normal to interface, σ_n is normal stress acting on the interface, k_s is the shear stiffness, Δ_s is displacement along the interface and, τ is shear stress acting on the interface.

To avoid overlapping of elements in compression, a large normal stiffness is required and the reverse is applicable for elements in tension which minimises the stresses in the interface.

To calculate the interface stiffness, if the stress and displacement is unknown, the following guideline can be used as given in the TNO DIANA user manual:

$$k_s = \frac{A^2}{t_{\text{inter}}} \frac{E_{\text{soil}}}{2(1+\nu_{\text{soil}})} \quad (3.18)$$

$$k_n = f_\alpha \cdot k_s \quad (3.19)$$

where E_{soil} is the Young's modulus of the sand; ν_{soil} is the Poisson's ratio of the sand; A is a reduction factor to make the interface weaker and more flexible than the soil (range from 0.5 to 1); t_{inter} is the thickness of the interface and; f_α is the multiplication factor (ranging from 10 to 100).

The cohesion and the friction angle can be calculated using:

$$c = A \cdot c_{\text{soil}} \quad (3.20)$$

$$\tan \phi = A \cdot \tan \phi_{\text{soil}} \quad (3.21)$$

where c_{soil} is the cohesion of the soil and ϕ_{soil} is the friction angle of the soil.

The dilatancy is assumed to be zero to avoid unrealistic volumetric strains during shear. The assumption is also made that the tensile stress cannot develop in the interface, resulting in a gap arising as the tensile stress becomes positive within the interface. This is modelled with a tension cut-off criteria and brittle gapping with zero tensile strength, f_t (TNO DIANA, 2012).

3.6. CONCLUDING SUMMARY

The importance of understanding the construction method and type of joint used for a slab on grade is discussed in this chapter. The purpose of the subgrade and sub-base was investigated and the behaviour of the interface between the sub-base and the concrete is explained. The above mentioned aspects of concrete are now used to define the parameters of the concrete when modelled in a FEM analysis. This information will form the basis for the experimental and numerical work in the following chapter.

CHAPTER 4: MATERIAL CHARACTERISTIC STUDY

The experimental work in this report is done in two parts. The first part is an extensive material parameter study to better understand the behaviour of the polypropylene fibre reinforced concrete (PPFRC), compared to conventional concrete. This is done through a series of tests, namely the compressive test, flexural test, wedge splitting test, and shrinkage test, which are all done on beam and cube specimens. The second part of the experimental work is a large scale test shown in Chapter 5. The results of the first part of the experimental work is then used to create a realistic finite element model shown in Chapter 6 that replicates the large scale test. This chapter shows the different material characteristics of PPFRC.

4.1. RESEARCH DESIGN

The material properties of the PPFRC required for the large scale experimental tests and analytical model are the compressive strength, the tensile behaviour, the fracture strength, the friction between the concrete and the soil and the shrinkage of the concrete. Four tests were completed to accumulate all the above mentioned parameters of the desired concrete given in Table 4.1. The compressive strength of the concrete was measured by conducting compressive cube tests, and the fracture energy is determined through results obtained from wedge splitting tests. The tensile and flexural behaviour was determined through three point beam tests. The friction between the soil and the concrete was calculated using Equation 3.18 to 3.21 and the shrinkage is measured with shrinkage tests and compared to the shrinkage calculated with the Model Code (2010) discussed in Section 2.1.4.

A mix with 28 day strength of 50 MPa and a slump of 110 mm was used since high workability was required for the large scale experiments. Although high compression

strength of the concrete is not usually required for slabs on grade, this type of concrete was used in this study because of its higher level of shrinkage. A high shrinkage in the concrete was a prerequisite of the mix, because the effect of macro polypropylene fibres on the shrinkage in concrete would be more visible if the concrete shrunk extensively. This was achieved with high fines content in the concrete mix, and high water content. The same mix design was used in all tests with the only difference being the fibre dosage that was added to the concrete. The design mix has a w/c ratio of 0.4 as depicted in Table 4.1. There were no admixtures added to the concrete as the use of admixtures could have an unmeasurable effect on the shrinkage. Only one type of cement was used in the mix design of this investigation.

Table 4.1: The designed concrete mix

Materials		RD	kg
Water		1	240
Binder	CEM I 52.5	3	600
Sand	Malmesbury	2.6	675
Stone	6mm	2.6	781

Three different fibre dosages were tested to compare the effect of the performance of the fibres. All the fibres were of the same origin. The fibre dosage for similar fibres that are best suited for industrial slabs on grade was tested by Van Der Westhuizen (2013). For this work 2 kg/m³, 5 kg/m³ and 8 kg/m³ macro polypropylene fibre dosages were chosen. This is also compared to conventional concrete of the same mix design. The properties of the fibres used in this report are given in Table 4.2.

Table 4.2: Properties of the fibre

Fibre Name	Rockstay CXO 50/30
Material	100% virgin polypropylene
Fibre type	Structural synthetic fibre
Use	Concrete reinforcement
Aspect Ratio	50
Fibre Length	30mm
Fibre diameter	0.8mm
Fibre shape	X-shaped
Secondary Anchorage	Non
Colour	Translucent
Fibre density	0.91 g/cm ³
Melting point	160° C
Thermal Conductivity	Low
Breaking strength	400 N/mm ²
Elongation	15% to 25%

4.2. TEST SETUP

4.2.1. COMPRESSIVE TEST

The compressive tests were performed with compliance to SANS 5863:2006. Four test cubes of 100 x 100 x 100 mm were casted for the different fibre dosages as described in Section 4.1 and they were compacted after casting according to SANS 5861-3. All the specimens were de-moulded 24 hours after casting and placed in curing tanks at 25 °C for 28 days. All cubes were weighed and measured before placed in a Contest compression testing machine. The maximum compressive force of each cube was then determined by compressing the cube until breaking point. The compressive strength was calculated by using:

$$f_{cc} = \frac{F}{A_c} \quad (4.1)$$

where f_{cc} is the compressive strength in MPa, F is the maximum load at failure in N, A_c is the cross-sectional area of the specimen on which the compressive force acts in mm².

4.2.2. SHRINKAGE TEST

The shrinkage tests were performed on 100 x 100 x 500 mm beams that rested on rollers to insure even shrinkage on the entire surface area. The specimens were placed next to the large scale test (see Chapter 5). This was done to measure the shrinkage of the concrete in the same environment as the large scale tests. Specimens of mix batches with similar fibre dosages were placed in a temperature controlled room in order to compare them with specimens placed in an uncontrolled environment. The deformation of each specimen was measured with a strain gauge seen in Figure 4.1. This deformation was estimated by measuring the deformation between two steel targets, glued 100 mm apart to the surface of the specimens 24 hours after casting. Figure 4.2 shows the targets that are connected to the specimens with epoxy.



Figure 4.1: The strain gauge

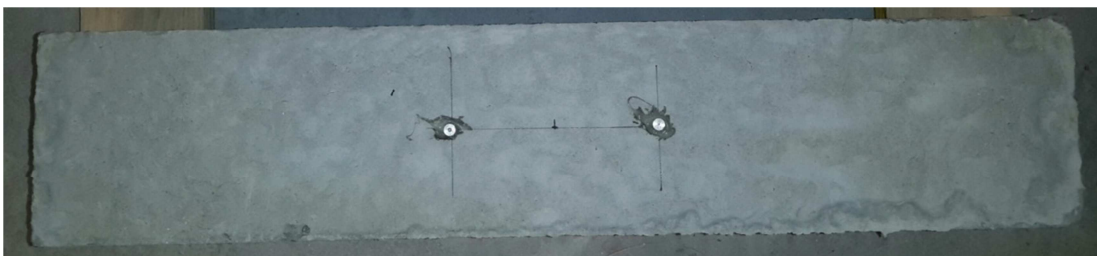


Figure 4.2: The targets used to measure the shrinkage

The shrinkage was determined by:

$$\varepsilon = \frac{L_i - L_0}{L_0} \quad (4.2)$$

where ε is the drying shrinkage strain, L_i is the length at a specific time between the two targets in mm, and L_0 is the initial length between the two targets in mm.

4.2.3. FLEXURAL TEST AND TENSILE BEHAVIOUR

The flexural behaviour was determined by means of a three point beam test using 150 x 150 x 500 mm beams. The test process is based on the EN 14651 (2007) and the three point beam test setup is shown in Figure 4.3 and 4.4. The distance between the axes of the supporting rollers are 450 mm and a centred load is applied at the top of the beam. All tests were conducted after 28 days of curing in a 25° C curing tank. The test specimens were notched 24 hours before testing with a 25 mm deep and 3mm wide notch at the bottom mid-span of the beam. The displacement of the specimens was measured using a steel frame to hold two Linear Variable Differential Transformers, (LVDT) in place. One LVDT should be placed on each side of the beam. A 2 MN Instron Materials Testing Machine that recorded the data at a rate of 5 Hz, was used to conduct the test. The load was increased at a constant displacement rate of 0.2 mm/min up to a deflection of 3.65 mm. Three specimens for each fibre dosage were tested.

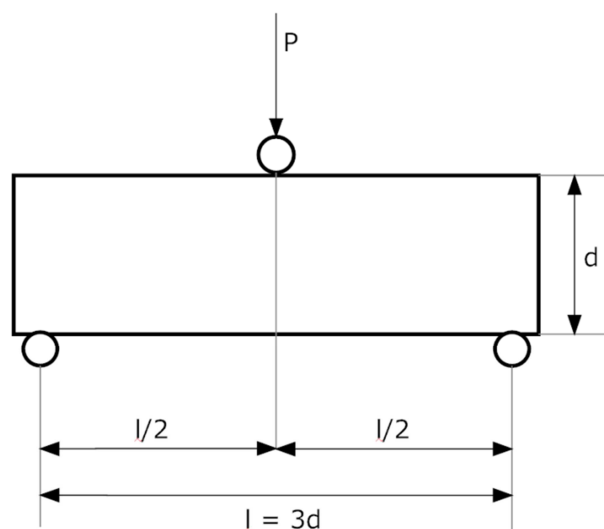


Figure 4.3: The setup for the three point beam test



Figure 4.4: The setup of the LVDT's for the three point beam test

The flexural strength is calculated by using:

$$f_{cf} = \frac{3F \times l}{2b \times d^2} \quad (4.3)$$

where f_{cf} is the flexural stress measured in MPa, F is the maximum load in N, l is the distance between supporting rollers in mm, b is the width of the specimen in mm, and d is the depth of the specimen in mm.

4.2.4. WEDGE SPLITTING TEST

The fracture energy of the fibre reinforced concrete is determined through calculations made from the results of the wedge splitting test (WST). The WST method for autoclaved aerated concrete (AAC) is given by RILEM (International Union of Testing and Research Laboratories for Materials and Structures, 1992) and modified to be used for FRC by Nordcn (2005).

The test was performed on a 100 x 100 mm cube supported on a base plate that differs from the prescribed line support in Figure 4.5. The plate can be seen in Figure 4.6 where the double linear line support is shown. The reason for this is to increase the stability of the test sample since it is not required to balance but can rather rest on the support. Figure 4.5 also

illustrates the loading schematics of the test. The test specimen has a 30 x 25 mm groove that is used to apply the load on the specimen and a 25 mm deep, 3 mm wide starter notch to initiate the crack.

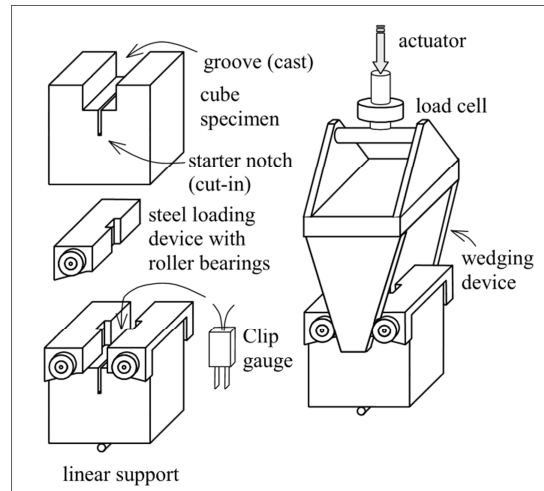


Figure 4.5: WST setup. (Nordcn, 2005)

The test setup applies a vertical compression force, F_v , onto the specimen that is converted into a splitting force, F_{sp} , with the use of the rollers as shown in Figure 4.5. The relationship between the two forces can be calculated by using:

$$F_{sp} = \frac{F_v}{2 \cdot \tan(\alpha_1)} \cdot \frac{1 - \mu \cdot \tan(\alpha_1)}{1 + \mu \cdot \tan(\alpha_1)} \quad (4.4)$$

where F_v is the vertical force applied on the specimen in kN, F_{sp} is the splitting force in kN, and α_1 is the wedge angle in degrees. In the Nordcn code, 15° is prescribed, but due to the lack of lab equipment to cut a 15° angle, an angle of 14° was used ($\alpha_1 = 14^\circ$). The friction coefficient (μ) of the rollers was ignored since the error in not including the friction is small, between 0.4 per cent and 1.9 per cent (Löfgren et al., 2013).



Figure 4.6: Wedge splitting test setup

Three samples of four different fibre dosages were tested and the crack mouth opening displacement (CMOD) and the vertical compressive force, F_v , were obtained. The results were then used to determine the splitting force by using Equation 4.4 and the force-CMOD graphs for each specimen was drawn. These graphs could then be used to calculate the splitting work, W_o , that is equal to the area under the force-CMOD graph. The splitting work is then divided by the area over which the concrete cracks to calculate the fracture energy, G_f , of the specimen as stipulated by Nordcn (2005) by using:

$$G_f = \frac{W_o}{A_{lid}} \quad (4.5)$$

where G_f is the fracture energy in N/m, A_{lid} is the crack area equal to the length of the crack times the width of the specimen in m^2 , and W_o is the splitting work done in N·m.

4.2.5. SIEVE ANALYSIS

A sieve analysis was done in accordance with the SANS 201. The results of the analysis were used to calculate the parameters of the soil supporting the concrete sample. These parameters were then used in the finite element analysis to model the behaviour of the soil. The sieve analysis is used to calculate the fines content of the aggregate. The sieve analysis

was performed with two gradings of natural sand that is locally found in South Africa called Malmesbury sand. The test consists of seven different size sieves. The sieves are stacked from the smallest sieve at the bottom to the largest sieve at the top. A quantity of 500 grams of sand was added to the top sieve after the sand was washed and dried in an oven for 24 hours. The stack of sieves are then shaken for ten minutes on a shaking machine, before each sieve is weighed separately to calculate the quantity of sand retained by the specific sieve size. After the sieve analysis is completed the dust content is calculated by:

$$\frac{(a-b)+c}{M_{Pt}} \times 100 \quad (4.6)$$

where a is the mass of the original test sample in g, b is the mass of the sample after washing in g, c is the mass of the material that passed the 75 µm sieve, M_{Pt} is the mass of the total test sample after sieving.

The fineness modulus is then calculated dividing the sum of the cumulative percentages of the material retained on each sieve by 100, excluding the material on the 75 µm sieve.

The fines content can be calculated by using:

$$\frac{(a-b)}{M_{Pt}} \times 100 \quad (4.7)$$

where a, b and M_{Pt} are defined as above.

4.3. RESULTS

4.3.1. COMPRESSION TEST

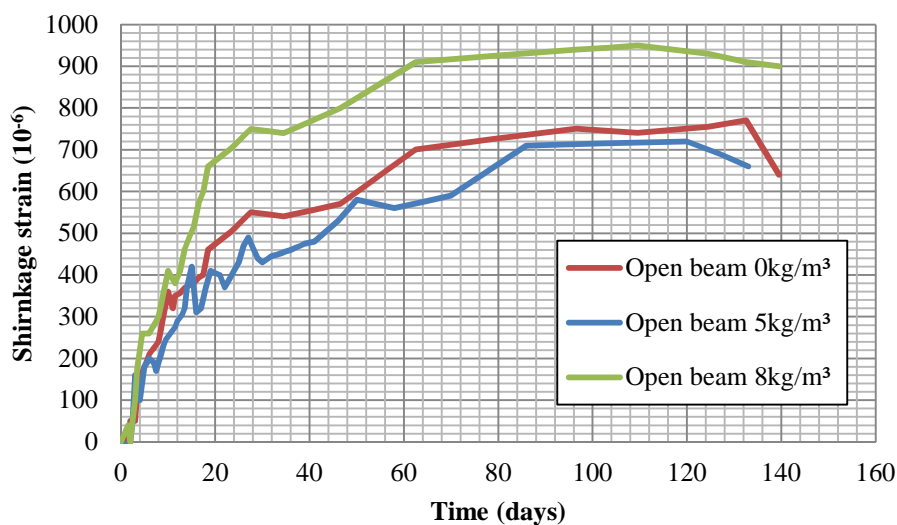
The compression force for test specimens, consisting of the same concrete mix but with different fibre dosages, was determined with the compression test. The fibre dosages used were no fibres, 5kg/m³ and 8 kg/m³ and the results of the test can be seen in Table 4.3. A schematic representation of the results can be seen in Figure 4.7.

Table 4.3: The compressive force for different fibre dosages

Fibre Volume	Density (kg/m ³)	Strength (MPa)
0 kg/m ³	2370	53.46
5 kg/m ³	2349	54.56
8 kg/m ³	2342	57.17

4.3.2. SHRINKAGE TEST

The shrinkage test was executed using the conventional concrete as well as PPFRC containing 5 kg/m³ and 8 kg/m³ fibres. Four test specimens were casted per fibre dosage. The test results can be seen in Figure 4.7 showing the shrinkage of the completely open specimens that were placed on rollers between the large scale tests as discussed in Chapter 5. Figure 4.8 shows the shrinkage results of specimens painted with a waterproofing paint on the bottom and the sides, preventing the evaporation of water from these sides. The function of the waterproofing is to replicate the effect of the soil under the concrete that reduces the effect of moisture loss at the bottom of the slab. Two specimens of each fibre dosage were tested in the same environment as the large scale tests.

**Figure 4.7: The shrinkage test results for open specimens**

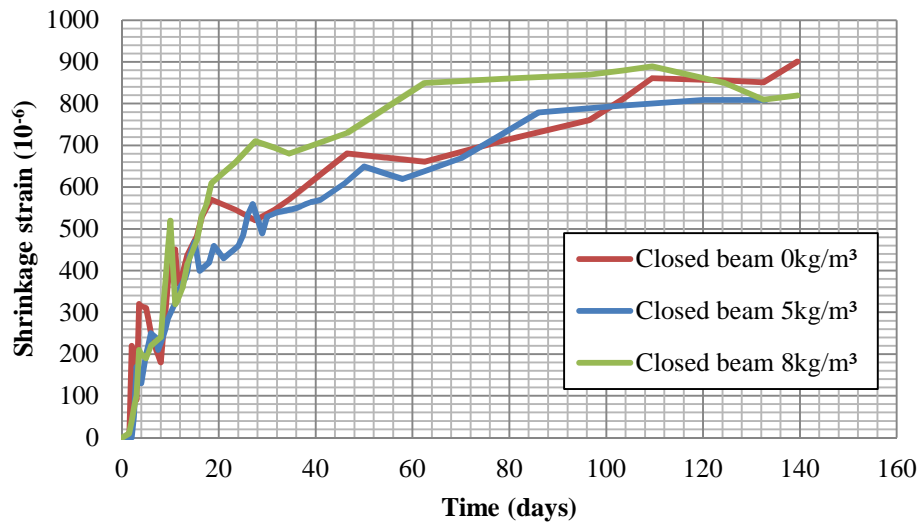


Figure 4.8: The shrinkage test results for the waterproofed beams

Similar specimens to the ones used for the open beams were placed in a temperature controlled room to test the effect of the environment on the drying shrinkage. The results for these tests are given in Figure 4.9.

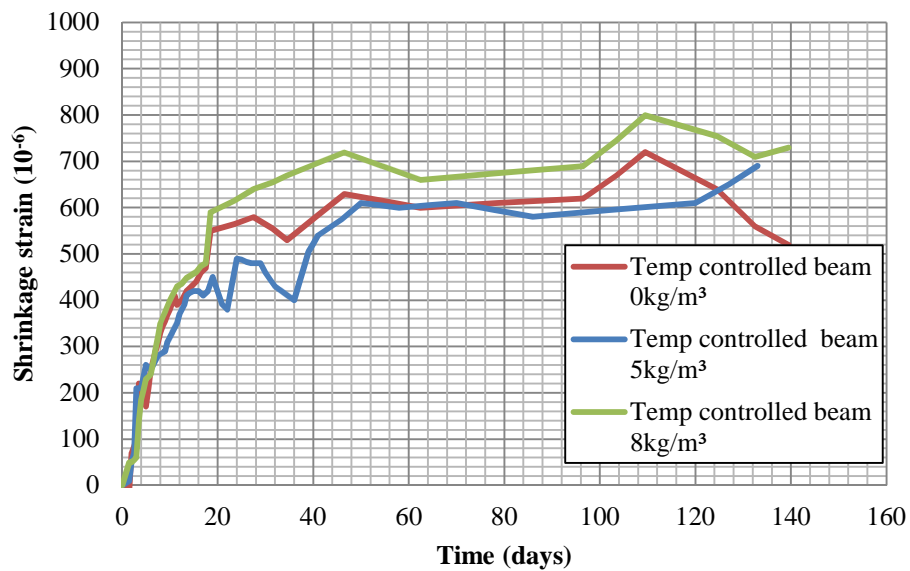


Figure 4.9: The shrinkage test results for beams tested in a temperature controlled room

Figure 4.10 to 4.12 compares the results of the open beam, closed beams and temperature controlled room beams with the same fibre dosage.

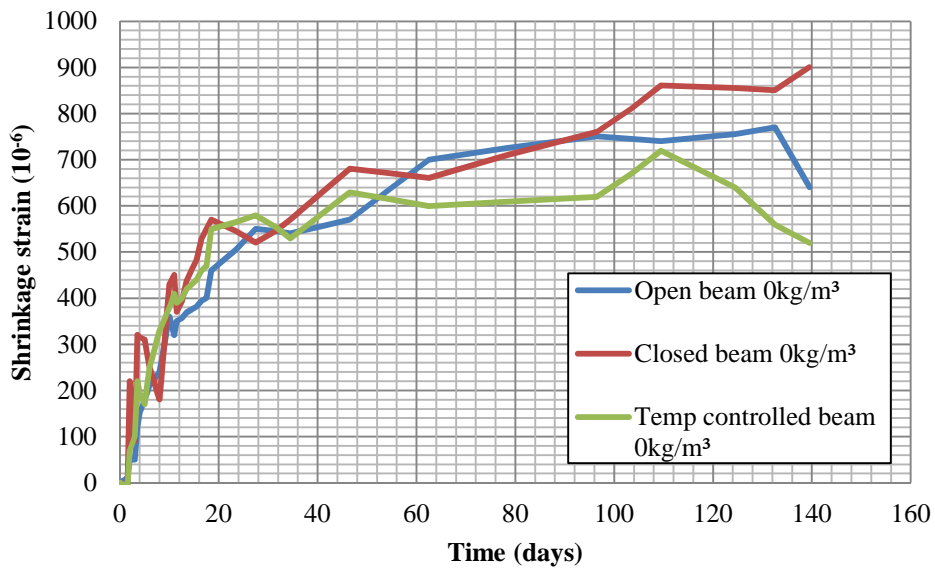


Figure 4.10: The shrinkage test results for beams containing no fibres

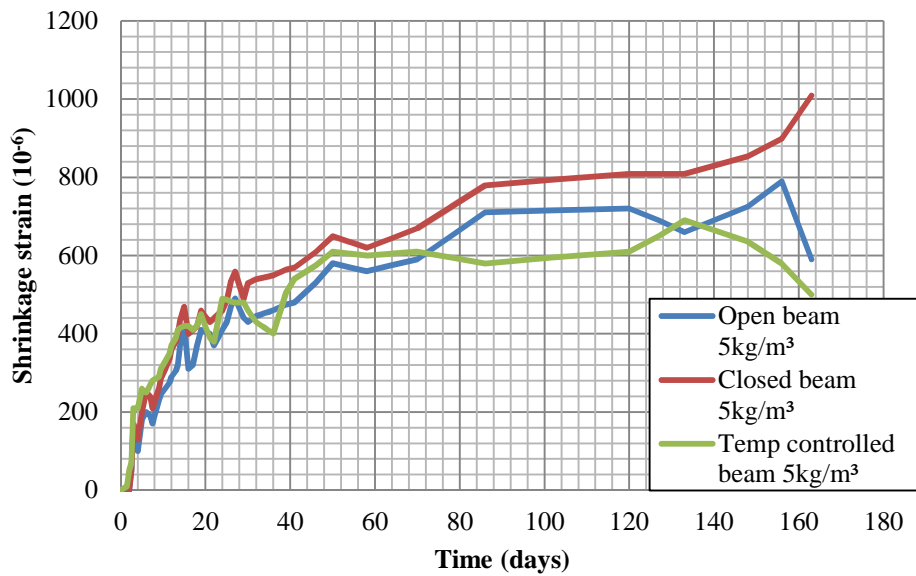


Figure 4.11: The shrinkage test results for beams containing 5kg/m^3 fibres

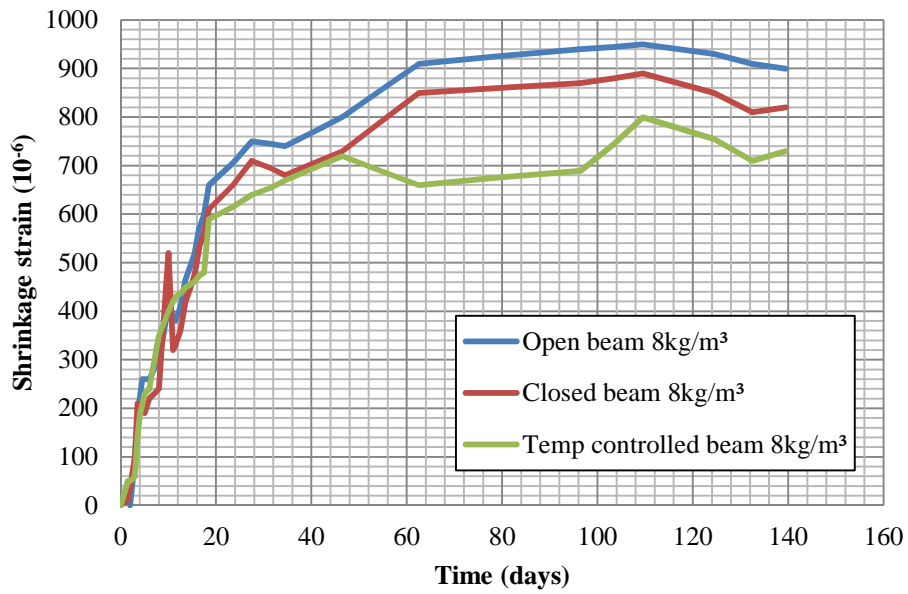


Figure 4.12: The shrinkage test results for beams containing 8 kg/m³ fibres

The temperature fluctuation in the temperature controlled room is shown in Figure 4.13.

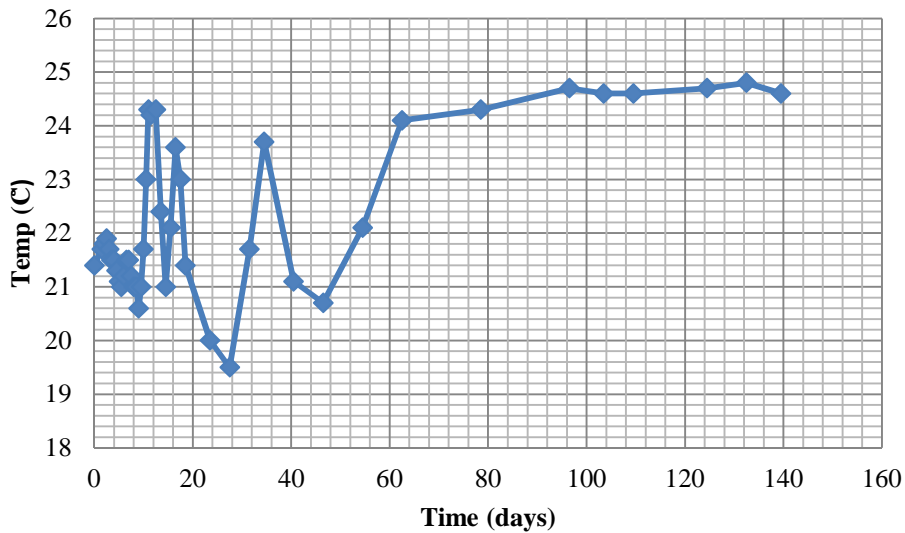


Figure 4.13: The temperature fluctuation in the temperature controlled room

Figure 4.14 shows the average shrinkage that was calculated using the model found in the Model Code, 2010, in Section 2.1.3. The calculations can be seen in Appendix 1. Figure 4.14 also compares the results calculated using the fib model code to the results obtained with the experimental work.

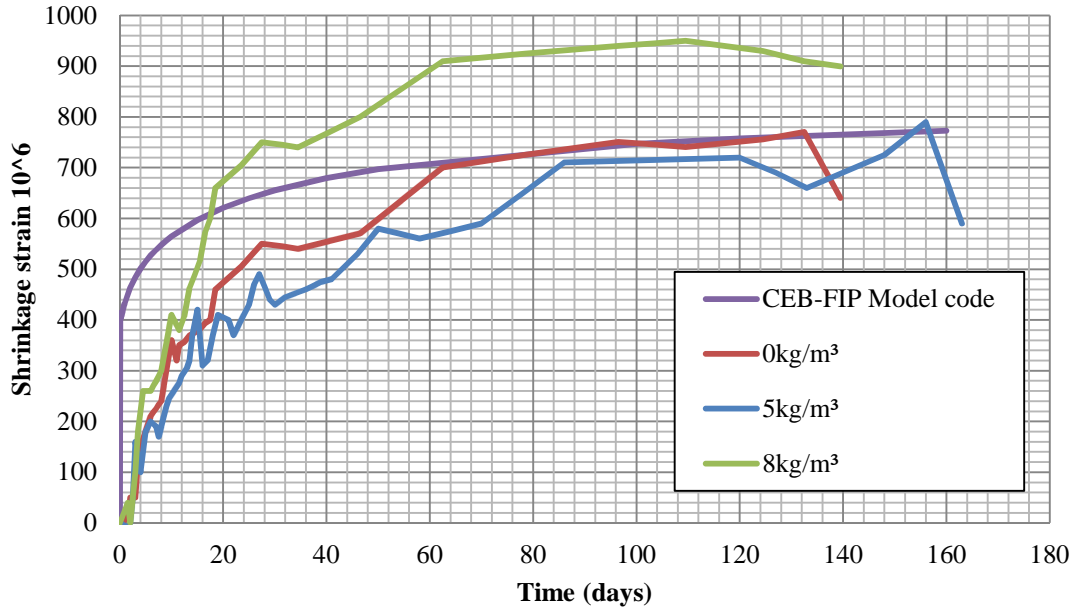


Figure 4.14: The shrinkage strain calculated with fib Model Code 2010 compared to experimental results

4.3.3 FLEXURAL TEST AND TENSILE BEHAVIOUR

The average flexural behaviour of conventional concrete, 5 kg/m³ PPFRC and 8 kg/m³ PPFRC is compared in a plot of the force over the deflection as seen in Figure 4.15. All the results from the flexural bending test are given in Appendix 2.

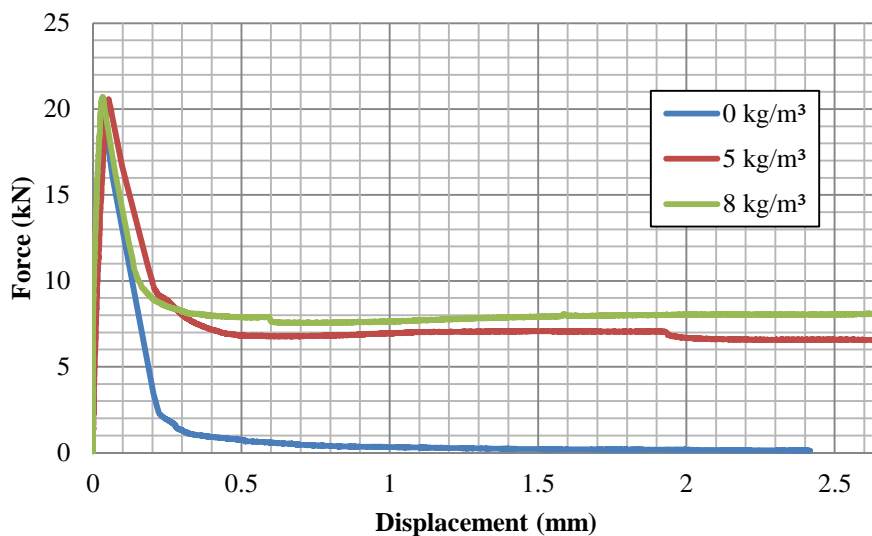


Figure 4.15: The average flexural behaviour of PPFRC for different fibre dosages

The equivalent flexural strength ratio, Re_3 values, for the PPFRC with two different dosages are given in Table 4.4. Table 4.4 gives the equivalent flexural strength ratio, Re_3 , for the different PPFRCs used. It also shows the coefficient of variance, COV, for the results of the Re_3 values.

Table 4.4: The Re_3 values for the fibre reinforced concrete

Fibre Dosage	Re_3 Value	COV
5 kg/m ³	0.21	32.7
8 kg/m ³	0.32	7.4

Table 4.5 gives the flexural strength, also known as the indirect tensile strength, of the concrete obtained through calculations with Equation 4.3, using the values of the three point beam test.

Table 4.5: The flexural strength of concrete containing different fibre dosages

Fibre dosage	Force (N)	Average flexural stress (MPa)
0 kg/m ³	21215	4.94
5 kg/m ³	18743	4.40
8 kg/m ³	20118	4.67

The tensile strength ($f_{ctk, 0.05}$) of the concrete was obtained from BS EN 1992-1-1:2004 for the cube strengths of the different fibre dosages as found in Section 4.3.2 and is shown in Table 4.6.

Table 4.6: The tensile strength and compressive strength of the different fibre dosages according to BS EN 1992-1-1:2004

Fibre dosage	Compressive strength (MPa)	Tensile strength (MPa)
0 kg/m ³	53.46	2.63
5 kg/m ³	54.56	2.68
8 kg/m ³	57.17	2.79

4.3.4. FRACTURE ENERGY OF PPFRC

The fracture energy was calculated with Equation 4.5 using the data collected from the wedge splitting test. The test was done with four specimens of four different fibre dosages each. The fibre dosages are 2 kg/m^3 , 5 kg/m^3 , 6 kg/m^3 and 8 kg/m^3 . Figure 4.16 gives the average force versus CMOD for the four different fibre dosages. The results for each fibre dosage can be seen in Appendix 3.

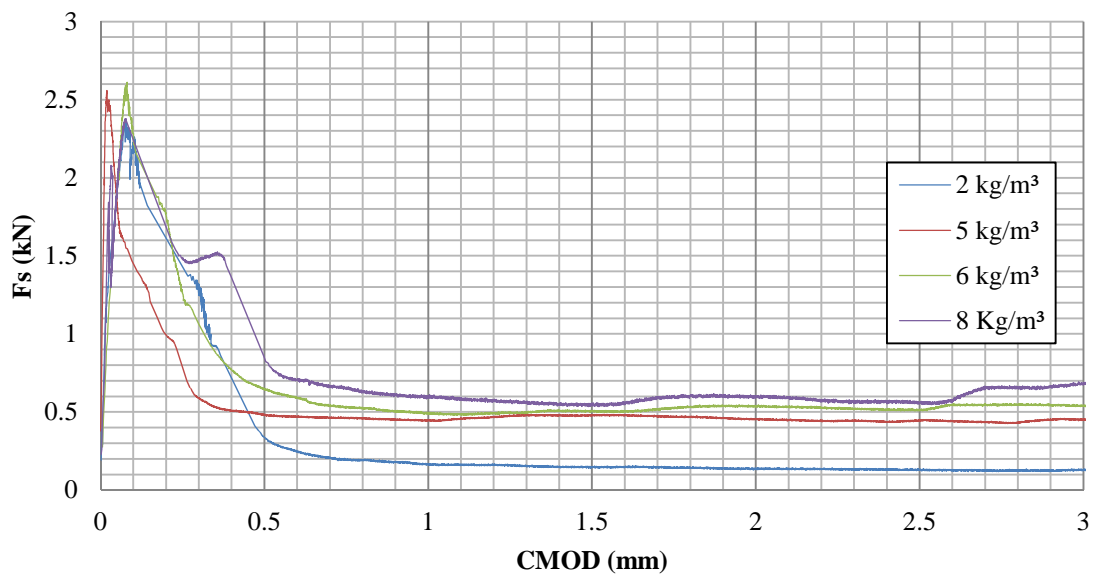


Figure 4.16: The force versus CMOD graph for different volume fibres

The fracture energy of the different fibre dosages was calculated using the area under the force versus CMOD graphs and divided by the ligament area. The results are shown in Table 4.7.

Table 4.7: The fracture energy recorded for selected fibre dosages per volume

Fibre Dosage	Fracture energy (G_f) (N/m)
2 kg/m^3	296.9
5 kg/m^3	766.7
6 kg/m^3	883.2
8 kg/m^3	1101.3

From the test specimens the fibre distribution could be found by counting the fibres in the broken specimens. The fibre distribution for different volumes of fibres is shown in Figure 4.17. The fibre distribution is also counted in three parts over the sample. The parts are made up out of the top third, the middle third and the bottom third. In all the samples the fibre distribution is higher at the bottom third with the top third having the second highest fibre count, indicating an even distribution of the fibres over the sample. Figure 4.18 shows the average count of fibres in three samples for the different fibre dosages. The figure indicated that the distribution is even in terms of the volume of fibres in the samples. Figures 4.19 to 4.22 show the cross sectional physical fibre distribution for 2 kg/m³, 5 kg/m³, 6 kg/m³ and 8 kg/m³.

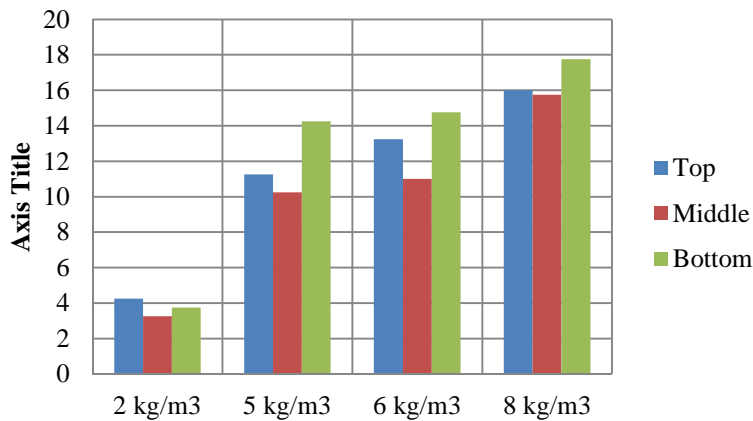


Figure 4.17: Spatial distribution of fibres for selected fibre dosages

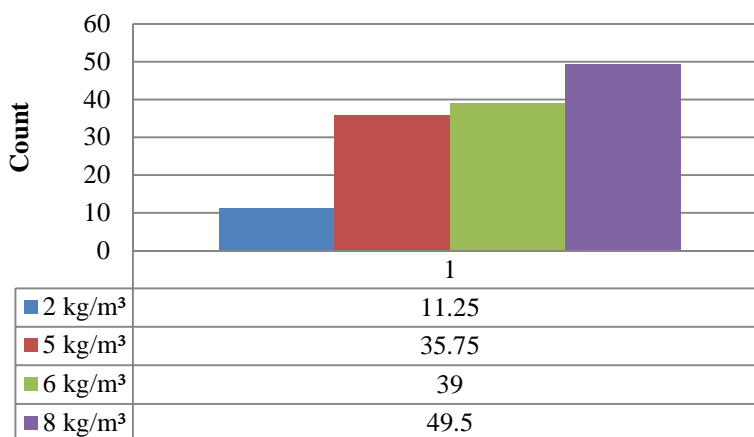


Figure 4.18: The average fibre count for four different fibre dosages



Figure 4.19: The cross sectional physical fibre distribution for a fibre dosage of 2 kg/m³



Figure 4.20: The cross sectional physical fibre distribution for a fibre dosage of 5 kg/m³



Figure 4.21: The cross sectional physical fibre distribution for a fibre dosage of 6 kg/m³



Figure 4.22: The cross sectional physical fibre distribution for a fibre dosage of 8 kg/m³

4.3.5. SIEVE ANALYSIS

The two different sand batches used in the concrete mix design and as the sub-base layer in the large scale tests, (See Chapter 5) were graded using a sieve analysis. The results of the sieve analysis can be seen in Figure 4.23.

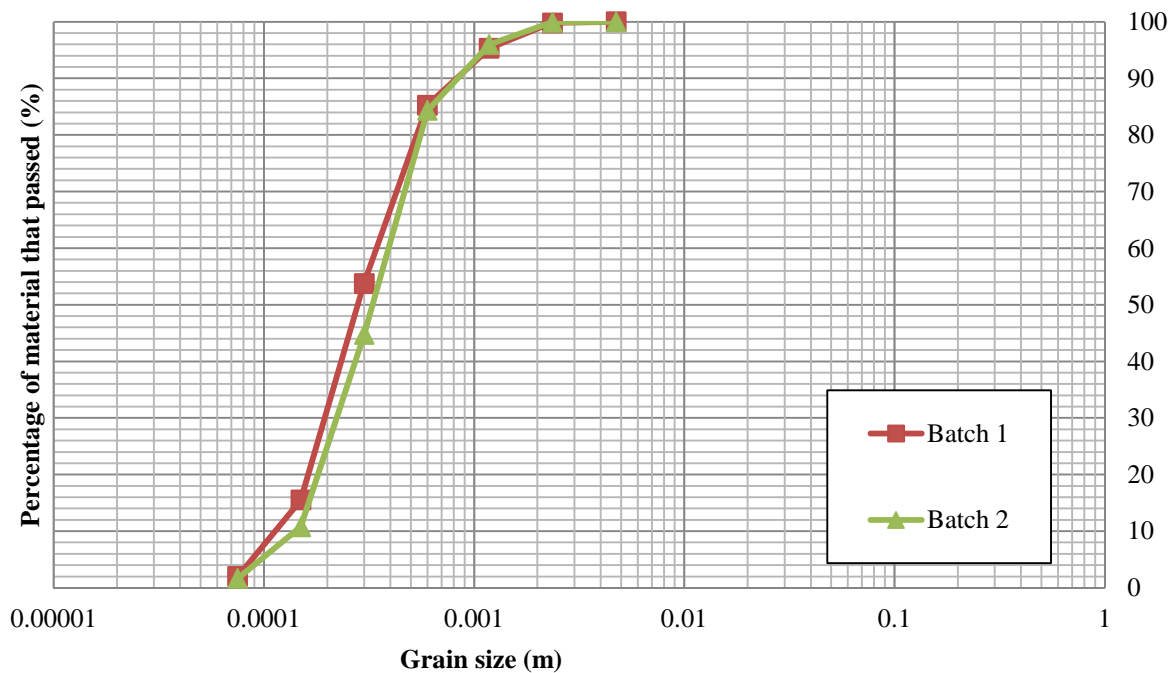


Figure 4.23: The sieve analysis results for the two batches of sand used

4.4. DISCUSSION

4.4.1. COMPRESSION TEST

The results of the compression tests showed that the use of high dosages polypropylene fibres does increase the compressive strength of conventional concrete. Although an increase in strength is found, it is only 6.5 per cent larger than the strength of conventional concrete. The use of high dosages of polypropylene fibres does increase the compressive strength of the concrete but not to such a large extent to see structural advantages in the concrete. Lower

dosages of polypropylene fibres had no impact on the compressive strength of the conventional concrete.

4.4.2. SHRINKAGE TEST

The shrinkage tests were done with four specimens consisting of 0 kg/m³, 5 kg/m³ and 8 kg/m³ fibre dosages placed in the same environment as the large scale test. Specimens of the same mixes were also placed in a temperature and humidity controlled room to evaluate the effect of the environmental change on the shrinkage in the concrete. Two specimens of the three fibre dosages were painted with a waterproofing paint on the bottom and the sides to limit the loss of moisture in those directions, resulting in a similar moisture movement as the large scale tests.

A concrete mix with a higher shrinkage than typical concrete used in slabs on grade was designed. This was done by designing the mix with a high fines content and an aggregate with a small particle size. The reason for choosing a mix design with a higher shrinkage is to achieve more cracks or larger crack openings, depending on the fibre dosage of the concrete.

The use of 5 kg/m³ fibres does show a small decrease in the shrinkage strain over 160 days. This same behaviour is seen in the temperature controlled specimens. For the specimens that were painted with the waterproofing paint, the shrinkage strains in the 0 kg/m³ and 5 kg/m³ specimens, are almost similar to the specimens with a 5 kg/m³ fibre dosage. This exhibited a less rapid increase in shrinkage over the first 40 days after casting, but becoming equal at about 80 days after casting. What is noted in all the tests specimens that cannot be explained without additional research, is the increase of 10 to 20 per cent in shrinkage strain after 10 days for all the specimens containing 8 kg/m³ fibres.

A close similarity in the shrinkage can be seen in the open and painted specimens with a slightly lower shrinkage in the painted specimens. This behaviour can be expected, since there are less open surfaces allowing moisture loss. The shrinkage behaviour of the specimens that were in the temperature controlled room is a bit more scattered, following the same trend as the specimens that were not in the temperature controlled room. At 60 days a drop in the shrinkage strain was noticed, but this drop can be explained because of

temperature fluctuation in the room, due to unexpected technical problems with the control unit.

The shrinkage strains that were found with the shrinkage test were compared to the strains calculated with the equations given in the fib Model Code 2010. The shrinkage calculated with the model code follows a very similar trend line to that of the conventional concrete. The shrinkage strain estimated using the model code, rapidly increases in the first few, but levels out faster than the shrinkage of the conventional concrete. The 5 kg/m³ PPFRC have a slightly lower shrinkage strain, suggesting that the use of polypropylene does decrease the shrinkage in the concrete. The test specimens containing 8 kg/m³ show a larger increase in shrinkage strain than that of conventional concrete. As stated before, this cannot be explained without further research.

4.4.3. FLEXURAL AND TENSION TEST

The results of the flexural and tensile test show that the fibre dosage does not increase the flexural strength of the concrete. This corresponds with the results found in literature. The flexural strength for the conventional and PPFRC concrete was 20 MPa. This is similar to the results Soutsos et al. (2012) found with regards to the shape of the load-displacement curve and the effect of higher fibre dosages. The equivalent flexural strength (Re3 value) of the design mix containing 5 kg/m³ and 8 kg/m³ polypropylene fibres indicate that at a higher fibre dosage the concrete has a higher equivalent strength over the total time of loading. The coefficient of variance (COV) indicates the inconsistency in the Re3 values that were obtained from test specimens containing the same fibre dosage. This shows that the use of a higher fibre dosage has a smaller variance in results. This is due to the higher fibre count allowing for a more even distribution of fibres over the micro-crack zone resulting in more micro-cracks being bridged.

4.4.4. FRACTURE ENERGY

The fracture energy was obtained using the wedge splitting test. The results were used to plot splitting force over CMOD graphs of four different fibre dosages. The splitting force over CMOD has a similar shape for all the different fibre dosages and is similar to the flexural tests load-displacement curves. The results for the splitting test (see Appendix 3), show a large variance for the different fibre dosages. This variance in results can be explained by the size of the test specimen. The smaller the test specimen the smaller the fracture ligament resulting in a larger scatter. A study done by Löfgren (2004) showed that the size of the specimen did not have any influence on the fracture energy, but it gave a larger scatter in results, similar to what was found in this study. The splitting force of 2.5kN was obtained for all the different test specimens. The fracture energy was calculated using the area under the splitting force over CMOD graphs of each fibre dosage, using Equation 4.5. The fracture energy of the conventional concrete is equal to 148 N/m with the PPFRC ranging from 297 N/m to 1101 N/m as the fibre dosage increase from 2 kg/m³ to 8 kg/m³. This increase in the fracture energy is due to the fibres' ability to bridge the crack and transfer the tensile forces in the concrete matrix.

The fibre count of the broken specimens was done to estimate the distribution of fibres and to determine the influence this has on the fracture properties of the concrete. The fibre distribution count not only showed the distribution over the crack, but also the distribution of the fibres over the depth of the specimens. For the 5 kg/m³ to 8 kg/m³ the distribution was even over the entire depth of the specimens, indicating a good distribution of the fibres after casting and compaction.

4.5. CONCLUDING SUMMARY

The parameter study was performed to provide clear insight of the mechanical behaviour of the PPFRC compared to conventional concrete. Different fibre dosages were compared and it was concluded that the use of macro polypropylene fibre does not increase the flexural strength, compressive strength and tensile behaviour of the concrete significantly. It was established that PPFRC does play a significant part in the increase of the equivalent flexural

strength (Re3 value). The fibres do not minimise the shrinkage in the concrete to a significant extent. These results form the basis for the discussions of the behaviour of the structures in the following chapters.

CHAPTER 5: LARGE SCALE TESTS OF SLABS ON GRADE

Large scale tests were done to determine the realistic behaviour of the PPFRC, compared to that of conventional concrete, when used for slabs on grade. This chapter discusses the setup, test methods, testing procedure and results of the large scale test.

5.1. TEST SETUP

The test setup is an 11 m wooden box with a width of 80mm and a depth of 200 mm. Because of the small width compared to the length of the slab it is assumed that the slab only spans in one direction. The reason for using a one direction spanning slab is to minimise the unnecessarily complicating factors that are introduced when a two direction spanning slab is used. The assumption was made that the one direction spanning slab will give a realistic representation of real, two direction spanning slabs as long as the sides along the length of the slab are free to move without restraint. Fibres are distributed at random and not only in one direction, resulting in the effects of the fibres being similar in both one direction as well as two direction tests. Tests on slabs spanning in one direction only, are less space consuming which allowed for more tests to be conducted at the same time.

The wooden boxes were first filled with 100 mm compacted Malmesbury sand, with a water content of 15.5 per cent. Damp soil under the concrete is required to help mitigate the plastic shrinkage in the concrete (National Ready Mixed Concrete Association, 1998). The soil represented a sub-base layer that is typically used in construction of slabs on grade in the Western Cape. The top 100 mm is then filled with either a conventional concrete or PPFRC, representing the slab. A 100 mm thick slab was used because thinner slabs are more likely to

crack. The effect of the slab thickness was also tested with one 150 mm concrete strip containing 5 kg/m^3 fibres. Figure 5.1 shows the basic layout of the test setup.

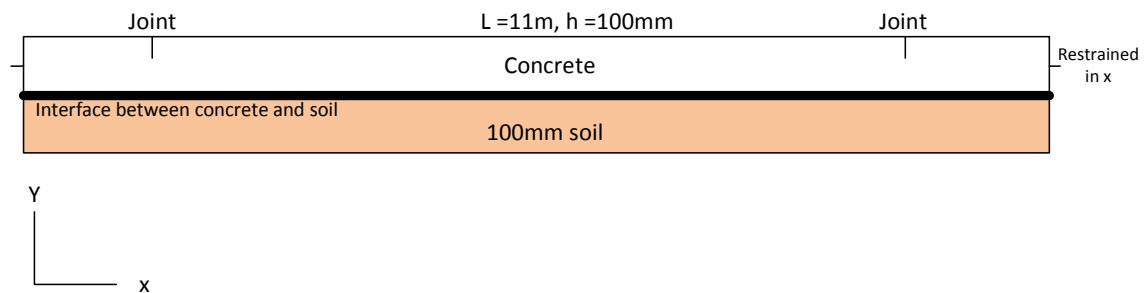


Figure 5.1: The layout of the large scale test

Nine of these concrete strips were tested, some with conventional concrete and some with different dosages PPFRC. Figure 5.2 shows a top view of the test setup of six of the concrete strips. Saw cut joints at different spacings were made in the different concrete strips. These joint spacings were either 4.5 m, 6 m or 9 m apart. Figures 5.3 to 5.5 show the layout of all the different joint spacings used in the large scale tests. These joint spacings were selected according to the commonly used spacing of 4.5 m. This was then increased to 6 m and 9 m to test the different effects of the spacings. The full range of tests conducted can be seen in Table 5.1. The conventional concrete strips are used as a control and was compared to the PPFRC to detect the effect of the fibres. The spacing between the joints differs to study the effect of the polypropylene fibres for different slab sizes.



Figure 5.2: Large scale test setup

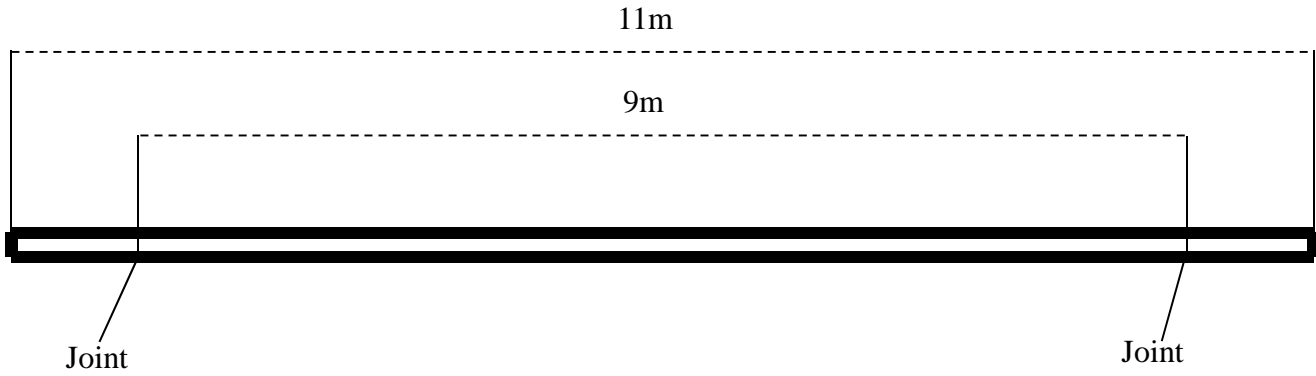


Figure 5.3: Concrete strip with 9 m spacing between saw cut joints

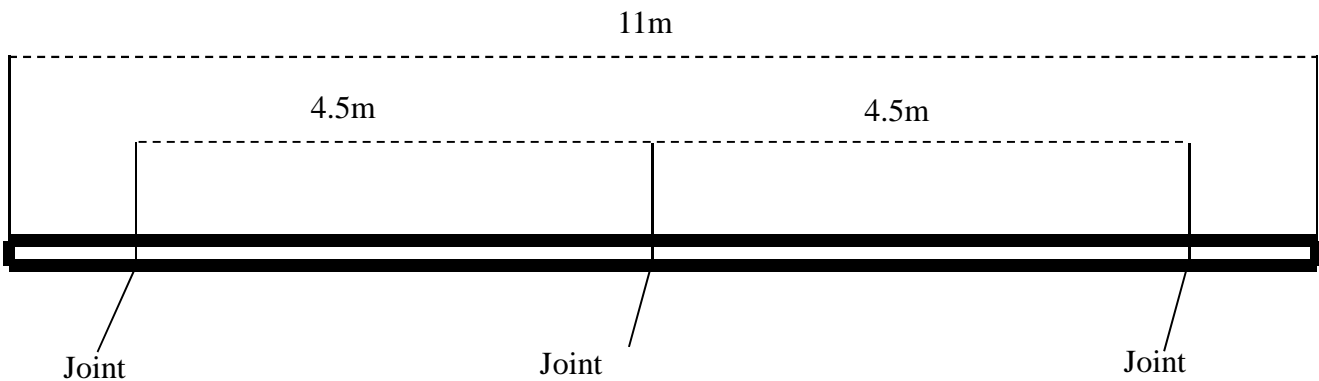


Figure 5.4: Concrete strip with 4.5 m spacing between saw cut joints

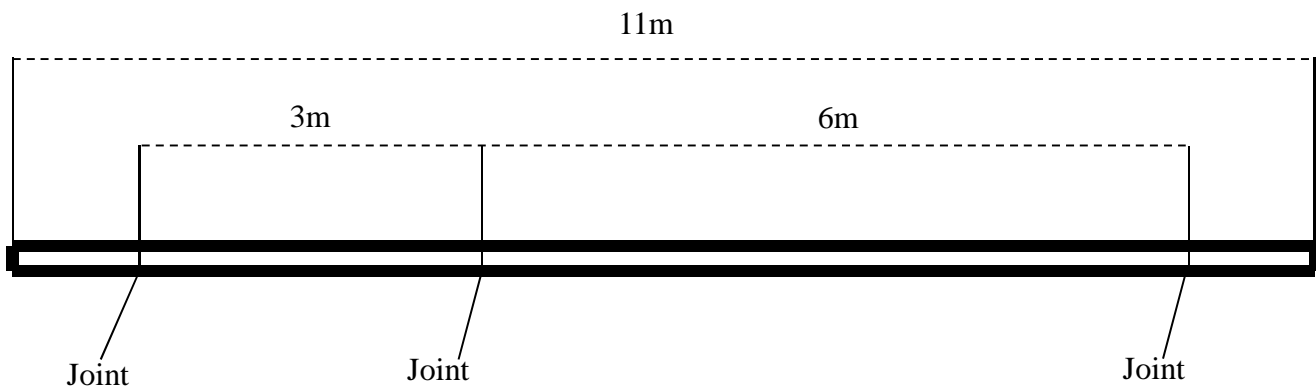


Figure 5.5: Concrete strip with 6 m and 3 m spacing between saw cut joints

The ends of the wooden boxes are bolted to a 200 x 200 x 20 mm angle section that is bolted to the laboratory floor (see Figure 5.6). The bolts are pre-tensioned to ensure that no movement could occur. This acts as the edges of a concrete slab where it is connected to the structure, restraining the slab against movement. The slab is connected to the angle section by a threaded steel bar that is bolted to one edge of the angle section and casted into the concrete. Edge joints were made 1m from both ends of the strips.



Figure 5.6: The angle section bolting the structure to the floor

The bar used to bolt the slab to the angle section was 12 mm threaded bar, with a length of 600 mm cast into the concrete. Threaded bar is used to minimise the effect of slip between the concrete and the steel. This restrains movement in the concrete that can cause an increase in shrinkage resulting in lower stresses in the concrete. The bar before and after casting, can be seen in Figure 5.7 and the calculations done to determine the length of the bar are given in Appendix 5.



Figure 5.7: The threaded bar restraining the concrete against movement

Two batches of sand were used as the base. Both batches were graded as shown in Section 4.3.5. The dampened compacted sand as seen in Figure 5.8 was hand compacted with a heavy steel plate welded to a steel rod. The steel plate is then repeatedly lifted and dropped onto the sand. This method was used because of the small dimensions of the structure, resulting in a lack of space for compaction equipment. To get a uniform consistency the steel plate was dropped 25 times before moving to the next section of soil. This was done to create a level surface for the concrete. This was desired to avoid uneven spots under the concrete resulting in crack formation in an unexplained location. The soil had to be damp to mitigate the effect of moisture loss at the bottom part of the slab which could increase the effect of plastic shrinkage.



Figure 5.8: The compacted sand layer before casting

The concrete mix used in the large scale test was the same as that for the parameter study given in Table 4.1. A high shrinkage mix was desired to exaggerate the effect of shrinkage in the structure, resulting in higher tensile stresses and more pronounced crack formations. An aggregate size of 6 mm was used to increase the workability of the concrete, which was important because of the confined dimensions, making casting and compacting difficult. This size of the aggregate also increased the shrinkage in the concrete. No admixtures were added to the concrete, since this could have an effect on the drying shrinkage, making it difficult to isolate the effect of the polypropylene fibres. Each strip was made up of an 88 litre mix by using a 120 litre pan mixer.

After the sand was compacted and the concrete was cast, the concrete was compacted with a poker vibrator that was placed into the top 50 mm of the concrete and moved along the strip. After compacting, the strips were covered with plastic and left to cure for 24 hours. After 24 hours, 5 mm saw cut joints were cut using an angle grinder. Firstly, joints were cut 1 m from the end of both the restrained edges and then at specified positions to make up 4.5 m, 6 m and 9 m spacings between joints (see Figure 5.3 to 5.5). All the saw cut joints had a depth of 25 mm. After this was completed, monitoring of the slabs commenced.

5.2. TESTING METHOD

To measure the shrinkage strain in the concrete a 100 mm strain gauge was used. The strain gauge measured the deformation between small metal discs called targets. The targets are flat on the one side and consist of a small hole on the other side. The flat side was glued on to the surface of the concrete and the other side was used to measure the deformation between the two targets with the strain gauge. The strain gauge can be seen in Figure 4.1. The results obtained from these measurements were the displacement of the concrete over time. Targets were placed over the joints and at the centre and quarters of each concrete strip. Extra targets were also placed at selected positions on each strip where cracks were expected to form. These positions were based on the theory explained in Figure 3.1 by Lee (2001).

Secondly the cracks widths were measured. This was done with the use of a special ruler (see Figure 5.9) that is used to measure the width of a crack. The first measurement was made at the time of formation. From there the growth in crack width was measured every 14 days.

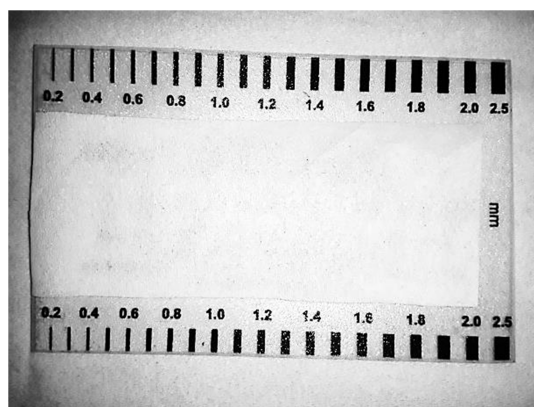


Figure 5.9: Ruler used to measure crack opening width

5.3. TESTING PROCEDURE

In total, nine tests were conducted. The tests had different fibre dosages, saw cut joint spacings and slab thicknesses. Table 5.1 gives a summary of all the tests done with a code given to each test representing the joint spacing, the fibre dosage, and the slab thickness. The “s” at the end of the code represents the soil that the slab was casted on, with s1 being the first batch and s2 the second batch.

Table 5.1: Summary of the large scale tests

Code	Distance between joints m	Fibres			Thickness (mm)		Friction	
		0 kg/m ³	5 kg/m ³	8 kg/m ³	100 mm	150 mm	Soil	Plastic
9,0,100,s1	9							
9,5,150,s2	9							
9,5,100,s1	9							
9,5,100,s1	9							
9,8,100,s2	9							
9,0,100,s2	9							
4,5,5,100,s1	4.5							
4,5,5,100,s1	4.5							
6,5,100,s1	6							

5.4. RESULTS

Data on crack formation was obtained in three phases. The first phase shows the number of cracks that opened, excluding the joints on all the 9 m joint spacing slabs, containing different fibre dosages, ranging from 0 kg/m³ to 8 kg/m³. This can be seen in Figure 5.10.

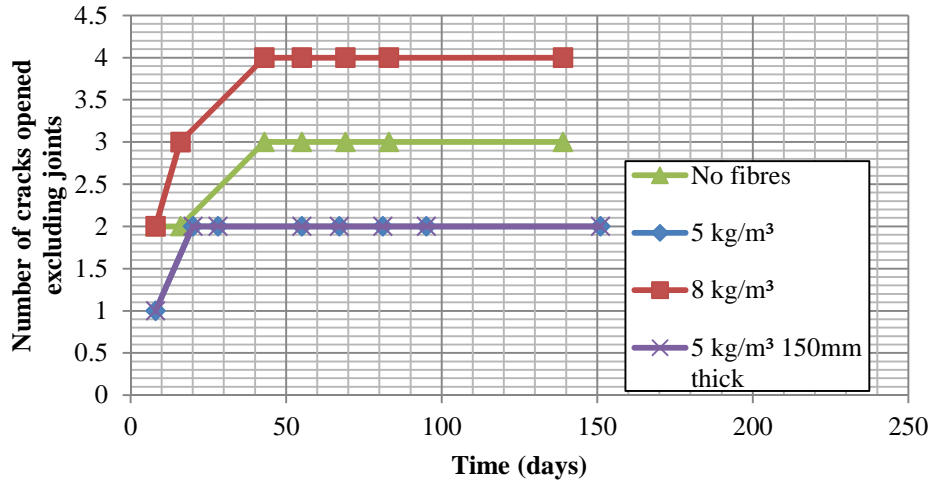


Figure 5.10: The number of cracks over time in slab with a 9 m joint spacing containing different fibre dosages

The number of cracks that formed in the slabs containing different saw cut joint spacings can be seen in Figure 5.11. All these results contain the same fibre dosages of 5 kg/m³.

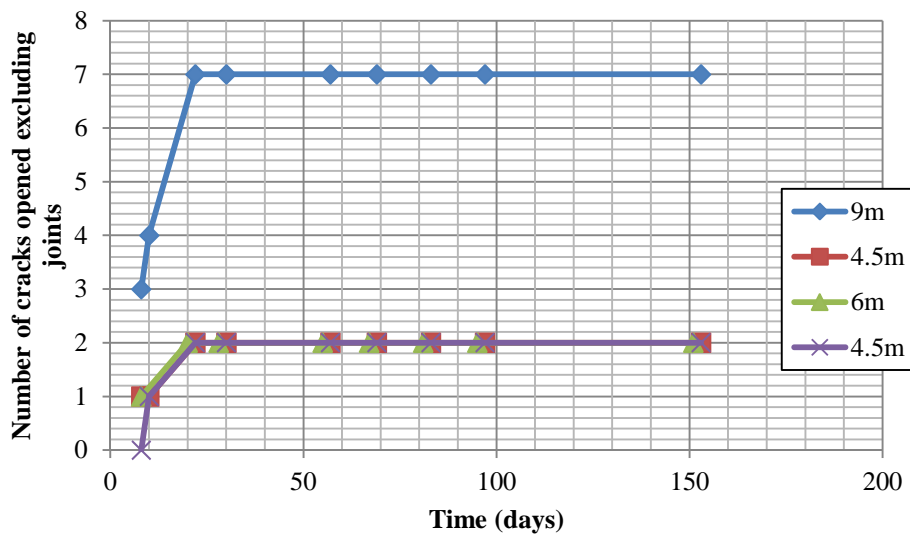


Figure 5.11: The number of cracks over time for slabs with different joint spacings containing 5 kg/m³ fibres

In the second phase the openings of the cracks were measured and compared. Firstly, the measurements of all the 9 m joint spacing slabs containing different fibre dosages, ranging from 0 kg/m³ to 8 kg/m³, were obtained (see Figure 5.12). Secondly, all the slabs with different saw cut joint spacings, all containing 5 kg/m³ fibres were measured (see Figure 5.13).

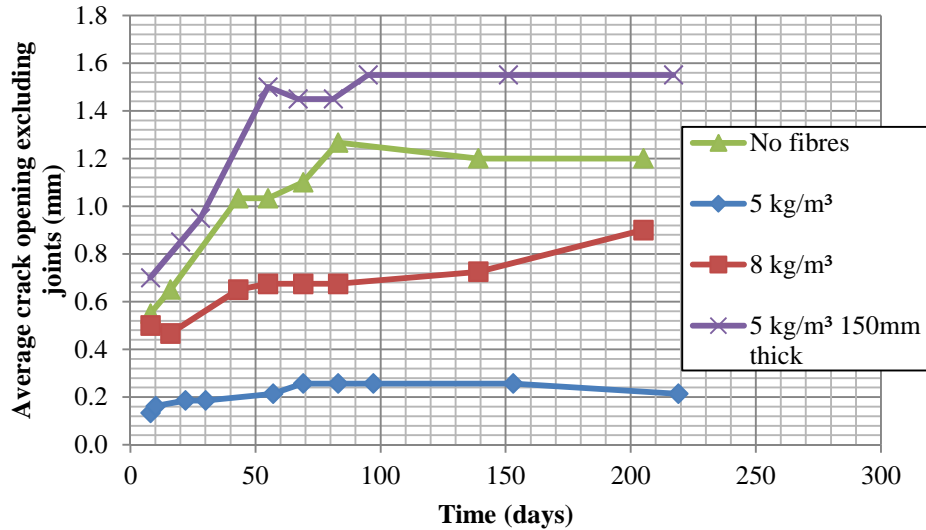


Figure 5.12: The average crack openings for 9 m joint spacing slabs containing different fibre dosages

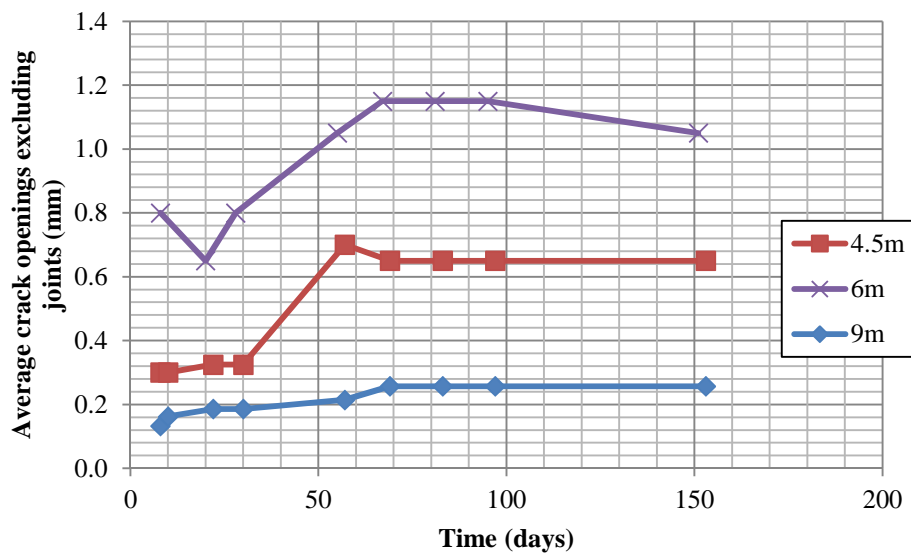


Figure 5.13: The average crack openings excluding joints for different saw cut joint spacings containing 5 kg/m³ fibres

All the above results for the crack count and crack width openings did not include the cracks that formed at the saw cut joints. In the third phase the width of the joint openings were measured. Firstly, the measurements of the joint openings of the 9 m joint spacing slabs, containing different fibres dosages, were compared. Secondly, the joint openings of different spacings between the saw cut joint, all containing a 5 kg/m³ fibre dosage, were measured and

compared. The first part can be seen in Figure 5.14 and the second part in Figure 5.15. Figure 5.16 shows a typical crack at a joint.

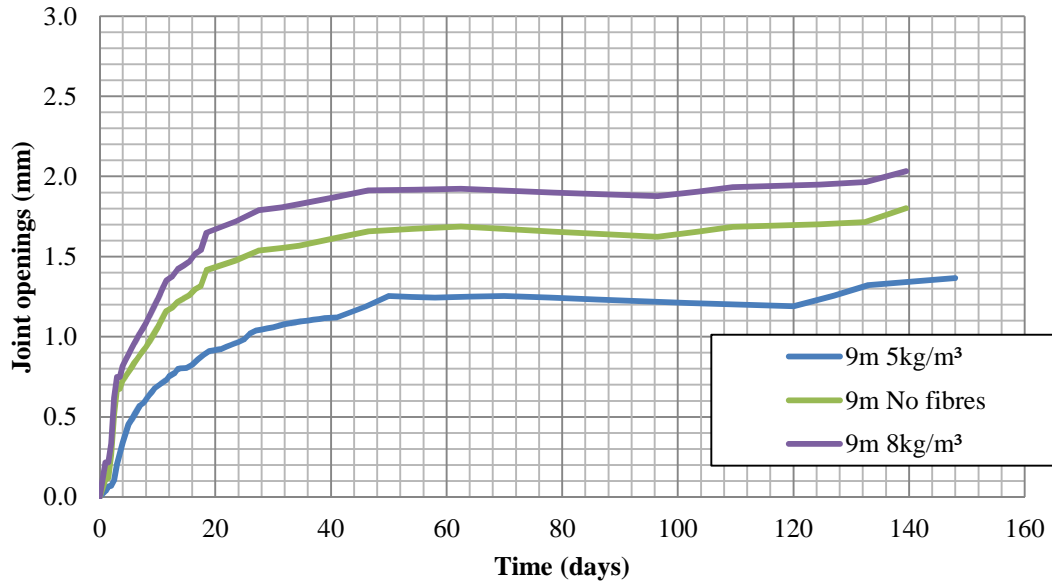


Figure 5.14: The joint openings for 9 m joint spacing slabs with different fibre dosages

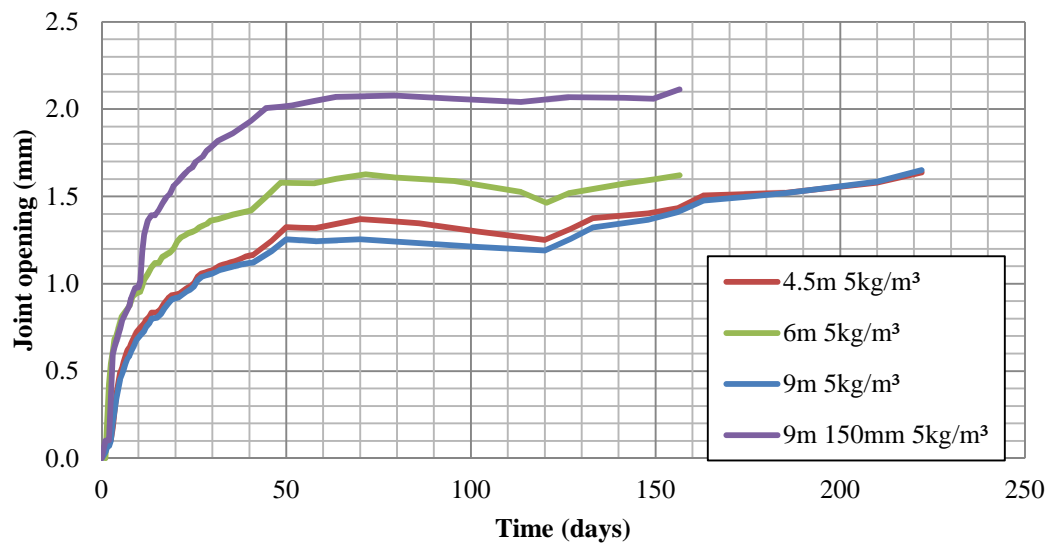


Figure 5.15: The joint openings of different joint spacings all containing 5 kg/m³ fibres



Figure 5.16: The crack at the joint

Figure 5.17 shows the total crack opening in all the 9 m joint spacing slabs containing different fibre dosages. This includes all the joint openings as well as the openings of the cracks between the joints.

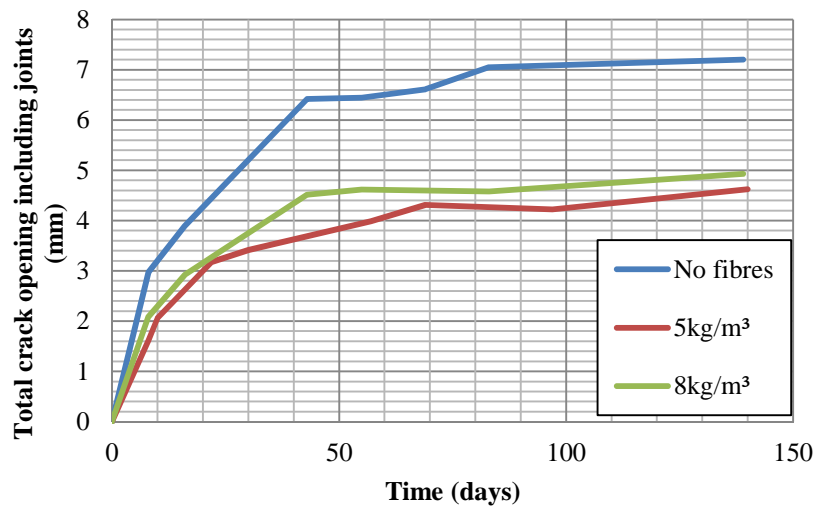


Figure 5.17: The total crack opening of a 9 m slab containing different fibre dosages.

Figure 5.18 shows the shrinkage strain at the centre of the 9 m joint spacing slabs containing different fibre dosages. It also compares the shrinkage strain of the 100 mm thick slab to that of the 150 mm slab.

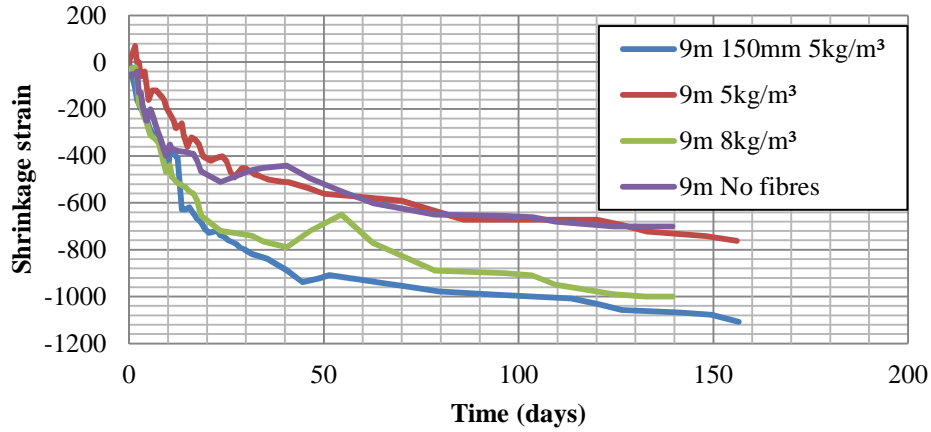


Figure 5.18: The shrinkage strain in 9 m joint spacing slabs containing different fibre dosages

All these results will be discussed in the following section. Figure 5.19 to 5.24 shows the location of the cracks that formed in each concrete strip. The red lines represent the cracks under the joints that formed first. The blue lines indicate the undesired macro cracks between the joints.

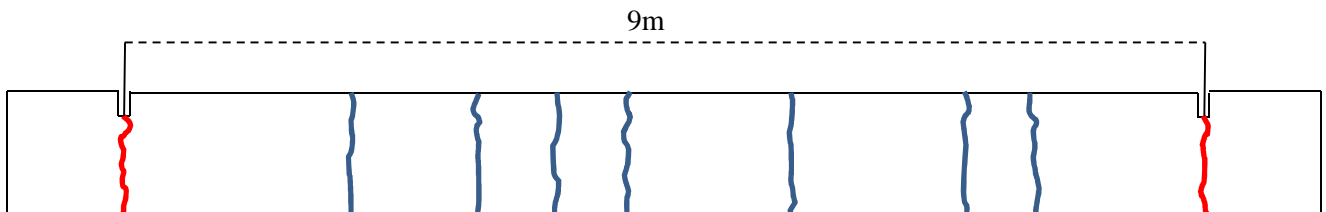


Figure 5.19: The crack pattern of a 9 m joint spacing slab containing 5kg/m³ fibres

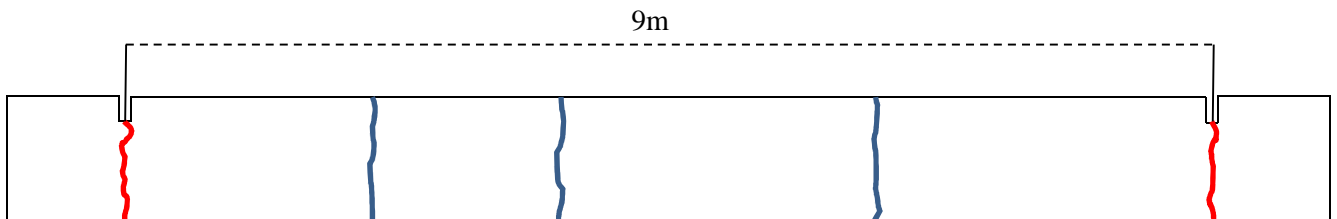


Figure 5.20: The crack pattern of a 9 m joint spacing slab containing no fibres

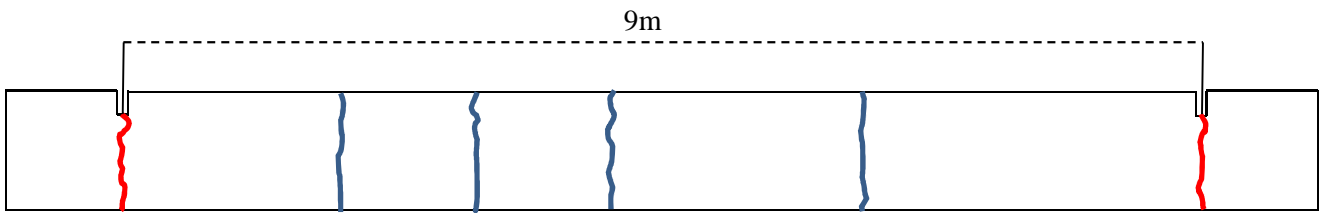


Figure 5.21: The crack pattern of a 9 m joint spacing slab containing 8 kg/m³ fibres

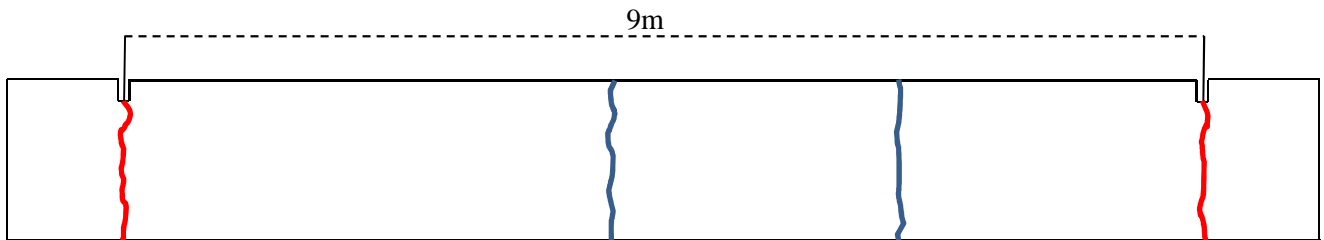


Figure 5.22: The crack pattern of a 150 mm thick 9 m joint spacing slab containing 5 kg/m³ fibres

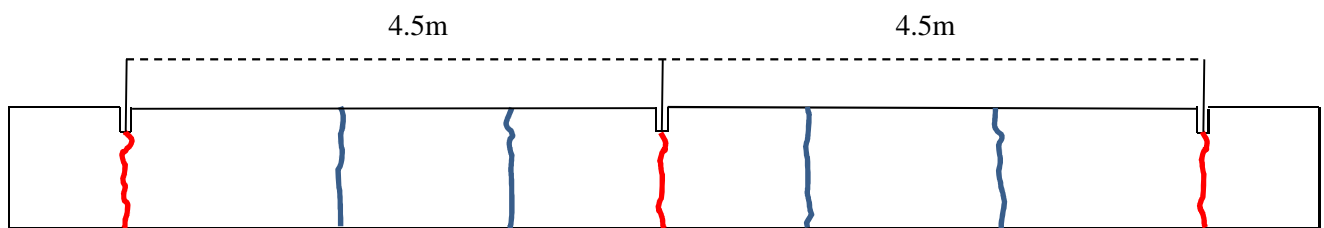


Figure 5.23: The crack pattern of a 4.5 m joint spacing slab containing 5 kg/m³ fibres

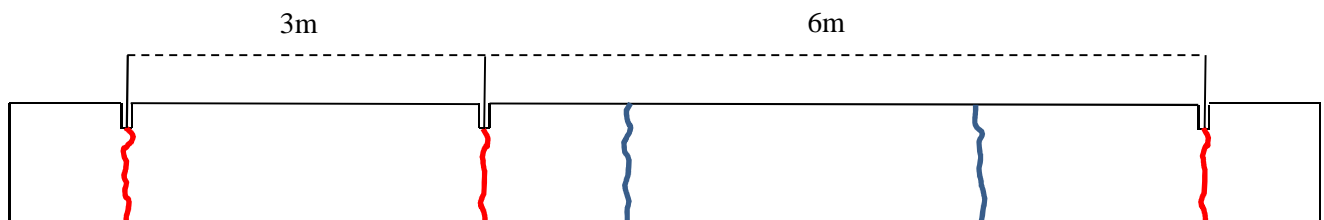


Figure 5.24: The crack pattern of a 6 m joint spacing slab containing 5 kg/m³ fibres

5.5. DISCUSSION

The large scale test was done to test the behaviour of PPFRC, compared to conventional concrete, when used in slabs on grade with different spacings between the saw cut joints. The goal of the test was to see if the use of PPFRC could be employed to increase the spacing between the joints, and to what extent the fibres could mitigate the formation of macro-cracks

in the slabs. To explain these effects the behaviour of the slabs was investigated in terms of the number of cracks formed, the width opening of the cracks and the width opening of the joints.

5.5.1. 9 m JOINT SPACING SLABS CONTAINING DIFFERENT FIBRE DOSAGES

The first comparison was the number of cracks formed over 150 days in six 9 m joint spacing slabs that contained different fibre dosages. The results of one of the slabs containing 5 kg/m³ fibres with a thickness of 100 mm were dismissed due to a practical error made in the casting process. To better explain the crack formation in the slabs, the results should be compared to the size of the crack openings over 150 days. For a fibre dosage of 5 kg/m³ seven small cracks formed throughout the slab, with an average crack opening width of 0.16 mm at the start of cracking, and a width of 0.22 mm at the end of 150 days. This was compared with the three cracks that formed in the slab containing no fibres with an average crack opening of 0.6mm, at the start of cracking, to double that of 1.2mm at 150 days. The same can be observed for the slab containing 8 kg/m³ fibres. Although only four cracks formed, it had an average crack opening of only 0.5 mm at the start growing to 0.6 mm at 150 days. The behaviour of the fibre leads to more cracks, compared to the number of cracks in the conventional concrete slabs, but the PPFRC had smaller average crack width openings. This behaviour can be explained by the fibres' bridging ability, holding the concrete together after micro-cracks formed. It can thus be concluded that the use of macro polypropylene fibres results in more cracks over the length of a slab, but with a smaller average crack opening than a similar slab containing no fibres.

The 150 mm slab with 5 kg/m³ fibres behaved differently from the 100 mm slab also with 5 kg/m³. In the 100 mm slab, only two cracks formed with a growing average crack opening of 0.7 mm at the start increasing to 1.58 mm at 150 days. No tests were conducted on a 150 mm slab containing no fibres. The behaviour could be explained when looking at the joint opening. The 150 mm slab had larger joint openings than the 100 mm slab containing 5 kg/m³ fibres. A smaller joint opening was expected since the larger effective thickness of the 150mm section meant less shrinkage compared to that of the 100mm section. This unexpected result could be due to the curling behaviour of the slab as drying starts taking place, but further investigation is required.

5.5.2. SLABS CONTAINING 5 kg/m³ FIBRES

The second comparison was between all the slabs containing 5 kg/m³ fibres with different saw cut joint spacings. Spacings of 4.5 m, 6 m and 9 m were used in the test. Firstly, the number of cracks formed in the slabs with different joint spacings were compared over a time period of 150 days. For a better explanation, the results should be compared with the size of the crack width openings formed over 150 days. It was found that with a fibre dosage of 5 kg/m³ all the slabs except the 9 m slab, formed two cracks over this time period. The 9 m slab formed seven cracks. The average crack width openings of the slabs were found to be different. For the 9 m joint spacing slab the average crack opening was 0.16 mm at the start of cracking and 0.22 mm at the end of 150 days. The 4.5 m joint spacing slab containing 5 kg/m³ fibres, gave a similar result to the 9 m joint spacing slab with average crack openings ranging from 0.08 mm to 0.12 mm over the time period. The 4.5 m joint spacing slab containing no fibres formed two cracks with an average crack width opening of 0.3 mm at the start and 0.62 mm at 150 days. The 6 m joint spacing slab containing 5 kg/m³ fibres had the largest average crack width opening starting at 0.8 mm and opened to 1.15 mm with only two cracks forming.

In all the slabs the average crack opening decreased near the end of the test. This is due to an increase in temperature corresponding to a change in seasons, resulting in thermal expansion which countered the shrinkage.

5.5.3. SLABS CONTAINING DIFFERENT FIBRE DOSAGES AND DIFFERENT SAW CUT JOINT SPACINGS

Phase three of the results give the joint width opening of all the slabs with different fibre dosages and different saw cut joint spacings. The joint openings of these slabs are all the same width and follow the same trend line as the crack width increases over time. The 4.5 m, 6 m and 9 m joint spacing slabs, all with a thickness of 100 mm, show similar growth of the joint openings, but the 150 mm thick slab, with a 9 m spacing between the joints had a significantly higher joint opening width. As mentioned above, this could be explained by the

increase in shrinkage due to the increase in thickness of the slab. More research must be done to fully understand the effect of the fibres on the thicker slab.

The total crack width opening, including the joints and the cracks in the slab, was also compared. It showed that the use of 5 kg/m^3 fibres significantly reduced the crack opening width of the slabs, compared to that of a slab containing no fibres. The use of 8 kg/m^3 fibres did decrease the crack width but to a lesser extent than a 5 kg/m^3 fibre dosage. This can be explained by the higher shrinkage strain in the slab containing 8 kg/m^3 that results in a larger crack width.

5.6. CONCLUDING SUMMARY

The large scale test was done to evaluate the behaviour of PPFRC compared to conventional concrete. It was found that with the use of fibres there was an increase in the number of cracks but that the average crack openings were smaller. It was determined that the optimum fibre dosage is 5 kg/m^3 , since a higher fibre dosage resulted in a higher post cracking stress transfer over the crack plane, therefore reducing the ability of the joint to open due to shrinkage.

It was proven that by adding 5 kg/m^3 fibres to a slab could improve the crack formation of the slab resulting in more but smaller, less visible cracks. The slabs with the smaller spacing between the saw cut joints gave almost exactly the same results as the 9 m joint spacing slab, indicating that the fibres did improve the properties of the concrete to an extent. It can thus be concluded that the use of polypropylene fibres may allow for an increase in joint spacings to some extent, but more tests should be conducted to support this.

More tests should be conducted in the same way to obtain more results on the behaviour of the PPFRC, but due to the scale of the test, this could not be done in the time frame of this study.

CHAPTER 6: VERIFICATION OF NUMERICAL MODEL

A Finite Element Method (FEM) analysis is used to evaluate the behaviour of PPFRC and its effect on the dimensions of the spacing between the saw cut joints on concrete floors on grade. The analyses also compare the structural behaviour of conventional concrete with PPFRC at different stages in time. The model, replicating the structure shown in Chapter 5, is simulated in FEM software called DIANA. This software was originally developed by TNO Building and Construction Research in the 1970's (TNO DIANA, 2003). It has the capability to analyse the early age behaviour of concrete. The results shown in Chapter 5 are used to verify the FEM model. For the purpose of verification seven large scale test results are compared to the FEM model.

6.1. TESTING PROCEDURE

The analyses used for the verification of the model are shown in Table 6.1 with the highlighted boxes indicating the active variables of each analysis.

Table 6.1: The tests used for verifications of the FEM model

Code	Distance between joints	Fibres			Thickness (mm)		Friction
		0 kg/m ³	5 kg/m ³	8 kg/m ³	100	150	
	m						Soil
9,0,100,s	9						
9,5,100,s	9						
9,8,100,s	9						
9,5,150,s	9						
4,5,5,100,s	4.5						
4,5,0,100,s	4.5						
6,5,100,s	6						

6.2. STRUCTURAL ANALYSIS DESIGN

A 2D plane stress model with 4-node elements was used in the structural analysis. Beam elements were considered, but it was incompatible with the interface elements that were required for the modelling of the layer between the soil and the concrete. A non-linear analysis was performed with force as the controlling convergence criteria. A combination of Newton-Raphson and Secant iterative solution methods were used to achieve convergence. The model geometry, mesh, interface, loads, boundary conditions, and crack modelling are discussed in the following section.

6.2.1. GEOMETRY

The model consists of a top part made up of concrete and a bottom part made up of soil. The two parts are separated by an interface. Both the concrete and the soil are 100 mm deep with the 5 mm interface in between. The structure is 11 m long with two joints spaced 4.5 m, 6 m or 9 m apart. The width (thickness) of the plane stress element is 80 mm for both the soil and the concrete. The interface between the concrete and the soil is added to represent the relationship between the normal and shear traction, and the normal and shear relative displacements of the concrete as it moves over the soil. Figure 6.1 shows the basic dimensions of the structure. Symmetry is not used as cracking is expected in the centre.

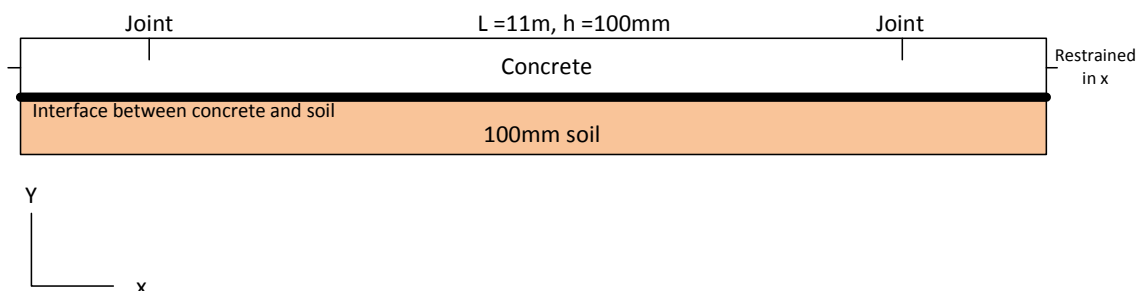


Figure 6.1: Basic layout of the model

6.2.2. MESH

The mesh of the concrete and the soil was generated using Quadrilateral, 4-node elements called Q8MEM with a mesh size of 5 mm over the entire structure. It was considered to use a finer mesh at the joints and a coarser mesh over the rest of the structure but, since random crack patterns are expected, this created a problem in convergence. The interface between the soil and the concrete is modelled L8IF element.

6.2.3. THE INTERFACE

As mentioned above, the interface between the concrete and the soil is made up out of L8IF elements. The interface is a 5 mm layer between the two materials that represents the friction in terms of traction and shear. This occurs as shrinkage in the concrete creates movement of the concrete over the soil. This behaviour was discussed in Section 3.6.3.

The surface between the soil and the concrete can be seen as fully bonded (rough interface). Maitra et al. (2009) state that the effective normal stiffness is the modulus of subgrade reaction (k) times the influencing area of the element. This value, along with the stiffness calculated with equations discussed in Section 3.6.3, gave large elastic stiffness values. This created convergence problems until the stiffness was reduced to a lower value. In an article by Eierle et al. (1999) it was suggested that this reduction in the stiffness can be allowed as long as it is greater than the stiffness of the soils. To model the interface between the soil and the concrete Coulomb Friction is used. The values required for the FEM model to analyse the friction on the interface, is shown in Table 6.2.

Table 6.2: The required parameters for the interface elements

Parameter	Program parameters	Value	Unit as entered into software
Normal stiffness (k_n)	DSTIF	9.04E7	N/m ³
Shear stiffness (k_s)	DSTIF	9.04E9	N/m ³
Coulomb Friction	FRICTI	N/A	
Cohesion (c)	FRCVAL	3450	
Friction angle (ϕ)		0.35	Rad
Dilatancy angle (ψ)		0.0	Rad
Gap forming	GAP	N/A	
Tensile strength (f_t)	GAPVAL	0	MPa
Shear retention	MODE2	1	
Reduced stiffness	MO2VAL	0.01	

6.2.4. LOADS

Only the own weight of the structure was applied to the system to isolate the effect of shrinkage strains on the slab. At a later stage loads can be applied, but this was not done as part of this study.

6.2.5. BOUNDARY CONDITIONS

Two sets of boundary conditions are required to replicate the large scale tests. Firstly, all the elements at the ends are constrained in the horizontal direction (x-direction) over the full depth of the member. This will constrain the structure from movement resulting in high tensile stresses in the concrete. This restraint can be seen in Figure 6.2. The slab will still be able to move in the vertical direction (y-direction) if the soil is compressed by the weight of the concrete.

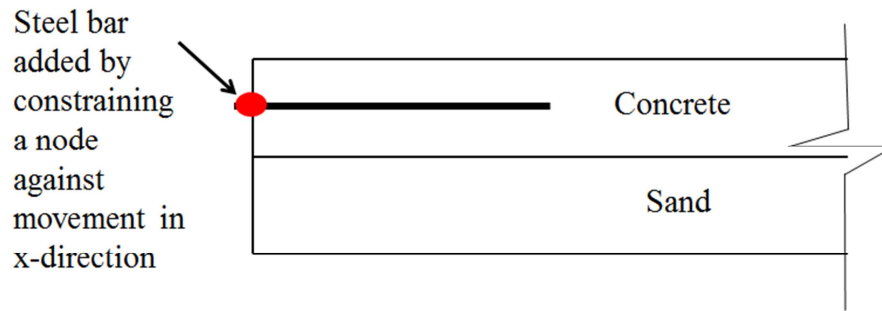


Figure 6.2: The constrain representing the steel bar in the concrete

The second boundary condition is the foundation of the member. The soil layer under the slab acts as the foundation of the slab. Studies have shown that the soil under a slab also undergoes movement with the slab as long as the friction between the soil and the concrete is not exceeded. The movement of the soil due to settlement, soil moisture migration and uneven fill can also have an influence on the slab (Rajani, 2002). For the purpose of this study perfect soil conditions were assumed as the complexity of soil modelling may affect the results of the drying shrinkage cracks. The perfect soil conditions refer to soil that only undergoes elastic deformation and is free of uneven compaction. The bottom of the soil was constrained against movement in all directions.

6.2.6. CRACKS

Without reinforcement concrete has a brittle cracking nature. Some FEM software has created cracking models to simulate this brittle behaviour. When fibres are added to the concrete the cracking behaviour is no longer brittle since the fibres act as reinforcement, holding the concrete together. Because the fibres are distributed randomly in the concrete matrix, predicting the behaviour of the FRC becomes more complex. To date no cracking model has been created to accurately take into effect the behaviour of FRC. To solve this problem the fracture energy of the concrete is changed to that of the PPFRC as found in the experimental work in Chapter 4. The Total Strain concept in the software, implements a non-

linear softening curve. A total strain crack model was used and the tensile behaviour in the concrete was related to the crack bandwidth in a Smeared Crack model.

6.3. MATERIAL PROPERTIES

As mentioned before, the model is made up out of three various materials namely: a bottom layer of sand, the interface between the sand and the concrete, and the concrete. The different material properties are specified in the following sections.

6.3.1. THE SAND

The bottom 100 mm of the model represents compacted Malmesbury sand. Models are available for modelling the behaviour of the soil, but plane stress elements cannot be used for these models. Specialised soil models are implemented for solid, plane strain or axisymmetric elements only. Since the primary focus is the stiffness of the soil layer and the interface between the two layers, a complicated soil model was not used. For this reason the soil is added as a plane stress element with linear elastic material property.

The supporting capacity and resistance against movement of the soil is important. The strength of the soil is impacted by the degree of compaction and its moisture content (Marais & Perrie, 1993). To model the compaction of the soil the density of the soil will be increased (density is the mass per unit volume). Table 6.3 lists all the parameters required by the software to model the soil.

Table 6.3: Sand parameters

Parameter	Program parameters	Value	Unit
Young's modulus	YOUNG	47	MPa
Poisons ratio	POISON	0.3	
Density	DENSIT	1400	kg/m ³

6.3.2. THE CONVENTIONAL CONCRETE AND PPFRC MATERIAL MODELS

The materials used in the analysis must replicate the materials used in the experimental work. The top 100 mm of the model represents the concrete with a high shrinkage capability. The linear elastic parameters required are the Young's modulus E , Poisson's ratio ν , and the mass density of the concrete. These parameters are similar for the conventional concrete and the PPFRC and can be seen in Table 6.4.

Table 6.4: Linear elastic material properties at 28 days

Parameter	Program parameters	Conventional concrete	5 kg/m³ PPFRC	Unit
Mass Density	DENSIT	2400	2400	kg/m ³
Poisson's Ratio (ν)	POISON	0.15	0.15	
Young's Modulus (E)	YOUNG	32	32	GPa

To analyse the cracking of both the conventional and the PPFRC concrete a static non-linear analysis must be done. In the software the concrete, known as a brittle material, undergoes cracking that can be modelled in a model called Multi-directional Fixed Cracking, with a constant stress cut-off as explained in Section 3.6.2. The linear tension softening in the model is determined by the fracture energy with constant shear retention and no plasticity. To accomplish this, the model requires the material parameters given in Table 6.5. The development of the fracture energy, tensile strength and the elasticity modulus increase over time and is calculated using the equations discussed in Section 2.1.2. This development is entered into software by using a function called MATURI referring to the material parameters of the concrete at a specified maturity of the concrete. The maturity value along with the material parameters is given in Table 6.5. Table 6.6 gives the input values used for the crack model, tension cut-off and tension softening used in the two different models. The tension softening is based on the softening diagrams given in Figure 3.7 in Chapter 3. When polypropylene fibres are added to the concrete the fracture energy (G_f) and the shape of the softening branch in the analysis will change (Westhuizen, 2013).

Table 6.5: The nonlinear parameters for concrete

	Tensile stress (f_t) (MPa)		Young's modulus (GPa)	
DIANA Program parameters	CRKVAL		YOUNG	
MATURI (days)	Conventional concrete	5 kg/m ³ PPFRC	Conventional concrete	5 kg/m ³ PPFRC
0	0.004	0.004	4.6	4
1	0.5	0.39	17.6	17
2	0.73	0.78	21.8	17.7
3	1.0	1.08	24	21.9
4	1.2	1.31	25.4	2.4
5	1.4	1.49	26.4	25.5
6	1.5	1.64	27.2	26.5
7	1.6	1.76	27.8	27.3
8	1.7	1.87	28.3	27.9
9	1.8	1.96	28.7	28.4
10	1.9	2.05	29.1	28.8
15	2.2	2.36	30.3	29.2
20	2.34	2.56	31.1	30.4
30	2.63	2.82	32.1	32.2
60	2.87	3.08	33.3	33.4
90	2.98	3.20	33.9	34.0
120	3.0	3.27	34.0	34.4

Table 6.6: The software parameters

Parameter	DIANA Program parameters	Description	Model used
Tension softening	TENSIO	The tension softening diagram used in the model	3
Shear retention	TAUCRI		0
Crack model	CRACK	The tension cut-off diagram used to describe the behaviour of failure	1

The shrinkage of the concrete is different for conventional concrete compared with the PPFRC. For this reason two different shrinkage models must be used to define the shrinkage. The shrinkage of the concrete is entered into the model in terms of shrinkage strain over time

measured in days. Figure 6.4 gives the shrinkage of the conventional concrete and the PPFRC. The shrinkage strain over time was obtained through the shrinkage test in Section 4.2.2.

To replicate the shrinkage in the concrete model an elasticity-based crack model that takes into account the temperature, concentration and the maturity of the concrete is used. The desired shrinkage strains are manually entered into the software as discrete shrinkage functions based on the element age and shrinkage at that age. The shrinkage strains used can be seen in Figure 6.3.

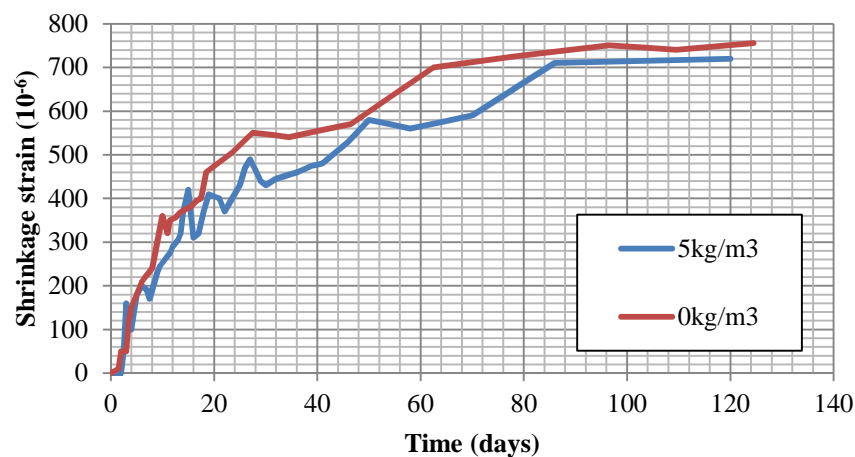


Figure 6.3: The shrinkage strain used in FEM analysis

The results obtained through using the material properties of conventional concrete and PPFRC in a FEM analysis follows.

6.4. RESULTS

Firstly, two FEM analyses were performed using conventional concrete and PPFRC containing 5 kg/m³ fibres. The results are divided into two comparable sections. Firstly, the results of the conventional concrete of the FEM analysis are compared to the results of the large scale test. Secondly the FEM analysis results of a PPFRC slab is compared to the large scale test made from the same material.

6.4.1. CONVENTIONAL CONCRETE

The results of the conventional concrete FEM model were compared to that of the large scale test in Chapter 5. Figure 6.4 shows the number of cracks that opened in both the model and experimental work.

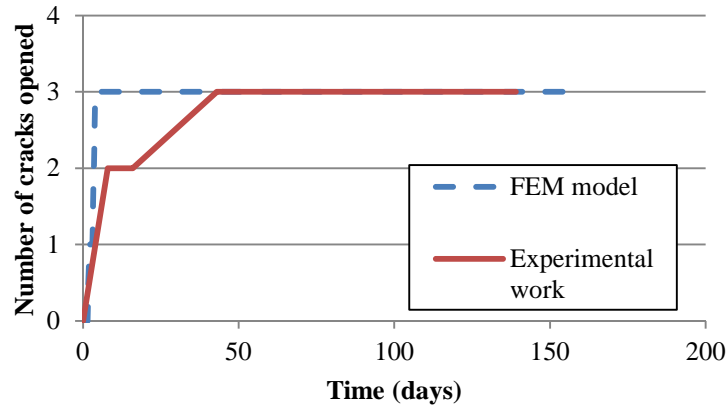


Figure 6.4: The number of cracks excluding joints in 9m joint spacing slab containing no fibres

Figure 6.5 compares the results of the size of the total crack opened between the joints in the experiment and the FEM model. Figure 6.6 gives the results of the average joint openings excluding joints of the FEM model and the large scale test. Figure 6.7 compares the total crack openings including the joint openings of the FEM analysis and experimental work.

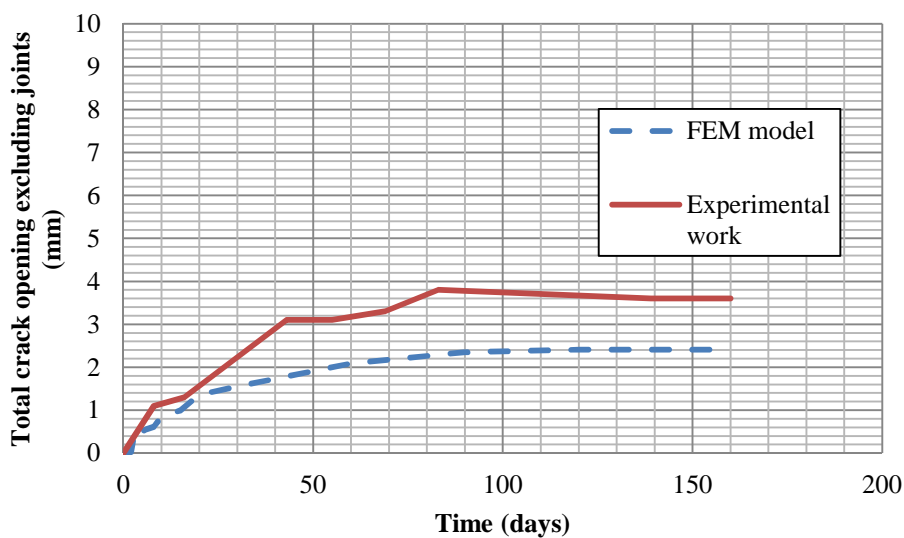


Figure 6.5: The crack opening width between joints in a 9m joint spacing slab containing no fibres

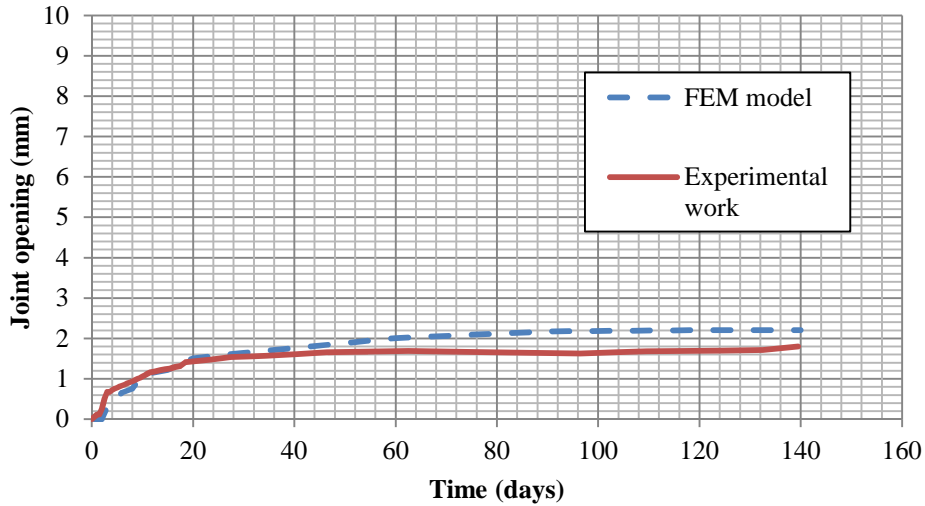


Figure 6.6: The average joint opening in a 9m joint spacing slab containing no fibres

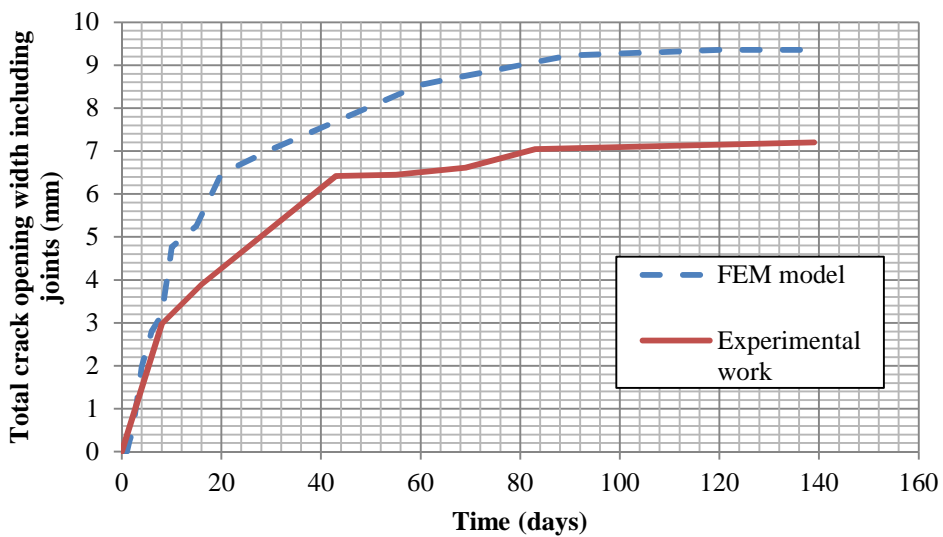


Figure 6.7: The total crack opening width including joints in a 9 m joint spacing slab containing no fibres

The result of the conventional concrete in the large scale test and the FEM model is discussed in Section 6.5. Figure 6.8 gives a summary of the crack openings in a 9 m joint spacing slab containing no fibres.

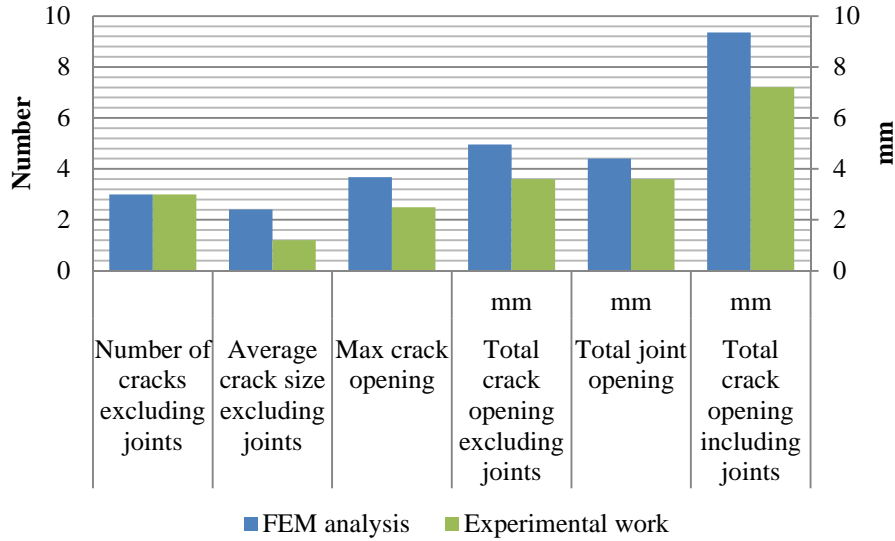


Figure 6.8: Combined FEM and experimental work results of a 9 m joint spacing slab containing no fibres (9,0,100,s)

6.4.2. POLYPROPYLENE FIBRE REINFORCED CONCRETE

The results of the FEM model of the PPFRC, containing 5 kg/m^3 , were compared to that of the large scale test. This model is the same model used for conventional concrete with the only difference being the material properties affected by the use of fibre in the concrete. Figure 6.9 shows the number of cracks that opened in both the FEM model and experimental work.

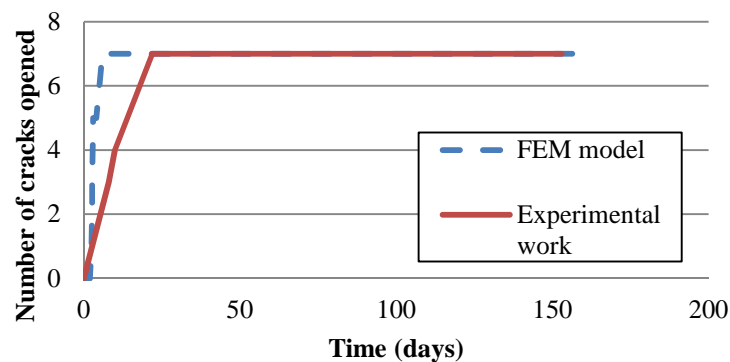


Figure 6.9: The number of cracks formed in a 9m joint spacing slab containing 5 kg/m^3 fibres

Figure 6.10 compares the results of the size of the crack openings in the experiment and the FEM model. Figure 6.11 gives the results of the average joint openings of the FEM model and the large scale test. Figure 6.12 compares the total crack opening of the joints and the cracks over the length of the slab. Figure 6.13 gives a summary of the crack openings in a 9 m joint spacing slab at 150 days.

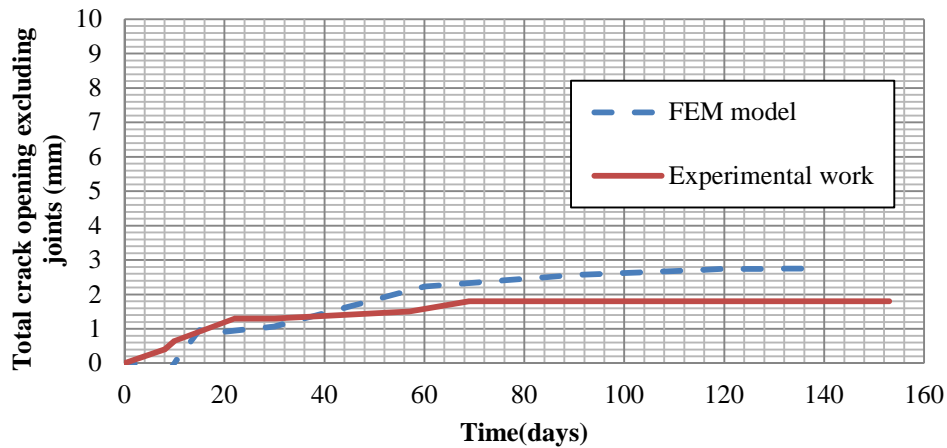


Figure 6.10: The crack opening width excluding joints in a 9 m joint spacing slab containing 5 kg/m³ fibres

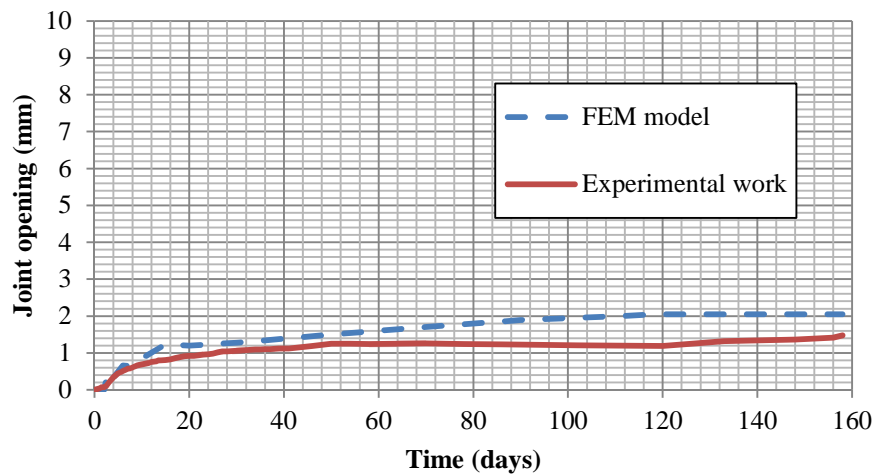


Figure 6.11: The average joint opening in a 9 m joint spacing slab containing 5 kg/m³ fibres

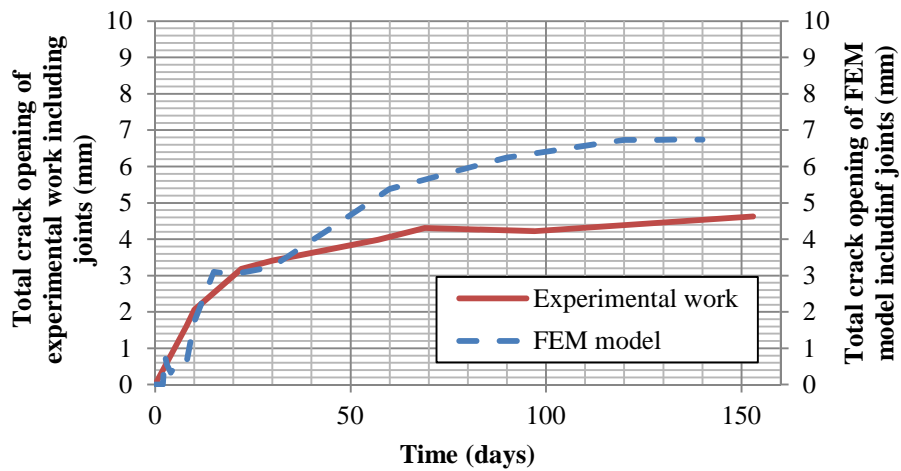


Figure 6.12: The total average crack opening in a 9 m joint spacing slab containing 5 kg/m³ fibres

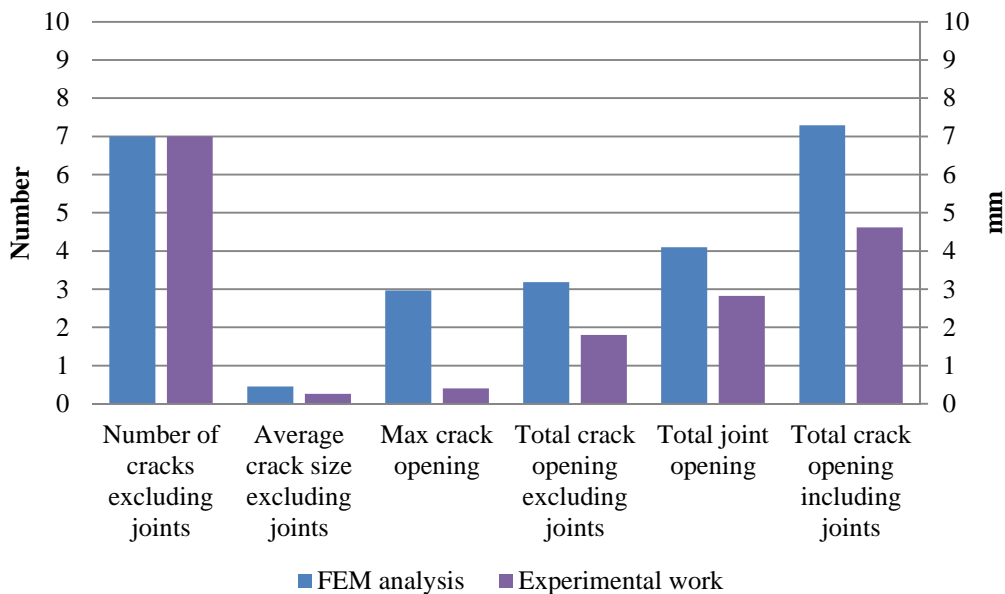


Figure 6.13: Combined FEM and experimental work results of a 9 m joint spacing slab containing 5 kg/m³ fibres (9,5,100,s)

6.4.3. OTHER RESULTS

The results shown in Figure 6.14 to 6.18 can also be used to verify the model. In this section the results of FEM analyses of 100 mm thick 4.5 m, 6 m and 9 m joint spacing slabs containing 5 kg/m³ are compared with the experimental work. A comparison between the FEM analysis and experimental work of a 100 mm thick 9 m joint spacings slab containing 8

kg/m³ fibres and a 150 mm thick slab containing 5 kg/m³ fibres is also shown. The development of the crack openings over time for the summarized results in Figure 6.14 to 6.18 can be seen in Appendix 6.

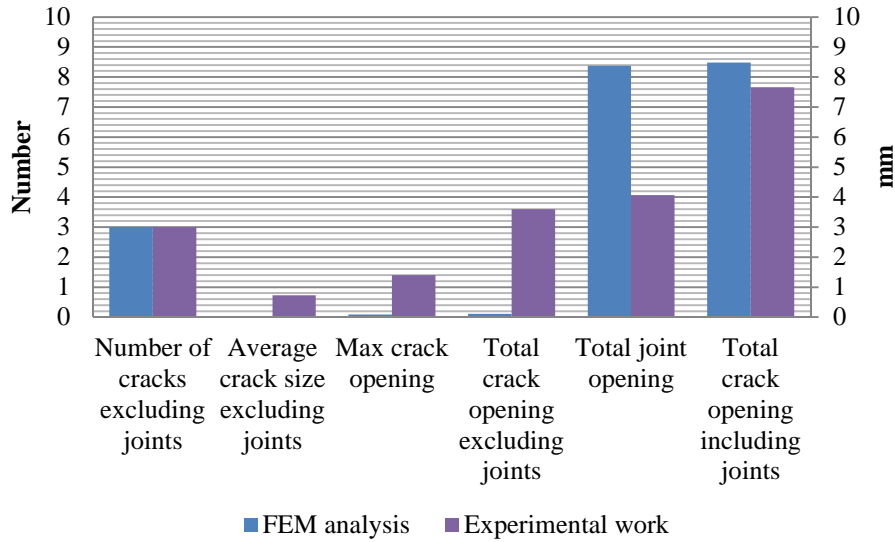


Figure 6.14: Combined FEM and experimental work results of a 9 m joint spacing slab containing 8 kg/m³ fibres (9,8,100,s)

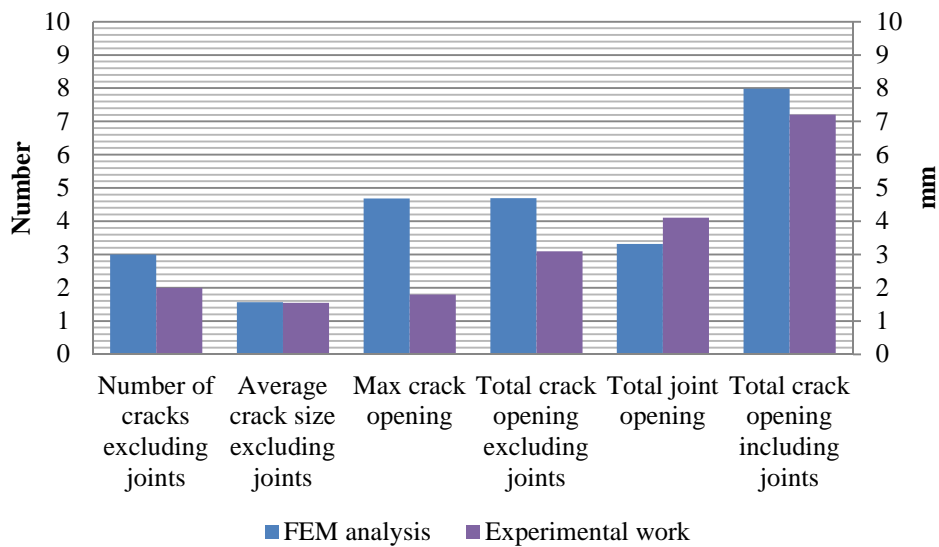


Figure 6.15: Combined FEM and experimental work results of a 9 m joint spacing slab containing 5 kg/m³ fibres (9,5,150,s)

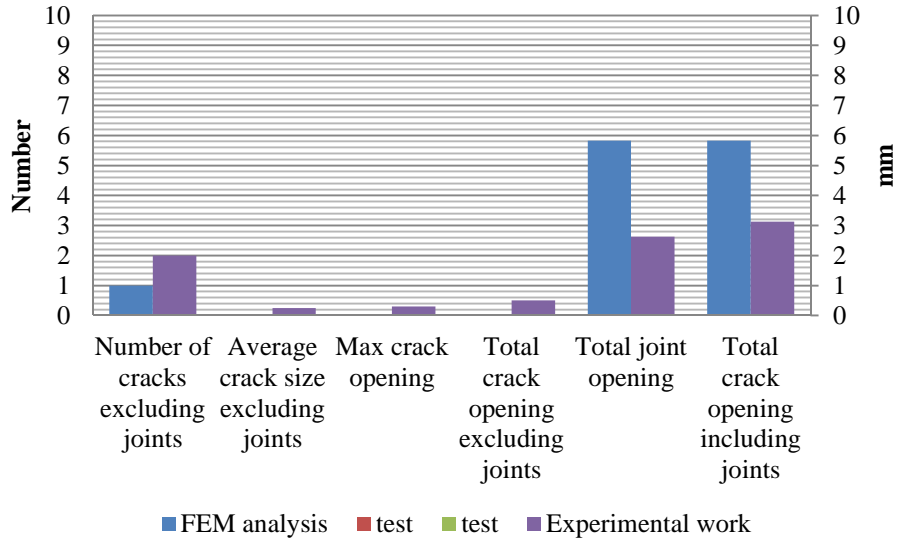


Figure 6.16: Combined FEM and experimental work results of a 4.5 m joint spacing slab containing 5 kg/m³ fibres (4.5,5,100,s)

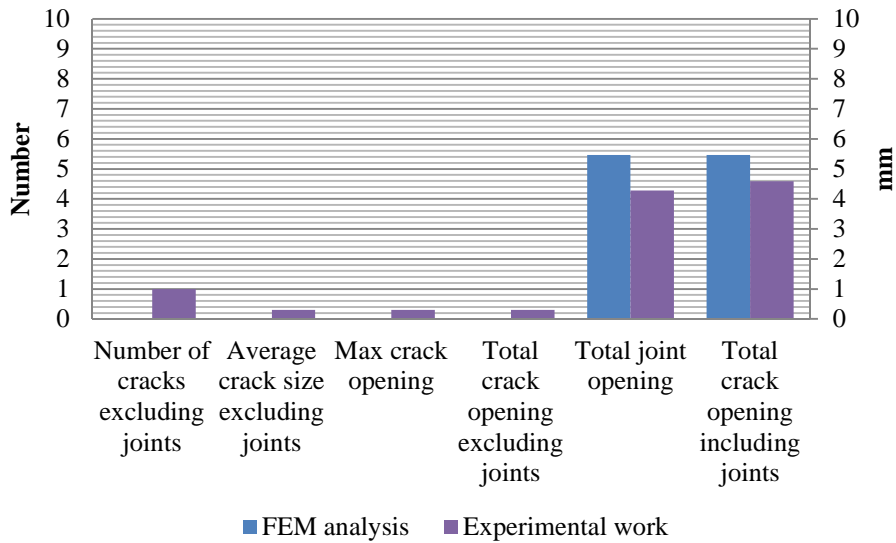


Figure 6.17: Combined FEM and experimental work results of a 4.5 m joint spacing slab containing no fibres (4.5,0,100,s)

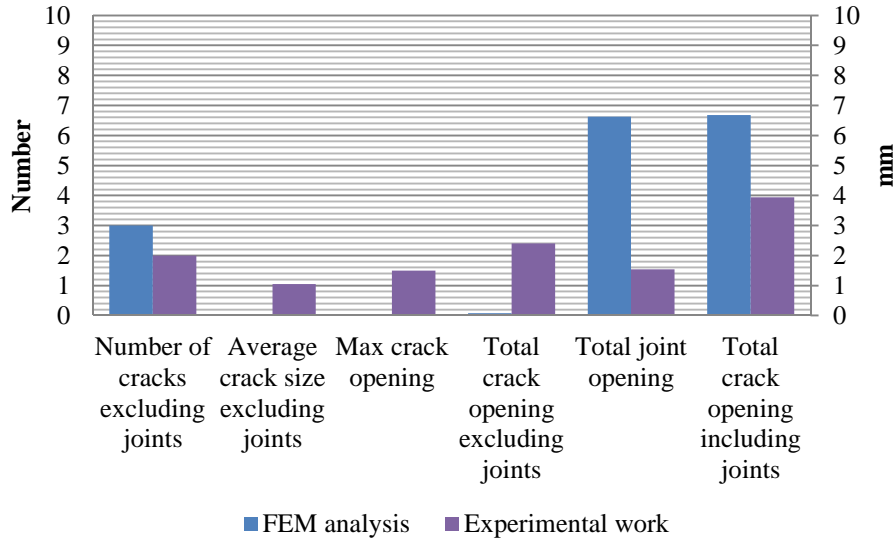


Figure 6.18: Combined FEM and experimental work results of a 6 m joint spacing slab containing 5 kg/m³ fibres (6,5,100,s)

6.4.4. JOINT OPENINGS

The average joint opening of a slab containing no fibres is compared to a slab containing 5 kg/m³ fibres in Figure 6.19. The FEM analysis of the same two slabs is also shown.

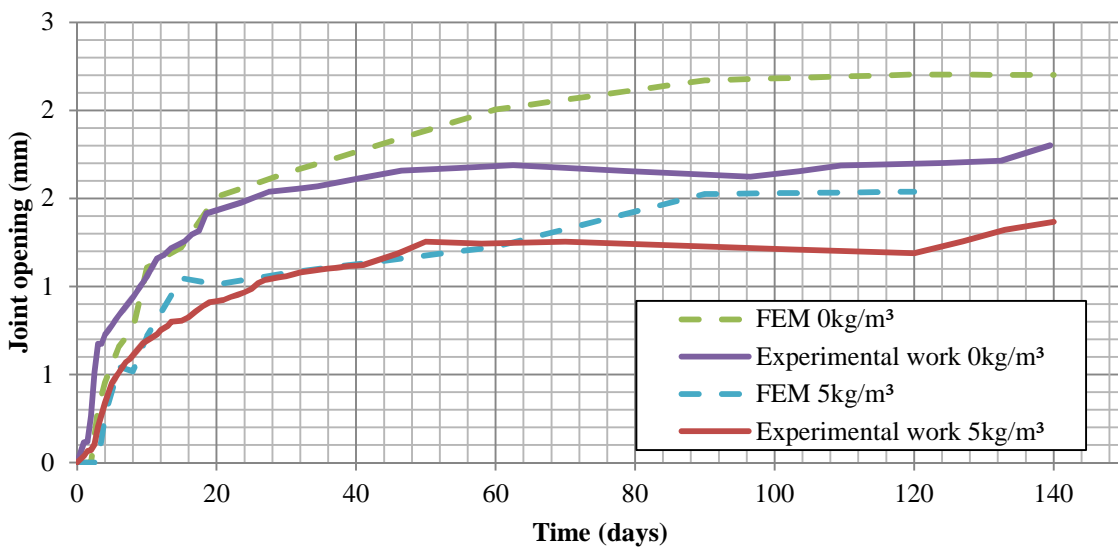


Figure 6.19: The average joint opening of 9 m joint spacing slabs containing 0 kg/m³ and 5 kg/m³ fibres

6.5. DISCUSSION

The number of cracks opened excluding joints, the average crack opening width and joint openings of the FEM analysis were compared with the experimental results to verify the accuracy of the FEM model. Firstly, a 100 mm thick, 9 m joint spacing slab containing no fibres was compared to a similar slab containing 5 kg/m³ fibres. This was done by first comparing the analysis with the experimental work for a slab containing no fibres where after the analysis and experimental work of a slab containing 5 kg/m³ were compared. Secondly, the FEM analyses representing five large scale experiments, all with different joint spacings, fibre content or slab thicknesses, were compared with the results of the experiments. These results were then used to establish the accuracy of the FEM model used in the analysis.

6.5.1. NUMBER OF CRACKS FORMED BETWEEN JOINTS

The first criteria for verification of the FEM model is the number of cracks formed between the saw cut joints. For a 9 m joint spacing slab with a thickness of 100 mm, containing either 0 kg/m³, 5 kg/m³ or 8 kg/m³ fibres, the same number of cracks opened in the analyses and the experimental work. Although similar numbers of cracks were formed, the maximum crack opening for a slab containing 5 kg/m³ fibres or less is much larger in the FEM analysis. This can be explained by the stochastic material distribution in the physical slabs, where due to the non-homogeneous behaviour of the concrete, cracks will form at random over the length of the slab. This is not the case for the FEM analysis, where it is noted that the first crack forms at an earlier stage in the centre of the slab. This crack width will increase until the tensile stresses in the slab reaches the tensile capacity of the concrete resulting in the next, much smaller crack. The same explanation can be used to clarify the difference in the FEM and experimental results of a 150 mm thick, 9 m joint spacing slab containing 5 kg/m³ fibres.

For a 9 m joint spacing slab containing 8 kg/m³ fibres the same number of macro cracks formed, but the maximum crack opening width is much smaller in the FEM analysis than in the experimental work. This is explained by the higher post cracking stress transfer over the crack plane in the model. With the increase in the fibres' volume the bridging effect of the fibres results in a higher stress transfer over the fibres. This means that instead of releasing

the tensile stress of the concrete after cracking, the stress remains in the concrete, resulting in more micro cracks forming. For the physical tests the stochastic distribution of the material creates weak spots in the concrete matrix resulting in some of the micro cracks opening to a greater extent to form macro cracks. Similar behaviour in the higher number of cracks opened and the larger maximum crack opening widths could be seen for 4.5 m and 6 m joint spacing slabs containing either 0 kg/m³ or 5 kg/m³ fibres. Since the tensile stresses in these slabs are lower, due to the shortened slab length, the cracks forming between the joints in the experimental work is due to the non-homogeneous nature of the physical materials.

The FEM model is expected to crack at an earlier stage than the experimental work. The reason for this is that the large scale test started at the day of casting, which included the curing time, the model did not take the curing time into account. Earlier cracking can also be because of the extent to which the friction increase differed between the model and the large scale tests. The reason for this difference is the effect of the environmental conditions and the soil sub-base. Perfect conditions are assumed in the model, resulting in all the cracks forming symmetrically at the same time. In the large scale test this was not the case as the cracks formed at the weakest point in the high stress zone, which lead to some cracks forming earlier than others. These cracks are likely to form at locations where poor compaction, poor stone distribution or an uneven base layer is present.

6.5.2. THE WIDTH OF THE CRACKS OPENED

The lower total crack opening including the joint openings of the experimental work that is noticed in all the comparisons, is due to the fact that in the FEM analysis the formation of micro cracks does not occur. In the experimental work some non-visible micro cracks formed that reduced the size of the macro cracks, resulting in a lower total crack opening width. Creep in the concrete also contributed in reducing the total crack width by relaxing some of the stresses in the concrete. Both the long and short term creep was ignored as the effect of creep falls outside the scope of this study.

The behaviour of the joint openings is controlled by the friction between the soil and concrete and the amount of cracks that opened between the joints. When adding all the crack opening widths of the analysis together, the opening over time follows the same trend line as the total

crack opening of the experimental work. This means that the same shrinkage deformation takes place in both the analysis and the experiment, which should be the case, since the shrinkage strain of the experiment was added to the model using the shrinkage strain over time graphs, obtained by the experiment. These graphs were entered into the model using a discrete shrinkage function. This also indicates that for the analysis the friction between the soil and concrete can be assumed to be acceptable.

Throughout the analysis small cracks formed on the bottom part of the concrete due to the curling effect, discussed in Section 2.1.3. This takes place until the stresses in the concrete become larger than the tensile capacity of the concrete at the bottom surface, resulting in the formation of cracks. This behaviour could not be measured in the experimental work but should be investigated. The same curling effect is also visible in the experimental work, raising the question on which surface of the slab do the cracks originate. A similar crack pattern for the cracks on the top surface of the concrete is seen, with the first crack occurring in the centre of the 9 m slab, followed by second and third cracks forming between the joints and the centre crack.

6.5.3. THE JOINT OPENINGS

The joint openings of the FEM analyses are in almost all the cases larger in size compared to the experimental work. There are two potential reasons for this. The first possibility is that the fracture energy entered into the model might be lower than the actual fracture energy in the experiments. This could be the case as the fracture energy used in the model was determined by the Wedge Splitting Test that uses a relatively small test sample compared to the dimensions of the experimental work. With the lower fracture energy it would seem that the fibres do not hold the joints together to the same extent as in the experimental work. But with an increase in fibre volume there will be a reduction in the joint opening. The second possibility for the larger joint openings is that the friction between the soil and the concrete could be lower in the model resulting in cracks opening wider. It could also be possible that the shrinkage strain entered into the model is higher than the actual shrinkage strain in the experiment. This is possible as the shrinkage entered into the model was measured from a shrinkage test that is conducted on a test specimen that is relatively small compared to that of the experiment. The exception in this is the 150 mm thick, 9 m joint spacing slab that

contained 5 kg/m³ fibres. This slab showed some unexpected results that could not be explained without additional research.

It should be noted that due to the ideal circumstances of the analysis the joints opened exactly the same on both sides of the slab. This will never be the case in reality as the joint openings are dependent on the shrinkage in the concrete matrix, the restraint of the concrete and the environmental effects at the location of the joint. Temperature effects are not taken into account in the analysis. This could be done with coupled analysis by using the FEM software with its coupling function. Further research could be conducted on the effect of temperature by means of a phase analysis in the current model. This was ignored in this study due to time constraints and because the exact shrinkage was used, taking temperature change into account to some extent.

6.5.4. THE AVERAGE CRACK OPENING WIDTHS

The average crack opening width excluding joints, showed almost similar results for most of the FEM analyses as well as the experimental works. This gives a good indication that the FEM model allowed for accurate cracking formation. The uncontrolled factors in the analysis and physical environment did not have an impact on the average crack opening width excluding joints. The only area where these results are not similar are in the 4.5 m and 6 m joint spacing slabs where the FEM analyses refrained from cracking, due to the low tensile stresses in the concrete after the joints' cracks. In the experimental work cracks could be due to the non-homogeneous nature of the concrete or sub-base.

6.6. CONCLUDING SUMMARY

A FEM model was developed to analyse the effects of macro polypropylene fibres in a concrete slab on grade. Seven analyses were performed, with different material properties, slab thickness and joint spacings. The results of the analyses were then compared to the results obtained with the large scale test in Chapter 5.

From the comparison it can be concluded that the FEM model gives a fairly accurate representation of the average crack formation in the experimental work. It should be noted that the behaviour of the concrete slab in reality will never be uniform for all slabs on grade, since the behaviour is highly dependent on the concrete matrix, the environmental conditions, the reinforcement, curing and the friction between the soil and the concrete.

The model is verified to work for the representation of the slabs on grade used in the experimental work. The model will now be used to analyse the effects of different fibre dosages and saw cut joint spacings in slabs on grade.

CHAPTER 7: FEM MODEL RESULTS

The FEM model described in Chapter 6 can now be used to analyse different parameters of slabs on grade. These parameters include fibre dosages, slab thicknesses, the spacing between the saw cut joints and the type of interface friction between the soil and the concrete. Table 7.1 shows all the analyses executed and the results are given in the following section. The results of the analyses are compared in terms of the effect the different parameters have on the maximum crack width and the total crack width of a slab on grade. The code used to define each analysis, as seen in Table 7.1, first indicates the length of the slab between saw cut joints, then the fibre dosage followed by the thickness of the slab and lastly, the friction between the concrete and sub-base where p stand for plastic and s stands for soil.

Table 7.1: The analyses conducted

Code	Distance between joints	Fibres			Thickness (mm)		Friction	
		0 kg/m ³	5 kg/m ³	8 kg/m ³	100m m	150m m	Soil	Plastic
	m							
9,0,100,s	9							
9,0,100,p	9							
9,0,150,s	9							
9,0,150,p	9							
9,5,100,s	9							
9,5,100,p	9							
9,5,150,s	9							
9,8,100,s	9							
4.5,0,100,s	4.5							
4.5,0,100,p	4.5							
4.5,0,150,s	4.5							
4.5,5,100,s	4.5							
4.5,5,100,p	4.5							
4.5,5,150,s	4.5							
4.5,8,100,s	4.5							
6,0,100,s	6							
6,5,100,s	6							

7.1. RESULTS

The results of all the conducted analyses are divided into four categories. Each category is used to establish the effect of different parameters such as the joint spacings, the fibre content, the slab thickness and the friction between the soil and the concrete. To fully evaluate these effects of polypropylene fibres, the results of each analysis is divided into five groups. Firstly, the number of cracks were compared, followed by the maximum crack width between the saw cut joints and the total crack opening width. The total crack width was divided into the total crack width between the joints and the total joint opening width. These five groups of each analysis are then compared to the other analyses.

7.1.1. DIFFERENT JOINT SPACINGS

Joint spacings of 4.5 m, 6 m and 9 m were analysed and compared. Figure 7.1 indicates the difference in total crack opening, maximum crack width and number of cracks for a 4.5 m, 6 m and 9 m joint spacing, all containing no fibres. Figure 7.2 and 7.3 also show the same comparisons, but for a 4.5 m, 6 m and 9 m joint spacing with a fibre dosage of 5 kg/m³ and 8 kg/m³.

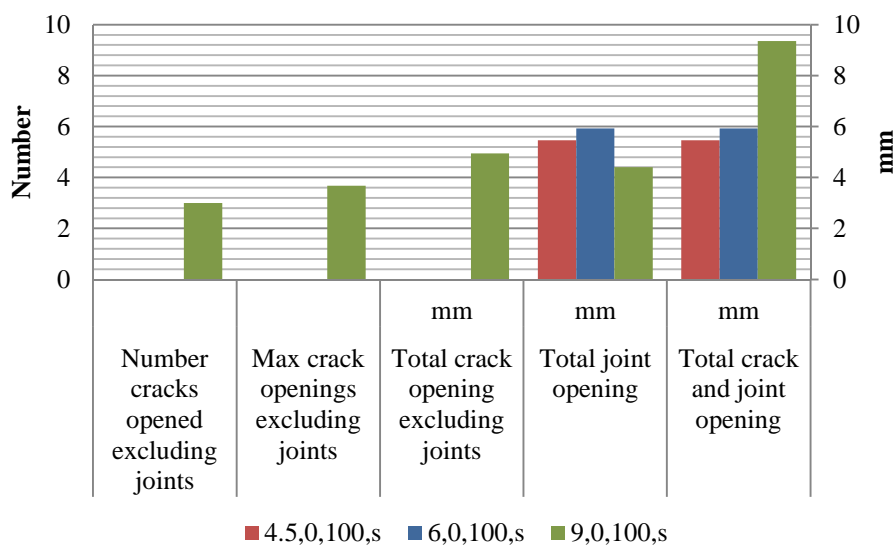


Figure 7.1: The crack opening of 4.5 m, 6 m and 9 m joint spacings containing no fibres

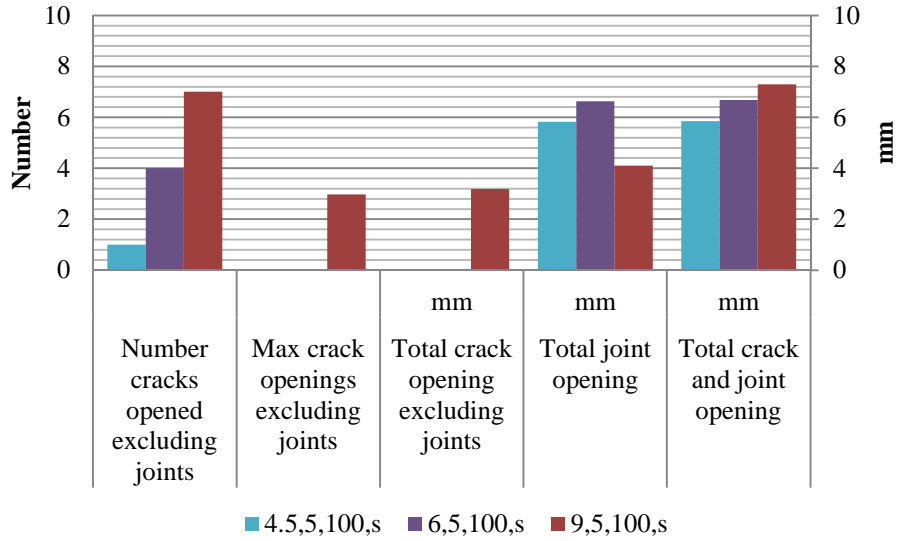


Figure 7.2: The crack opening of 4.5 m, 6 m and 9 m joint spacings containing 5 kg/m³ fibres

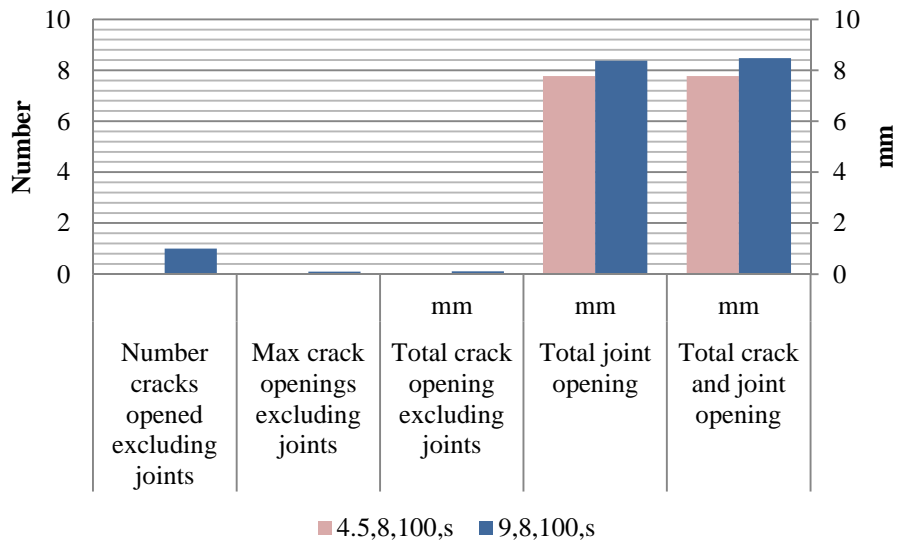


Figure 7.3: The crack opening of 4.5 m and 9 m joint spacings containing 8 kg/m³ fibres

Figure 7.4 and 7.5 indicates the total crack width; maximum crack width between joints: the number of cracks opened in a 4.5 m and 9 m slab with a thickness of 150 mm. Slabs containing no fibre were compared to slabs containing 5 kg/m³ fibres.

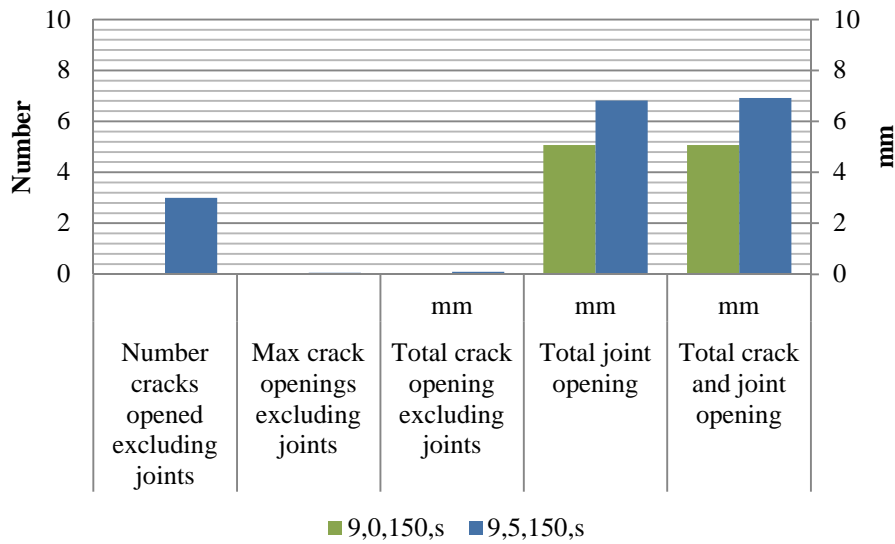


Figure 7.4: The crack opening of 9 m joint spacing slab with a slab thickness of 150 mm containing no fibres or 5 kg/m³ fibres

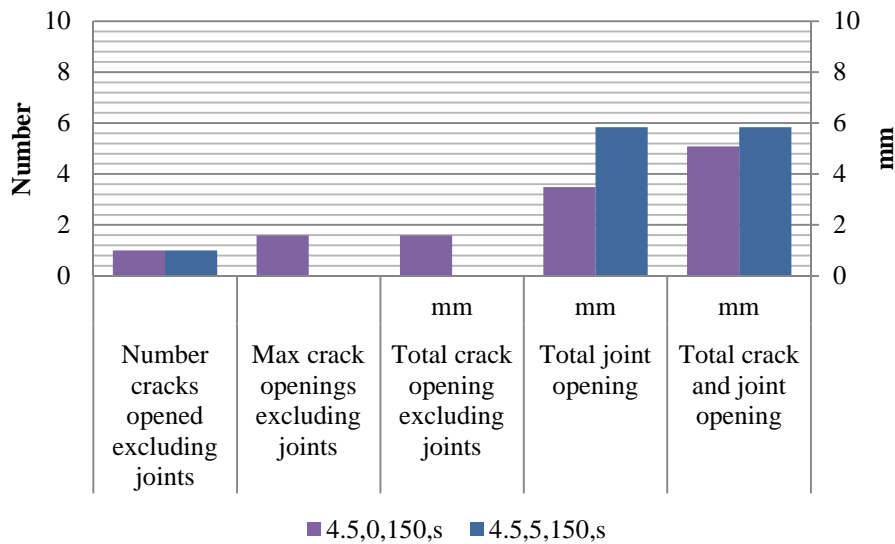


Figure 7.5: The crack opening of 4.5 m joint spacing slab with a thickness of 150 mm containing no fibres or 5 kg/m³ fibres

7.1.2. DIFFERENT FIBRE DOSAGES

The effect of different fibre dosages on the crack width in slabs on grade are given in this section. This is done by using different fibres dosages in slabs with the same slab thickness, joint spacing and interface friction. Figure 7.6 shows a 9 m joint spacing slab with a thickness of 100 mm and a sand sub-base under the concrete. Fibre dosages of 0 kg/m³, 5 kg/m³, and 8 kg/m³ were compared. Figure 7.7 and 7.8 give similar results for a 4.5 m and 6 m joint spacing slab.

Figure 7.9 shows the crack distribution of a slab containing no fibres. It is then compared with Figure 7.10 and 7.11 showing a slab containing 5 kg/m³ and 8 kg/m³ fibres.

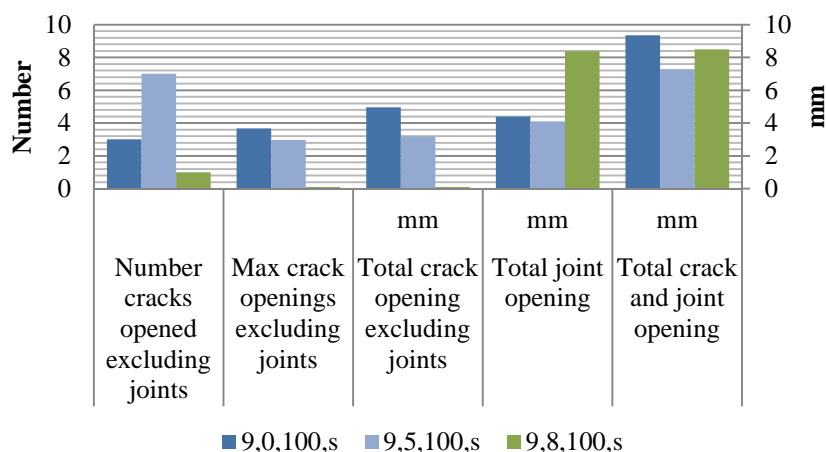


Figure 7.6: Comparing the crack openings of 9 m joint spacing slabs containing different fibre dosages

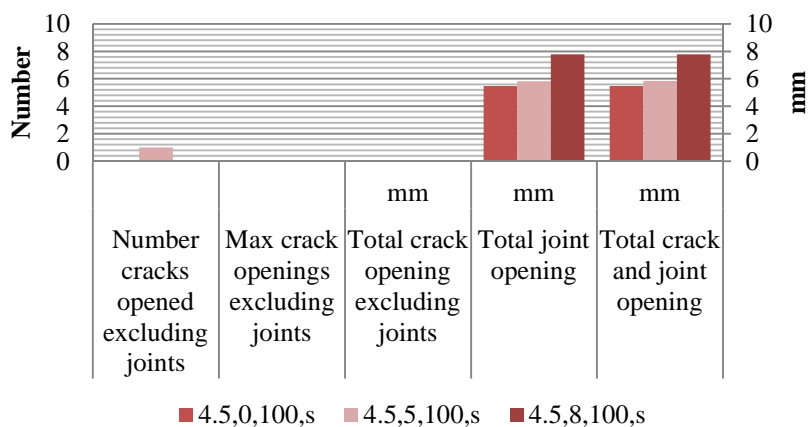


Figure 7.7: Comparing the crack openings of 4.5 m joint spacing slabs containing different fibre dosages

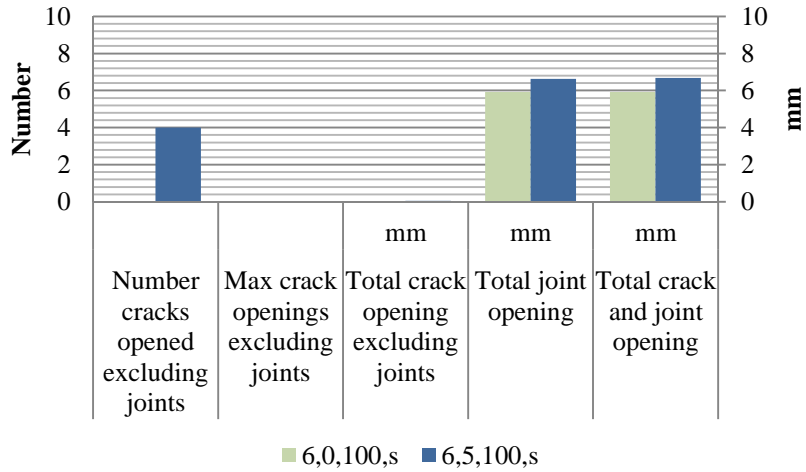


Figure 7.8: Comparing the crack openings of 6 m joint spacing slabs containing different fibre dosages

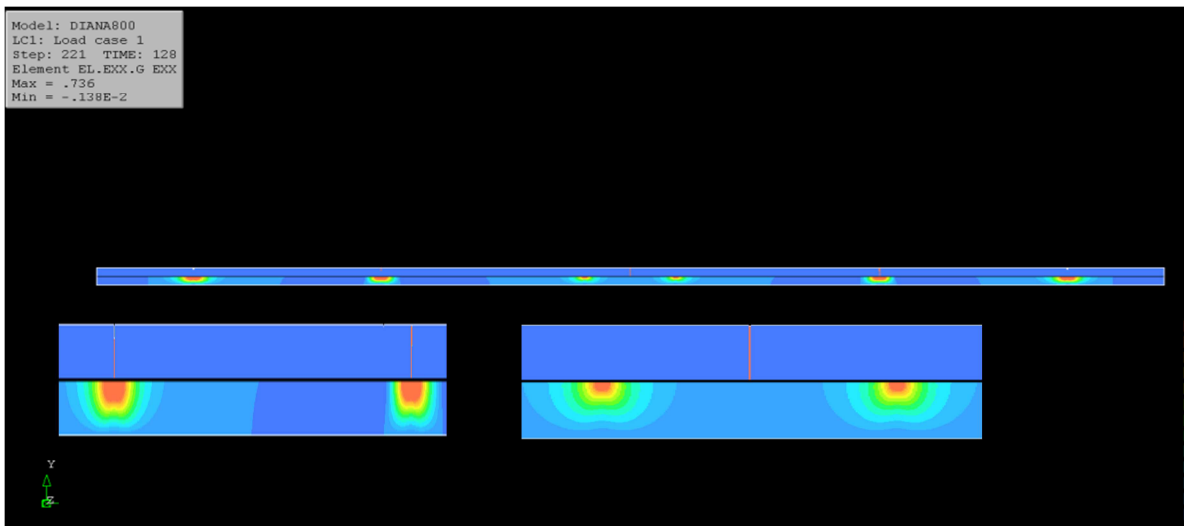


Figure 7.9: The crack distribution in FEM for a 9,0,100,s slab

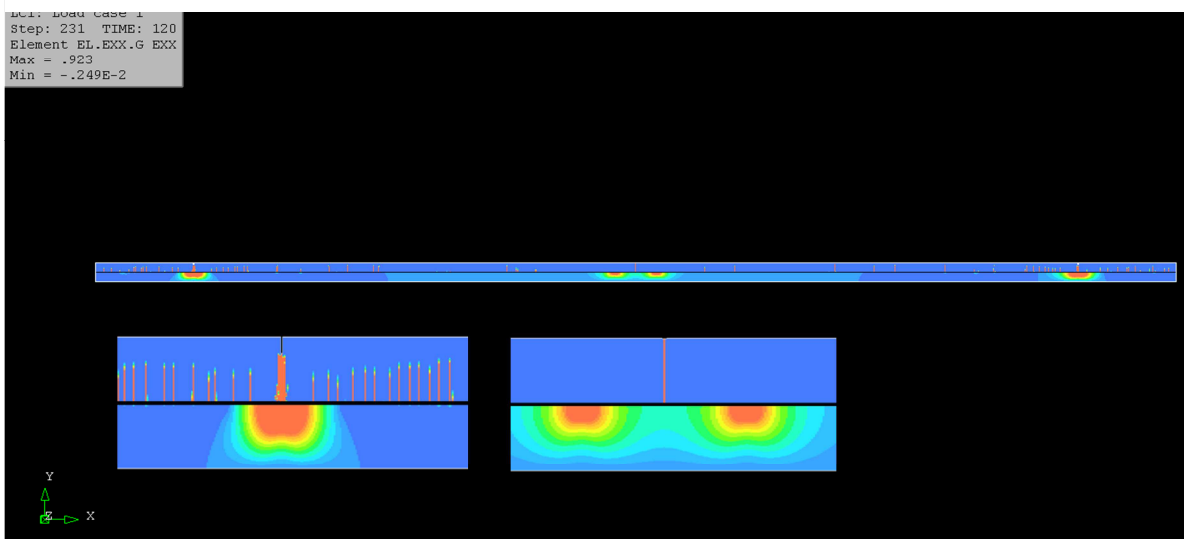


Figure 7.10: The crack distribution in FEM for a 9,5,100,s slab

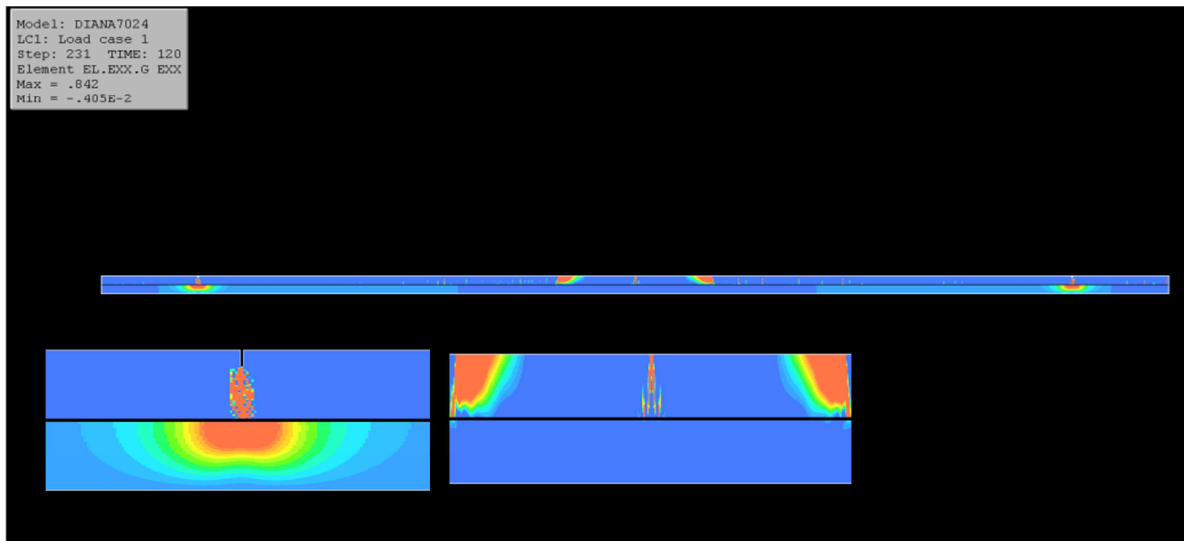


Figure 7.11: the crack distribution in FEM for a 9,8,100,s slab

7.1.3. DIFFERENT SLAB THICKNESSES

The thickness of the slab can have an effect on the extent of crack formation in a slab on grade. Figure 7.12 and 7.13 shows the results of two 9 m joint spacing slabs with a thickness of either 100 mm or 150 mm. The slabs contained a dosage of 0 kg/m³ or 5 kg/m³ fibres.

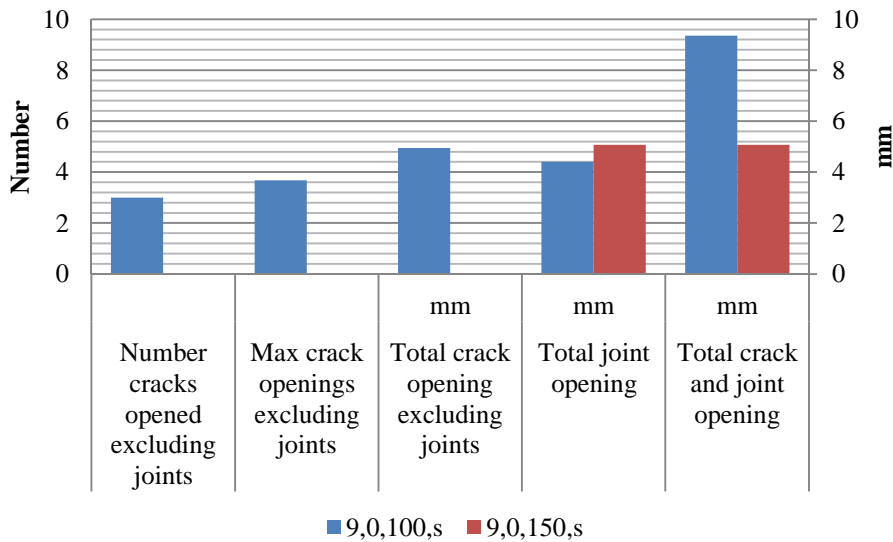


Figure 7.12: Comparing the crack openings of 100 mm thick 9 m joint spacing slabs with a 150 mm thick 9 m joint spacing slab, both containing no fibres

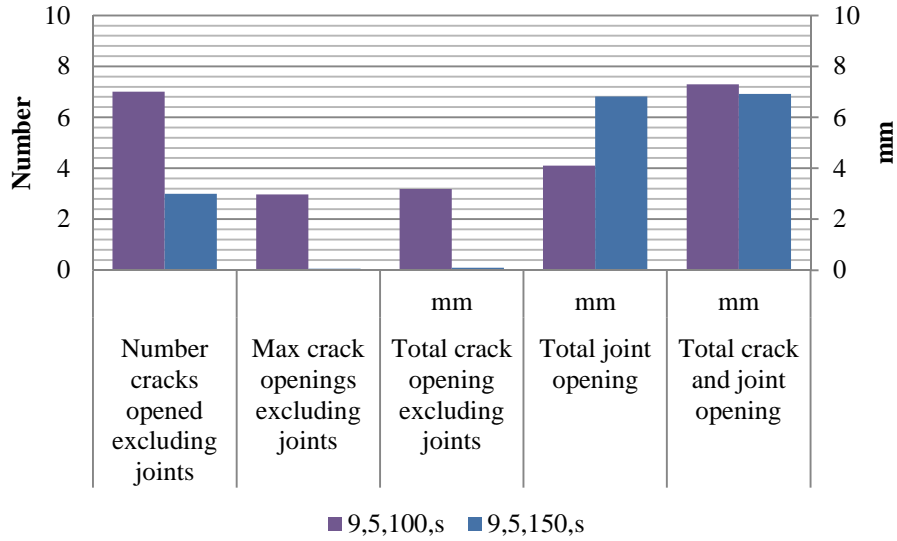


figure 7.13: comparing the crack openings of 100 mm thick 9 m joint spacing slabs with a 150 mm thick 9 m joint spacing slab, both containing 5 kg/m³

Figure 7.14 and 4.15 show the results for analyses conducted on a 4.5 m joint spacing slab with a thickness of either 100 mm or 150 mm.

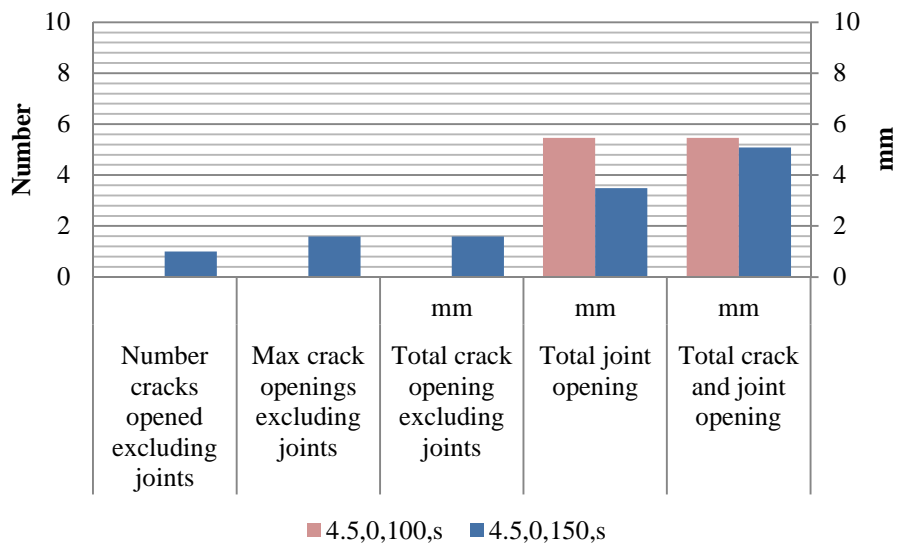


Figure 7.14: Comparing the crack openings of 100 mm thick 4.5 m joint spacing slabs with a 150 mm thick 4.5 m joint spacing slab, both containing no fibres

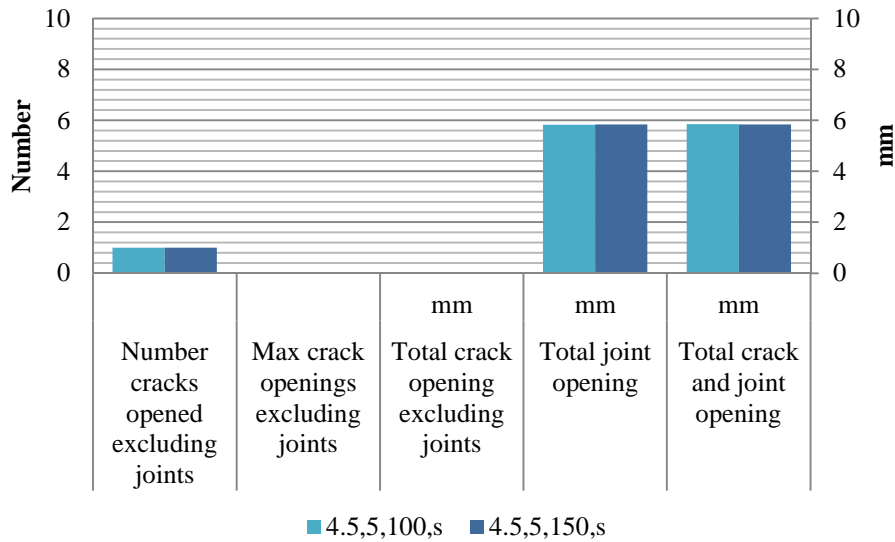


Figure 7.15: Comparing the crack openings of 100 mm thick 4.5 m joint spacing slabs with a 150 mm thick 4.5 m joint spacing slab, both containing 5 kg/m³

7.1.4. DIFFERENT FRICTION BETWEEN SOIL AND CONCRETE

The analyses were conducted first with a high friction between the concrete and the soil representing the behaviour of the concrete resting on a sand sub-base. Secondly, it was assumed that there is a plastic sheet between the concrete and the soil resulting in a lower friction coefficient. Figure 7.16 and 7.17 displays the results of a 9 m joint spacing slab with a fibre dosage of 0 kg/m³ or 5 kg/m³. The two frictions discussed above are compared in Figure 7.16 and 7.17, where “s” is the concrete on sand and “p” is the concrete on plastic sheeting. Figure 7.18 and 7.19 shows similar results for a 4.5 m joint spacing slab.

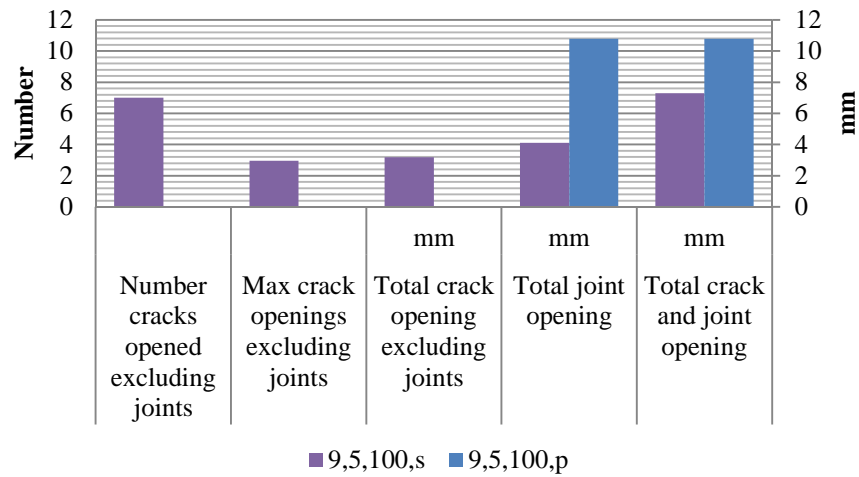


Figure 7.16: Comparing the crack openings of 100 mm thick, 9 m joint spacing slab resting on either soil or plastic, both containing 5 kg/m³

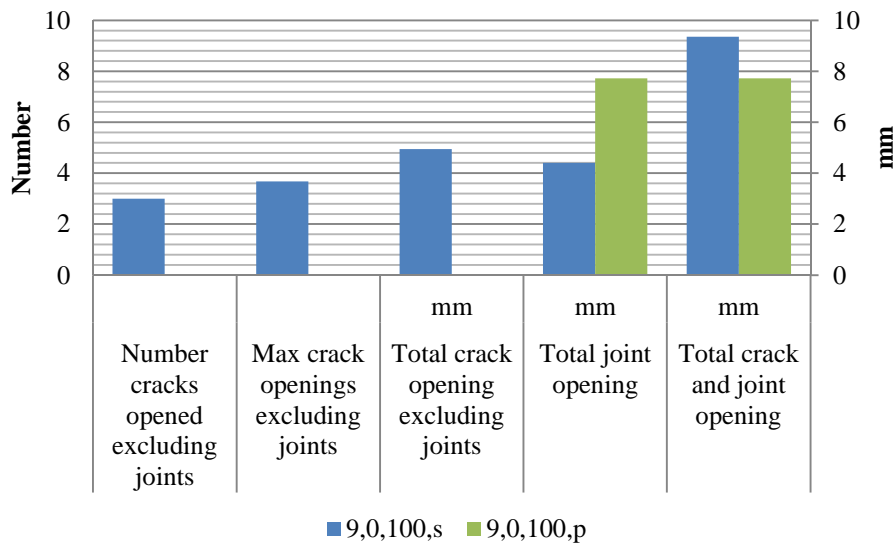


Figure 7.17: Comparing the crack openings of 100 mm thick, 9 m joint spacing slab resting on either soil or plastic, both containing no fibres

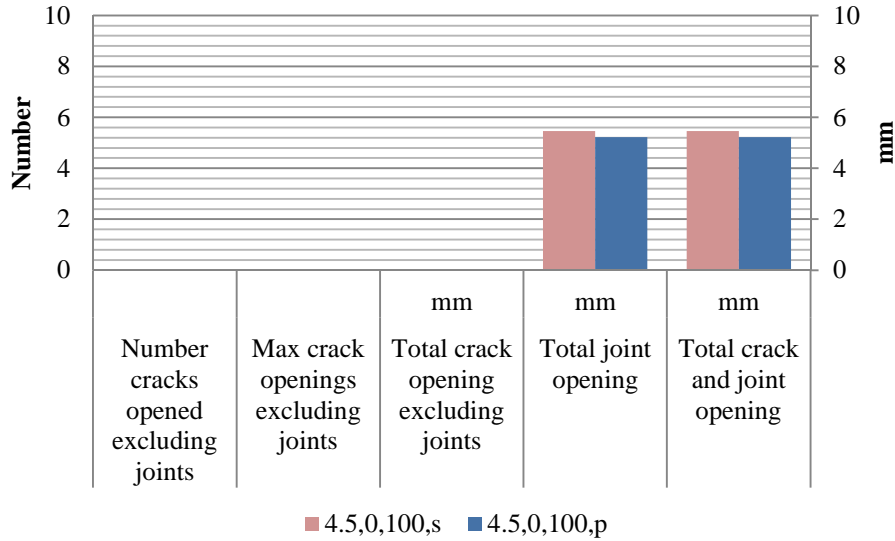


Figure 7.18: Comparing the crack openings of 100 mm thick, 4.5 m joint spacing slab resting on either soil or plastic, both containing no fibres

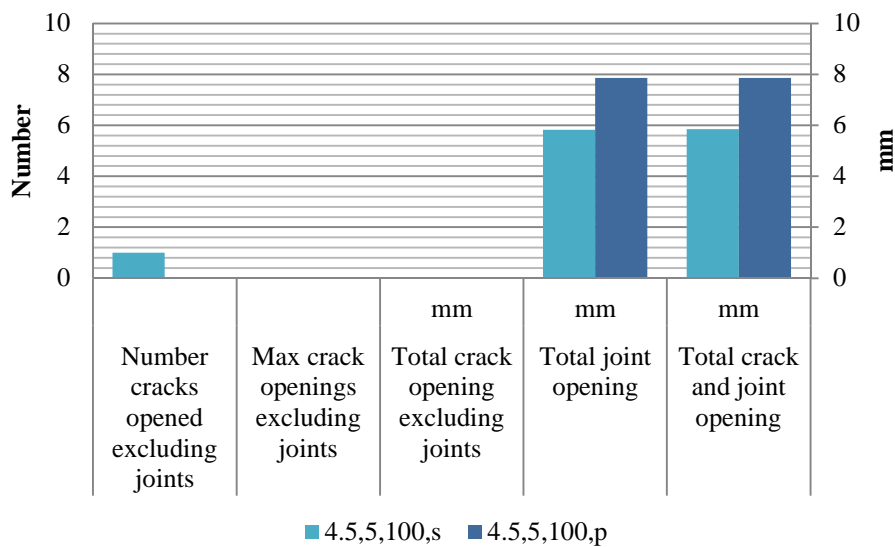


Figure 7.19: Comparing the crack openings of 100mm thick, 4.5 m joint spacing slab resting on either soil or plastic, both containing 5 kg/m³

7.2. DISCUSSION

The results of seventeen FEM analyses were compared to estimate the effect of the fibre dosage, slab thickness, spacing between the joints and the degree of friction between the concrete and the soil. These factors influenced the maximum crack width between joints, the total crack opening and the number of cracks that opened in a slab on grade.

7.2.1. THE EFFECT OF THE SIZE OF THE SPACING BETWEEN SAW CUT JOINTS

Firstly, the effects of three different joint spacings were compared. These spacings are 4.5 m, 6 m and 9 m, representing slabs with these lengths between the saw cut joints. Slabs containing no fibres with the joints spaced 4.5 m or 6 m apart have no crack opening between the joints. Since these slabs only cracked at the joints, with their main purpose that of initiating cracks to reduce tensile stresses, it is assumed that these slabs perform as anticipated by design guidelines. When 5 kg/m^3 macro polypropylene fibres were added to the concrete a crack formed between the joints with a spacing of 4.5 m. This is discussed below. In the 9 m joint spacing slab, containing no fibres, three cracks formed between the joints with a large maximum crack width and total crack width. This supports the behaviour of concrete slabs on grade in practice, exhibiting that the use of slabs with a joint spacing larger than 6 m will result in macro-cracks forming between the joints.

When the same three slabs are analysed with a fibre dosage of 5 kg/m^3 , cracks are found between the joints of all three slabs. The number of visible cracks formed in the slabs amplified with an increase in slab length. This increase in the number of crack formations leads to a decrease in the size of the total crack opening width between the joints. This crack increase also means that the joint opening width decreases, defeating the purpose of the joints. This behaviour can be explained by the bridging ability of the fibres after a crack has formed. When the cracks form at the joints, the fibres hold the cracks together, resulting in a restraint against shrinkage in the slab. Consequently the tensile stresses in the slab increases, leading to high stresses between the joints that can initiate crack formation when exceeding the tensile capacity of the concrete. The same bridging effect starts taking place across the new crack, again resulting in a small stress release in the slab. A post cracking stress transfer takes place over the crack plane in the concrete. Small cracks will form as long as the tensile stress is greater than the tensile capacity of the concrete. As a result the maximum crack widths in the slabs are small in comparison to that of the slabs containing no fibres.

When the fibre dosage is increased to 8 kg/m^3 the bridging effect of the fibres is much higher, resulting in a higher post stress transfer, where the next crack forms almost at the same time as the previous crack due to the stress transfer. Consequently there is a shift in crack formation between micro-cracks and macro-cracks, which implies that no single crack formed between the joints. Instead various micro-cracks formed all over the length of the

slabs during the analyses. Due to the stochastic distribution of the material properties of the physical slab, more macro-cracks will occur in the physical test.

7.2.2. THE EFFECT OF THE FIBRE DOSAGE ON THE CRACK WIDTHS

The analysis of conventional concrete in a 9 m joint spacing slab with a thickness of 100 mm and a sand sub-base layer was compared with the analysis of a similar slab containing a fibre dosage of 5 kg/m³ and 8 kg/m³. Compared to the slab containing 5kg/m³ fibres the conventional concrete slab had a larger total crack opening excluding the joint, a larger joint opening and a larger total crack opening including the joints. It did have fewer cracks opened between the joints but on average the cracks opened to a greater magnitude. This can be explained by the bridging ability of the fibres discussed above. In the analysis of a slab containing 8 kg/m³ fibres the quantity of cracks between the joints declined and no large cracks formed in the slab. Because of the low crack forming between the joints, the joints opened to a greater extent than the slab made from conventional concrete and 5 kg/m³ PPFRC. The same analyses were done for a 4.5 m and 6 m joint spacing slab showing results similar to a 9 m joint spacing slab containing 5 kg/m³ fibres. Apart from a minor increase in the amount of cracks forming between the joints, the use of polypropylene fibres in 4.5 m and 6 m joint spacing slabs had no real impact on the crack formation or total crack width.

7.2.3. THE EFFECT OF THE SLAB THICKNESS ON THE CRACK WIDTH

For a 9 m joint spacing slab containing no fibres the analysis of the 100 mm thick slab was compared to the analysis of a 150 mm slab. The 100 mm slab had more cracks forming between the joints and a larger total crack width. The 150 mm slab revealed that the increase in slab thickness resulted in fewer cracks forming and a lower joint opening width. When the same analyses were conducted with a fibre dosage of 5 kg/m³, the 150 mm slab tended towards a lower quantity of crack forming between the joints, but the maximum crack width and the total crack width were larger. These results are not fully understood and additional research is required to explain this behaviour. The slab thickness had no significant effect on the crack formation for a 4.5 m joint spacing slab containing no fibres and 5 kg/m³ fibres.

7.2.4. THE EFFECT OF FRICTION ON THE WIDTH OF THE CRACKS

Lastly, the effect of the friction between the soil and the concrete was analysed. When looking at a 9 m joint spacing slab containing no fibres the slab with a soil sub-base had three cracks formed between the joints, with a larger total crack opening than that of a slab resting on a plastic sheet having no cracks opened between the joints. The sheet reduced the friction between the soil and the concrete. This reduction is preferred, since the friction between the concrete and the soil is the cause of an increase in tensile stresses in the slab, resulting in crack formation. An increase in the fibres' dosage in the concrete had no effect on the cracking formation when plastic sheet was used. All the slabs cracked at the joints and shrunk freely without being restrained to a great enough extent for high tensile stresses to form in the slab. This meant that apart from the joint cracks there were no cracks in the slabs resting on plastic sheets.

7.2. CONCLUDING SUMMARY

The FEM analyses of a 4.5 m, 6 m and 9 m joint spacing slab containing 0 kg/m³, 5 kg/m³ or 8 kg/m³ fibres were conducted to determine the effect of the macro polypropylene fibres on cracking formation. The conclusion can be made that the use of these fibres had no significant improvement in decreasing the drying shrinkage crack formation in slabs on grade. The fibres in a 9 m joint spacing slab resulted in a decrease in the joint openings that consequently lead to higher tensile stresses in the slab. Additional cracks formed because of the high tensile stress compared to that of a slab containing no fibres. Although there was an increase in the number of cracks formed, the crack width was drastically reduced due to the bridging ability of the fibres.

The addition of macro polypropylene fibres in 4.5 m and 6 m joint spacing slabs have no real impact on the crack formation or total crack width. Thicker slabs or plastic sheeting under the concrete will help to mitigate the formation of cracks.

CHAPTER 8: CONCLUSION

The purpose of this study was to determine the effect of South African produced macro polypropylene fibres on drying shrinkage cracks that form in slabs on grade. This effect was then applied to investigate the possibility of increasing the spacings between the saw cut joints in slabs on grade. Firstly, a full parameter study was done on fibre reinforced concrete, determining the fibres' influence on the compressive strength, shrinkage, tensile strength and fracture strength of the concrete. Then large scale tests were conducted to determine the effect of the fibre reinforced concrete on slabs on grade. The results of the large scale tests were then compared to a FEM analysis designed to replicate the behaviour of the experimental work. The following conclusions were made.

8.1. THE PARAMETER STUDY

- The use of high volumes macro polypropylene fibres only relatively increased the compressive strength of conventional concrete. This increase is not significant enough to induce structural advantages when using macro polypropylene fibres.
- The use of the fibres increased the flexural strength of the conventional concrete.
- The drying shrinkage of the concrete is reduced with the use of macro polypropylene fibres, but only up to a fibre dosage of 5 kg/m^3 . This reduction in drying shrinkage is relatively low.
- The fracture energy of conventional concrete is increased with the increase in the macro polypropylene fibre dosage.

8.2. LARGE SCALE TEST

- The addition of macro polypropylene fibres increased the number of drying shrinkage cracking over the length of a slab on grade compared to that of a slab containing no fibres.
- The increased number of cracks had a smaller average crack width than the cracks formed in a similar slab containing no fibres. Although the use of macro polypropylene fibres reduced the size of the macro crack width, it lead to the formation of additional cracks.
- The use of polypropylene fibres had no significant effect on the slabs with joint spacings of 4.5 m and 6 m.

8.3. FINITE ELEMENT ANALYSIS

- The use of polypropylene fibres in 4.5 m and 6 m joint spacing slabs had no real influence on the crack formation or total crack widths compared to that of a conventional concrete slab.
- Plastic sheeting between the soil and the concrete resulted in no cracks forming between the joints. The use of macro polypropylene fibres had no influence when plastic sheeting was used.
- With the increase in joint spacing the macro polypropylene fibres restrained the joints from opening to a great enough extent to decrease the high tensile stresses in the slab. The effect of these high tensile stresses was crack forming between the joints. As the concrete cracks the stresses in the concrete are transferred by the fibres as it bridges the crack. Instead of releasing the tensile stresses in the concrete, the crack now transfers the stresses and although the fibres hold the crack together and reduce the crack width, the still high tensile stresses lead to additional cracks forming. Using up to 5 kg/m^3 macro polypropylene fibres help control the width of macro cracks in a slab on grade but it can lead to an increase in the number of macro cracks forming.

- Using fibre dosages higher than 5 kg/m^3 resulted in higher post stress transfer over the crack plains, therefore reducing the ability of the joint to open, due to shrinkage that increased the extent of cracks forming over the length of the slab.
- It can be concluded, based on the finite element analyses and the experimental work, that adding macro-synthetic fibres to concrete will increase the number of cracks between joints, especially if the joint spacing is increased. Using plastic sheet does however prevent cracks from forming between the joints, even if the joint spacing is increased to 9 m.

8.4. FUTURE RESEARCH

- With the increase in macro polypropylene fibre dosage it is expected that the drying shrinkage of the concrete decreases. This was not the case for tests done with a fibre dosage of 8 kg/m^3 where higher shrinkages than that of the conventional concrete were obtained. Additional research is required to explain this behaviour.
- More large scale tests would give a better understanding of the behaviour of the PPFRC, but due to the scale of the test and the time constraint of this study only a limited amount of tests could be completed. More research is required to explain the behaviour of slabs thicker than 100 mm.
- For a 9 m joint spacing slab containing no fibres, the analysis of the 100 mm thick slab is compared to the analysis of a 150 mm slab. The 100 mm slab had more cracks forming between the joints and a larger total crack opening width. The 150 mm slab indicated that the increase in slab thickness resulted in better crack formation behaviour and a reduction in the joint opening widths. When the same analyses were conducted with a fibre content of 5 kg/m^3 , the 150 mm slab did have a decrease in the number of cracks forming between the joints, but the maximum crack opening width, and total crack opening width were larger. This behaviour is not fully understood and should be investigated.

BIBLIOGRAPHY

- ACI Committee 360. (2006). *Design of Slabs-on Grade ACI360R-06*. American Concrete Institute.
- 201, S. (2002). *Sieve analysis, fines content and dust content of aggregates*. SABS.
- ACI 209R-92. (1997). *Prediction of creep, shrinkage and temperature effects in concrete structures*. ACI Committee 209.
- ACI Committee 209. (2008). *ACI 209.2R-08 Guide for Modeling and Calculating Shrinkage and Creep in Hardened Concrete*. Farmington Hills: American Concrete Institute.
- ACI Committee 544. (2002). *ACI 544.1R-96: State-of-the-Art Report on Fiber Reinforced Concrete*. ACI Committee 544.
- Akarapu, S., Sharp, T., & Robbins, M. O. (2010). *Stiffness of Contacts Between Rough Surfaces*. Baltimore, USA: Department of Physics and Astronomy, Johns Hopkins University.
- Alhozaimy, A. M., Soroushian, P., & Mirza, F. (1996). Mechanical Properties of Polypropylene Fibre Reinforced Concrete and the Effects of Pozzolanic Materials. *Cement & Concrete Composites* 18, 86-92.
- Arslan, H. (2005). Finite Element Study of Soil Structure Interface Problem. *EJGE*.
- ASTM C1550. (2012). *Standard Test Method for Flexural Toughness of Fiber Reinforced Concrete (Using Centrally Loaded Round Panel)*. ASTM Standard. West Conshohocken Pennsylvania: ASTM International.
- ASTM C78. (2010). *Standard Test Method for Flexural Strength of Concrete (Using Simple Beam with Third-Point Loading)*. West Conshohocken Pennsylvania: ASTM International.
- ASTM D 2487 - 06. (2000). *Standard Practice for Classification of Soils for Engineering Purposes (Unified Soil Classification System)*. West Conshohocken, US: ASTM International.

- ASTM INTERNATIONAL C1581/C1581M-09a. (2009). *Standard Test Method for Determining Age at Cracking and Induced Tensile Stress Characteristics of Mortar and Concrete under Restrained Shrinkage*. West Conshohocken Pennsylvania, USA: ASTM INTERNATIONAL .
- Banthia, N. (2004). *Fiber Reinforced concrete*. Vancouver, Canada: University of British Columbia.
- Banthia, N., & Gupta, R. (2006). Influence of polypropylene fiber geometry on the plastic shrinkage cracking in concrete. *Cement and Concrete Research* 36, 1263-1267.
- Barcelo, L., Boivin, S., Acker, P., Touin, J., & Clavaud, B. (2001). Early age shrinkage of concrete: Back to physical mechanisms. *Concr. Sci. Eng.* 3, 85-91.
- Barcelo, L., Moranville, M., & Clavaud, B. (2005). Autogenous shrinkage of concrete: a balance between autogenous swelling and self-desiccation. *Cement and Concrete Research* 35, 177-183.
- Barros, J. (1999). *Analysis od concrete slabs supported on soil*. Semni, Spain: Metodos numericos en ingenieria.
- Barros, J. A., & Figueiras, J. A. (2011). Model for the analysis of steel fibre reinforced concrete slabs on grade.
- Bazant, Z. P., & Baweja, S. (2000). *Creep and Shrinkage Prediction Model for Analysis and Design of Concrete Structures: Model B3*. Farmington Hills, Michigan: Am .Concrete Institute.
- Beaudoin, J. J. (1990). *Handbook of Fibre-Reinforced concrete*. New Jersey: Noyes Publications.
- Boshoff, W. P., & Combrinck, R. (2013). Modelling the severity of plastic shrinkage cracks in concrete. *Cement and Concrete Research* 48, 34-39.
- Bothma, J. (2013). *The Structural use of synthetic fibres: Thikness design of concrete slabs on grade*. Setellenbosch: Stellenbosch University.
- Brandt, A. M. (2008). Fibre reinforced cement-based (FRC) composites after over 40 years of development in building and civil engineering. *Composite Structures* 86, 3-9.

- British Standards Institute. (2007). *BS EN 14651: Test Method for Metallic Fibre Concrete - Measuring the Flexural Tensile Strength. Standard*. London: British Standards Institute.
- BS 8110. (1997). *Structural use of concrete*. British Standards Institute.
- BS EN 1992-1-1:2004. (2004). *Eurocode 2: Design of concrete structures Part 1-1: General rules and rules for building*. UK: British Standards.
- Carino, N. J., & Clifton, J. R. (1995). *Prediction of Cracking in Reinforced Concrete Structures NISTIR 5634*. Gaithersburg: National Institute of Standards and Technology.
- fib Model Code 2010. (2011). *Model Code 2010 Final draft*. Special Activity Group 5.
- Cement & Concrete Institute. (2009). *Fulton's concrete technology*. Midrand, South Africa: Cement & Concrete institute.
- Choi, J.-H., & Chen, H.-L. R. (2011). Analysis of Shrinkage and Thermal Stresses in Concrete Slabs Reinforced with GFRP Rebars. *Journal of Materials in Civil Engineering*, 621-627.
- Choi, S. Y., Park, J. S., & Jung, W. T. (2011). A study of the shrinkage control of fiber reinforced concrete pavement. *Procedia Engineering 14*, 2815-2822.
- Concrete Society Technical Report No. 65. (2007). *Technical Report No. 65 Guidance on the use of Macro-synthetic-fibre-reinforced Concrete*. Blackwater, Camberley, UK: The Concrete Society.
- Dahl, A. (1985). *Plastic Shrinkage and Cracking Tendency of Mortar and Concrete Containing Fibermesh*. Trondheim, Norway: FCB Cement and Concrete Research Institute.
- Dellate, N., Mack, E., & Cleary, J. (2007). *Evaluation of high absorptive materials to improve internal*. Cleveland, OH, USA: Cleveland State University.
- Dove, J. E., & Jarrett, J. B. (2002). Behavior of dilative sand interface in a geotribology framework. *Geotechnical Geoenvironment Engineering*, 25-37.

- Duncan, J. M., & Clough, G. W. (1971). Finite element analysis of retaining wall behavior. *Journal of Soil Mechanics and Foundations Division, ASCE*, 97(SM12), 1657-1673.
- EFNARC. (1996). *European specification for sprayed concrete*. Aldershot: EFNARC.
- Eierle, B., & Schikora, K. (1999). Computational Modelling of Concrete at Early Ages using DIANA. *DIANA World*, 2/99.
- Goel, R., Kumar, R., & Paul, D. K. (March 2007). Comparative Study of Various Creep and Shrinkage Prediction Models for Concrete. *Journal of Materials in Civil Engineering*, 249 - 260.
- Gomez, J. E., Filz, G. M., & Edeling, R. M. (1999). *Development of an Improved Numerical Model for Concrete-to-Soil Interfaces in Soil-Structure Interaction Analyses*. US Army Corps of Engineering.
- Gomez, J. E., Filz, G. M., & Edeling, R. M. (2000). *Extended Load/Unload/Reload Hyperbolic Model for Interfaces: Parameter Values and Model Performance for the Contact Between Concrete and Coarse Sand*. Washington, DC: US Army Corps of Engineers.
- Grzybowski, M., & Shah, S. P. (1989). Shrinkage Cracking in Fiber Reinforced Concrete. *ACI Materials Journal*, Vol. 41, No. 148.
- Hannant, D. J. (1978). *Fibre Cements and Fibre Concretes*. Salisbury: John Wiley & Sons, Ltd.
- Hanson, T. C., & Mattock, A. H. (1966). The influence of the size and shape of member on shrinkage and creep of concrete. *Journal of the American Concrete Institute*, 63, 267-290.
- Hillerborg, A., Modeer, M., & Pettersson, P. E. (1976). Analysis of crack formation and crack growth in concrete by means of fracture mechanics and finite elements. *CEMENT and CONCRETE RESEARCH*, Vol. 6. pp. 773-782.
- Hryciw, R. D., & Irsyam, M. (1993). Behavior of sand particles around rigid ribbed inclusions during shear. *Soil and Foundations* 33(3), 1-13.

- Hu, L., & Pu, J. (2004). Testing and Modeling of Soil-Structure Interface. *Journal of Geotechnical and Geoenvironmental Engineering*. Vol. 130, 851-860.
- Idiart, A. E. (2009). *Coupled analysis of degradation processes in concrete specimens at the meso-level*. DEPARTMENT OF GEOTECHNICAL ENGINEERING AND GEOSCIENCES. Barcelona: UNIVERSITAT POLITÈCNICA DE CATALUNYA.
- Igarashi, S., Bentur, A., & Kovler, K. (2000). Autogenous shrinkage and induced restraining stresses in high-strength concretes. *Cement and Concrete Research* 30, 1701-1707.
- International Union of Testing and Research Laboratories for Materials and Structures. (1992). RILEM Determination of the specific fracture energy and the strain softening of AAC. In I. U. Structures, *Technical Recommendations for the Testing and Use of Construction Materials* (pp. 156-157). London: E & FN SPON.
- Jianyong, L., & Yan, Y. (2001). A study on creep and drying shrinkage of high performance concrete. *Cement and Concrete Research* 31, 1203-1206.
- Kakooei, S., Akil, H. M., Jamshidi, M., & Rouhi, J. (2011, September 28). The effect of polypropylene fibres on the properties of reinforced concrete structures. *Construction and Building Materials*, 27, 73-77.
- Kayali, O., Haque, M. N., & Zhu, B. (1999). Drying shrinkage of fibre-reinforced lightweight aggregate concrete containing fly ash. *Cement and Concrete Research* 29, 1835-1840.
- Kristiawan, S. (2013). Performance Criteria to Assess Shrinkage Cracking Tendency in Concrete Overlay. *Procedia Engineering* 54, 82-100.
- Labib, W., & Eden, N. (2004). *An investigation into the use of fibres in concrete industrial ground-floor slabs*. Liverpool Jhon Moores University. Liverpool: School of the Built Environment.
- Lee, S. (2001). Behavior of Concrete Slabs under Friction Drag. *KSCE Journal of Civil Engineering*, Vol. 5, No. 2, pp. 141-145.
- Leonards, G. A. (1965). *Experimental study of the static and dynamic friction between soil and typical construction materials*. New Mexico: Air Force Weapons Laboratory.

- Litton, R. W. (1974). *A contribution to the Analysis of Concrete Structures Under Cyclic Loading*. Berkeley: University of California.
- Löfgren, L. (2004). *The wedge splitting test - a test method for assessment of fracture parameters of FRC?* Chalmers: Dep. of Structural and Mechanical Engineering, Chalmers University of Technology.
- Löfgren, L., Olesen, J. F., & Flansbjer, M. (2013). Retrieved 07 21, 2013, from Tekna: https://www.tekna.no/ikbViewer/Content/225412/S78%2520-%2520L%25C3%25B6fgren%2520et%2520al%25202005-05-10%2520FINAL_just%2520af%2520DB.pdf
- Maitra, S. R., Reddy, K. S., & Ramachandra, L. S. (2009). Experimental Evaluation of interface friction and study of its influence on concrete pavement response. *Journal of Transportation Engineering*, 563-571.
- Manolis, G. D., Gareis, P. J., Tsonos, A. D., & Neal, J. A. (1997). Dynamic Properties of Polypropylene Fiber-Reinforced Concrete Slabs. *Cement and Concrete composites* 19, 341-349.
- Marais, L. R., & Perrie, B. D. (1993). *Concrete industrial floors on the ground*. Midrand: Portland Cement Institute.
- Nagarkar, P., Tanmble, S., & Pazare, D. (1987). *Study on fibre reinforced concrete*.
- Nakamura, T., Mitachi, T., & Ikeura, I. (1999). Direct shear testing method as a means for estimating geogrid-sand interface shear-displacement behavior. *Soils Found*, 39(4), 1-8.
- National Ready Mixed Concrete Association. (1998). *CIP 5 - Plastic Shrinkage Cracking*. Retrieved August 07, 2014, from NRMCA: <http://www.nrmca.org/aboutconcrete/cips/05p.pdf>
- Neville, A. M., & Brooks, J. J. (2001). *Concrete Technology (revises edition - 2001 Standards)*. Harlow: Addison Wesley Longman.
- Newman, J., & Choo, B. S. (2003). *Advanced Concrete Technology concrete properties*. Burlington: Butterworth-Heinemann.

- Nordcn. (2005). *Wedge Splitting Test Method (WST): Fracture Testing of Fibre-Reinforced Concrete (Mode I) (NT Build 511)*. Norway: Nordic Innovation Centre.
- Odendaal, C. M. (2015). *Establishment of Performance-Based Specifications for the Structural Use of Locally Available Macro-Synthetic Fibres*. Stellenbosch: Stellenbosch University.
- Odman, S. T. (1968). Effects of variations in volume, surface area exposed to drying, and composition on shrinkage. *RILEM/CEMBUREAU International Colloquium on the Shrinkage of Hydraulic Concretes*, (p. vol 1). Madrid.
- Older, C. (1937). *Bates experimental road or highway research in Illinois*. Springfield, Illinois.
- Ostergaard, L. (2003). *Early-Age Fracture Mechanics And Cracking of Concrete Experiments and Modelling*. Denmark: Technical University of Denmark.
- Padron, I., & Zollo, R. F. (1990). Effect of Synthetic Fibers on Volume Stability and Cracking of Portland Cement Concrete and Mortar. *ACI Materials Journal*, Vol. 87, No. 4, 327-332.
- Passuello, A., Moriconi, G., & Shah, S. P. (2009). Cracking behavior of concrete with shrinkage reducing admixtures and PVA fibers. *Cement & Concrete Composites*, 699-704.
- Pelisser, F., Neto, A. B., Rovere, H. L., & de Andrade Pinto, R. C. (2010). Effect of the addition of synthetic fibres to concrete thin slabs on plastic shrinkage cracking. *Construction and Building Materials* 24, 2171-2176.
- Peterson, M. S., Kulhawy, F. H., Nucci, L. R., & Wasil, B. A. (1976). *Stress-deformation behavior of soil-concrete interfaces*. NY: Contract report B-49 to Niagara Mohawk Power Corporation, Syracuse.
- Peterson, P. E. (1980). Fracture energy of concrete: method of determination. *Cement and Concrete Research* Vol 10, 78-89.
- Potyondy, J. (1961). Skin friction between various soils and construction materials. *Geotechnique* 11(4), 339-353.

- Powers, T. (1965). Mechanisms of shrinkage and reversible creep of hardened cement paste. London: Cement and Concrete Association.
- Rajani, B. (2002). Behaviour and Performance of Concrete Sidewalks. *Construction Technology Update No. 53*.
- RILEM. (1976). *International symposium on carbonation of concrete*. Cement and Concrete Association.
- Rots, J. G. (1988). *Computational modeling of concrete fracture*. Delft: Delft University of Technology.
- SABS 864:1994. (1994). *Concrete tests - Flexural strength of hardened concrete*. SABS.
- Saetta, A. V., Schrefler, B. A., & Vitalian, R. V. (1993). THE CARBONATION OF CONCRETE AND THE MECHANISM OF MOISTURE, HEAT AND CARBON DIOXIDE FLOW THROUGH POROUS MATERIALS. *Cement and Concrete Research Vol 23*, 761-772.
- SANS 10100-1:2000. (2000). *Code of practice for the structural use of concrete. Part 1*. Pretoria: South African Bureau of Standards.
- SANS 5863:2006. (2006). *Concrete test - compressive strength of hardened concrete*. Pretoria: South African Bureau of Standards.
- SANS 5864:2006. (2006). *Concrete tests - flexural strength of hardened concrete*. Pretoria: South African Bureau of Standards.
- SANS 861-3. (1994). *Concrete tests - Making and curing of test specimens*. SABS.
- SANS 863:2006. (2006). *Concrete tests - Compressive strength of hardened concrete*. SABS.
- Singh, S. K. (2010). *Polypropylene Fiber Reinforced Concrete: An Overview*. Roorkee: Roorkee & Honorary Secretary Institute of Engineering.
- Soutsos, M. N., Le, T. T., & Lampropoulos, A. P. (2012). Flexural performance of fibre reinforced concrete made with steel and synthetic fibres. *Construction and Building Materials 36*, 704-710.

- Tapcu, B., & Canbaz, M. (2007). Effect of different fibers on the mechanical properties of concrete containing fly ash. *Construction Building Materials*, 1486-1491.
- Technical Report No. 34. (2003). *Concrete industrial ground floors: A guide to design and construction. Technical Report No. 34*. UK: the concrete society.
- The Concrete Institute. (2013). *Fibre reinforced concrete*. Midrand: The Concrete Institute.
- TNO DIANA. (2003). *History of TNO DIANA BV*. Retrieved Nov 27, 2014, from TNO DIANA: <http://tnodiana.com/History>
- TNO DIANA. (2012). *DIANA-9.4.4 User's Manual - Geotechnical Analysis*. The Netherlands: TNO DIANA.
- TNO DIANA Material Lib. (2012). *DIANA User manual - Material Lib*. Delft ,The Netherlands: TNO DIANA BV.
- Troxell, G. E., Raphael, J. M., & Davis, R. E. (1958). Long-time creep and shrinkage tests of plain and reinforced concrete. *Proceedings ASTM 58*, (pp. 1101-1120).
- Tschegg, E. K., & Linsbauer, H. N. (1986). Fracture energy determination of concrete with cube shaped specimens. *Zement und Beton*, 38-40.
- Uesugi, M., & Kishida, H. (1987). Tests of the interface between sand and steel in simple shear apparatus. *Geotechnique 37(1)*, 45-52.
- Van Der Westhuizen, D. (2013). *Using Synthetic Fibres in Concrete to Control Drying Shrinkage Cracking in Concrete Slabs-on-Grade*. Stellenbosch: University of Stellenbosch.
- Walker, W. W., & Holland, J. A. (January 1, 1999). *The First Commandment for Floor Slabs: Thou Shalt Not Curl nor Crack... (Hopefully)*. Concrete International.
- Wittmann, F. H., & Bluhwiler, E. (1990). The wedge splitting test, a new method of performing stable fracture mechanics test. *Engineering Fracture Mechanics*. 35, 117-125.
- Zhang, L., Wang, X., & Zheng, G. (2009). Effect of polypropylene fibers on the strength and elastic modulus of soil-cement. *Geosynthetics Civil Environment Eng*, 386-391.

APPENDIX 1: THE CALCULATION OF THE SHRINKAGE STRAIN USING CEB-FIP MODEL CODE

TABLE 1: THE PARAMETERS USED FOR CEB-FIP MODEL CODE CALCULATIONS

F _{cm}	54
A _{as}	600
α _{ds1}	6
α _{ds2}	0.012
H	0.722021661

TABLE 2: THE CALCULATION OF SHRINKAGE STRAIN USING THE CEB-FIP MODEL CODE

Time (days)	Autogenous shrinkage			Drying shrinkage					Total shrinkage	
	β _{as} (t)	ε _{cas0} (fcm)	ε _{cas} (t)	ε _{cdso} (fm)	β _{RH} (RH)		β _{ds} (t1-ts)	ε _{cds} (t,ts)	ε _{cs}	ε _{cs} (10 ⁶)
0	0	-0.00046106	0	0.00046032	-0.7564	0.957563	0	0	0	0
0.1	0.061287	-0.00046106	-2.8257E-05	0.00046032	-0.7564	0.957563	1.105976	-0.00039	-0.0004133	413.3423
0.2	0.085559	-0.00046106	-3.9448E-05	0.00046032	-0.7564	0.957563	1.048994	-0.00037	-0.0004047	404.6931
0.3	0.103758	-0.00046106	-4.7839E-05	0.00046032	-0.7564	0.957563	1.031871	-0.00036	-0.0004071	407.1218
0.4	0.118818	-0.00046106	-5.4782E-05	0.00046032	-0.7564	0.957563	1.023619	-0.00036	-0.0004112	411.192
0.5	0.131877	-0.00046106	-6.0803E-05	0.00046032	-0.7564	0.957563	1.018761	-0.00035	-0.0004155	415.5214
0.6	0.143516	-0.00046106	-6.6169E-05	0.00046032	-0.7564	0.957563	1.015561	-0.00035	-0.0004198	419.7735
0.7	0.154081	-0.00046106	-7.1041E-05	0.00046032	-0.7564	0.957563	1.013293	-0.00035	-0.0004239	423.8553
0.8	0.163798	-0.00046106	-7.5521E-05	0.00046032	-0.7564	0.957563	1.011603	-0.00035	-0.0004277	427.7468
0.9	0.172823	-0.00046106	-7.9682E-05	0.00046032	-0.7564	0.957563	1.010293	-0.00035	-0.0004315	431.4519
1	0.181269	-0.00046106	-8.3576E-05	0.00046032	-0.7564	0.957563	1.00925	-0.00035	-0.000435	434.9827
2	0.246362	-0.00046106	-0.00011359	0.00046032	-0.7564	0.957563	1.004593	-0.00035	-0.0004634	463.3728
3	0.292778	-0.00046106	-0.00013499	0.00046032	-0.7564	0.957563	1.003055	-0.00035	-0.0004842	484.2378
4	0.32968	-0.00046106	-0.000152	0.00046032	-0.7564	0.957563	1.002289	-0.00035	-0.000501	500.9852
5	0.360593	-0.00046106	-0.00016625	0.00046032	-0.7564	0.957563	1.00183	-0.00035	-0.0005151	515.078
6	0.387311	-0.00046106	-0.00017857	0.00046032	-0.7564	0.957563	1.001524	-0.00035	-0.0005273	527.2904
7	0.410895	-0.00046106	-0.00018945	0.00046032	-0.7564	0.957563	1.001306	-0.00035	-0.0005381	538.0879
8	0.432029	-0.00046106	-0.00019919	0.00046032	-0.7564	0.957563	1.001142	-0.00035	-0.0005478	547.7753
9	0.451188	-0.00046106	-0.00020802	0.00046032	-0.7564	0.957563	1.001015	-0.00035	-0.0005566	556.5645
10	0.468714	-0.00046106	-0.00021611	0.00046032	-0.7564	0.957563	1.000914	-0.00035	-0.0005646	564.6096
15	0.53911	-0.00046106	-0.00024856	0.00046032	-0.7564	0.957563	1.000609	-0.00035	-0.000597	596.9603
20	0.591158	-0.00046106	-0.00027256	0.00046032	-0.7564	0.957563	1.000456	-0.00035	-0.0006209	620.9045
25	0.632121	-0.00046106	-0.00029145	0.00046032	-0.7564	0.957563	1.000365	-0.00035	-0.0006398	639.7587
30	0.665609	-0.00046106	-0.00030689	0.00046032	-0.7564	0.957563	1.000304	-0.00035	-0.0006552	655.1778
40	0.717736	-0.00046106	-0.00033092	0.00046032	-0.7564	0.957563	1.000228	-0.00035	-0.0006792	679.1847
50	0.756883	-0.00046106	-0.00034897	0.00046032	-0.7564	0.957563	1.000183	-0.00035	-0.0006972	697.2183
100	0.864665	-0.00046106	-0.00039866	0.00046032	-0.7564	0.957563	1.000091	-0.00035	-0.0007469	746.8802
120	0.888183	-0.00046106	-0.00040951	0.00046032	-0.7564	0.957563	1.000076	-0.00035	-0.0007577	757.7182
160	0.920327	-0.00046106	-0.00042433	0.00046032	-0.7564	0.957563	1.000057	-0.00035	-0.0007725	772.5319

APPENDIX 2: RESULTS OF FLEXURAL TESTS

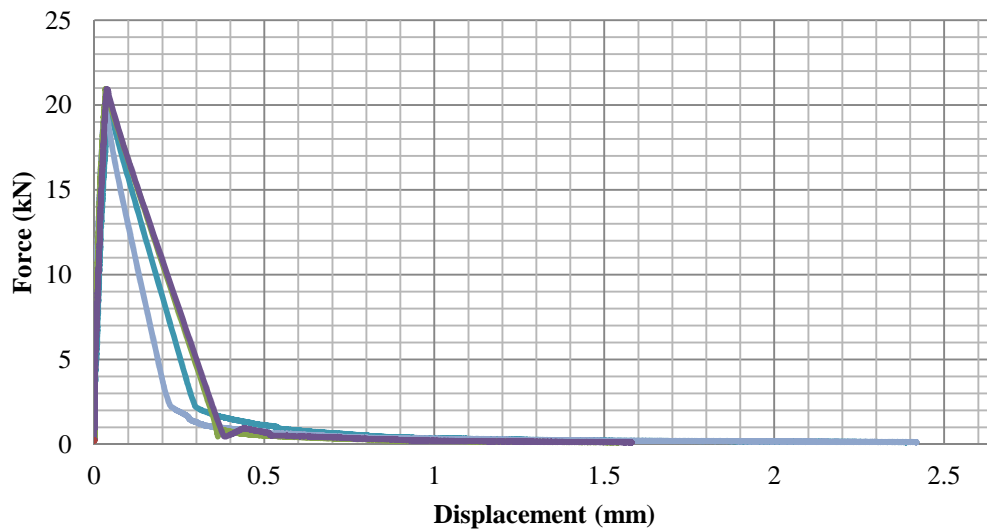


Figure 0.1: The flexural test results for no fibres

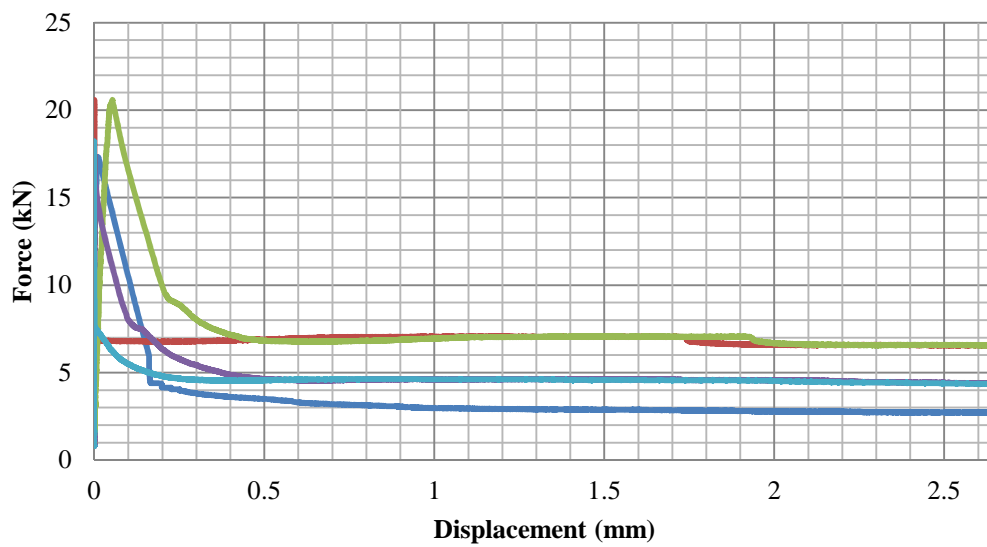


Figure 0.2: The flexural test results for 5kg/m³ fibres

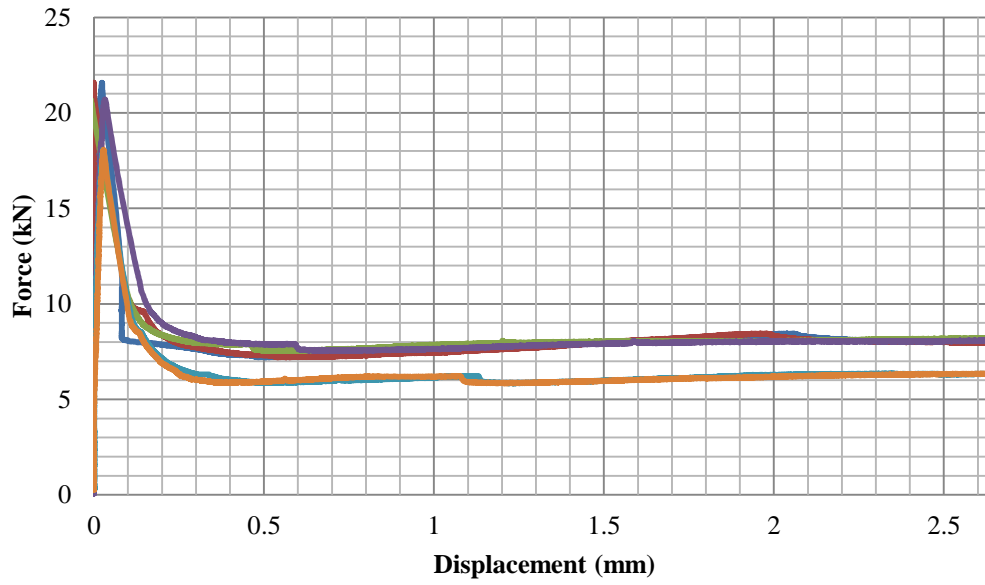


Figure0.3: The flexural test results for 8kg/m³ fibres

TABLE 1:THE FLEXURAL STRENGTH AND DATA FROM FREXURAL TESTS

Casting	Testing	Sample	d(m)	b(m)	mass	F(N)	l(m)	fcfMpa)	Ave fcf (Mpa)
5kg/m ³ 22April 2014	20- May- 14	1	0.15 2	0.7	37.54	17355.8 3	0.45	0.72	0.79
		2	0.15 2	0.69 6	37.5	20601.9 7	0.45	0.86	
		3	0.15 1	0.7	37.28	18269.7 3	0.45	0.77	
No fibres 6 Mei 2014	3 Junie 2014	1	0.15 4	0.69 8	37.83	20938	0.45	0.85	0.89
		2	0.15 5	0.69 7	39.89	24656	0.45	0.99	
		3	0.14 8	0.69 9	38.02	19888	0.45	0.88	
		4	0.15 2	0.69 3	40.05	19378	0.45	0.82	
8kg/m ³ 6 Mei 2014	3 Junie 2014	1	0.15 5	0.71	38.91	18074	0.45	0.72	0.83
		2	0.15 3	0.7	38.23	20704	0.45	0.85	
		3	0.15	0.71	38.43	21576	0.45	0.91	

APPENDIX 3: RESULTS OF FRACTURE ENERGY TEST

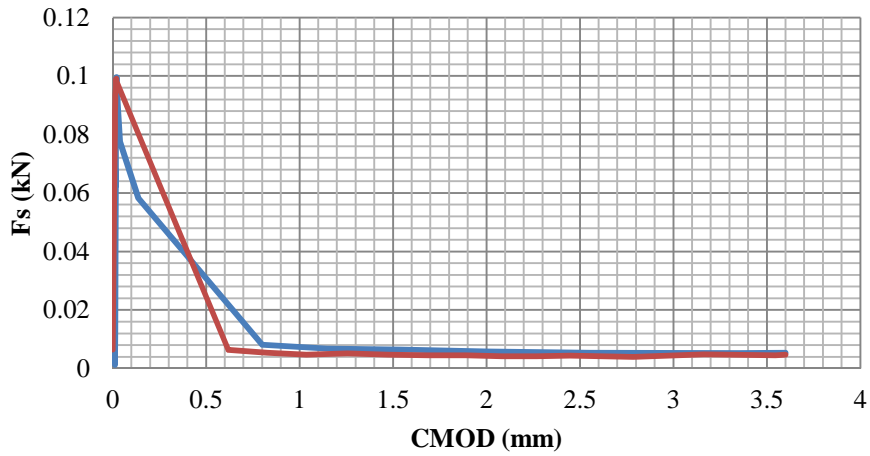


Figure 0.1: 2kg/m³

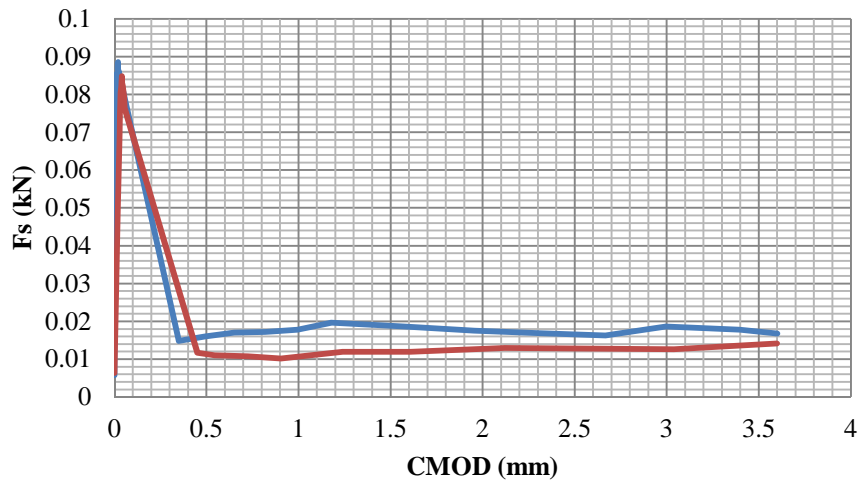


Figure 0.2: 5kg/m³

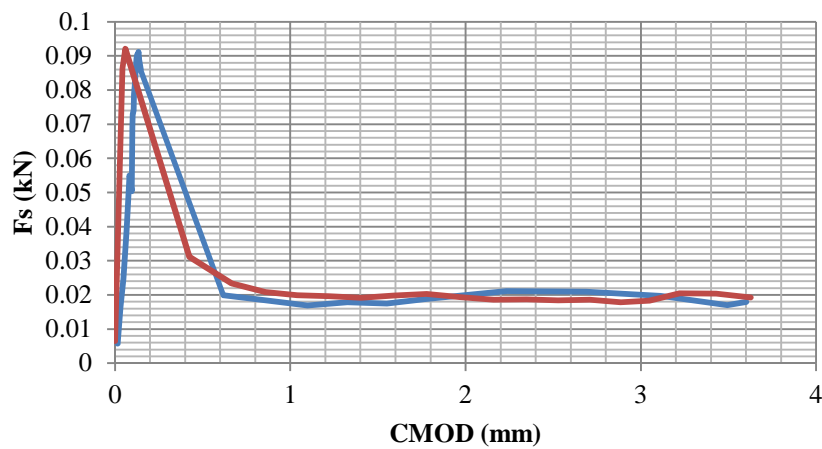


Figure 0.3: 6kg/m³

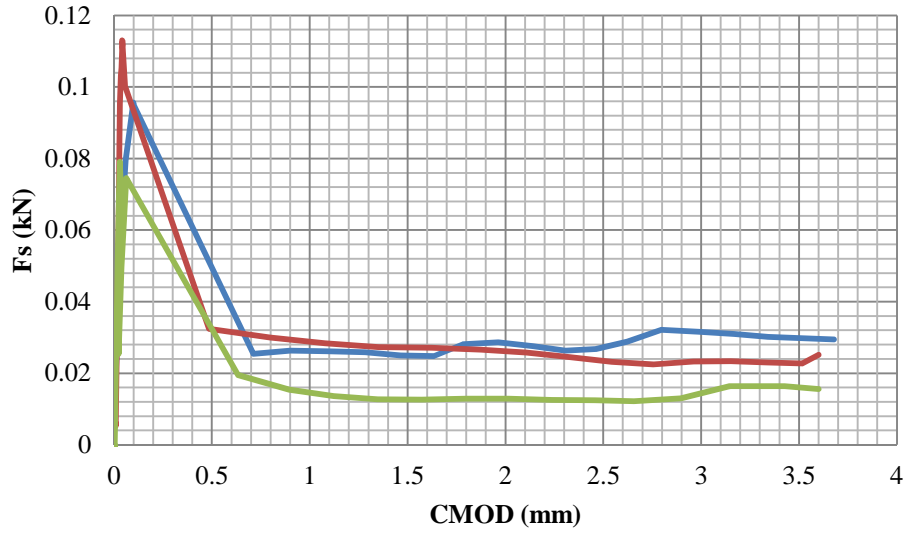


Figure 0.4: 8kg/m^3

APPENDIX 4: SIEVE ANALYSIS RESULTS

Sieve unit	Grain size	Sieve mass before	Sieve mass after	Individual mass retained R	Individual percentage retained	Cumulative percentage (4750µm to 150µm sieves)	Percentage of material that passed	Percentage of material that passed (rounded off)
µm	m	g	g	g	%	%	%	%
4750	0.00475	596	596	0	0	0	100.00	100
2360	0.00236	548	549	1	0.20	0.20	99.80	100
1180	0.00118	480	502	22	4.50	4.71	95.29	95
600	0.0006	467	516	49	10.03	14.73	85.27	85
300	0.0003	410	564	154	31.51	46.25	53.75	54
150	0.00015	390	577	187	38.26	84.51	15.49	16
					84.51	150.40		
75	0.000075	432	498	66	13.51		1.98	2
Pan (mass c)		564	574	10	2.05			
Mass a-b				11.6	2.37			
Subtotal 2(a-b+c)				21.6	4.42			
Total mass		3887	4376	488.7	100.00			
Mass		g						
a		500.3						
b		488.7						
Fineness modulus		1.50 %						
Dust content		4.32 %						

Sieve unit	Grain size	Sieve mass before	Sieve mass after	Individual mass retained R	Individual percentage retained	Cumulative percentage (4750µm to 150µm sieves)	Percentage of material that passed	Percentage of material that passed (rounded off)
µm	m	g	g	g	%	%	%	%
4750	0.00475	627.9	627.9	0	0	0	100.00	100
2360	0.00236	519	519.5	0.5	0.101853738	0.10	99.90	100
1180	0.00118	481.6	500.8	19.2	3.91118354	4.01	95.99	95
600	0.0006	467.6	524.8	57.2	11.65206763	15.67	84.33	85
300	0.0003	409.9	604.3	194.4	39.60073335	55.27	44.73	54
150	0.00015	391.2	557.9	166.7	33.95803626	89.22	10.78	16
					89.22	164.27		
75	0.000075	433.2	477.8	44.6	9.13		1.65	2
Pan (mass c)		565.8	573.6	7.8	1.60			
Mass a-b				9.4	1.91			
Subtotal 2(a-b+c)				17.2	3.50			
Total mass		3896.2	4386.6	490.9	100.00			
Mass		g						
a		500.3						
b		490.9						
Fineness modulus		1.64 %						
Dust content		3.44 %						

Batch 1

Grain size	Percentage of material that passed
mm	per cent
0.00475	100
0.00236	99.79537549
0.00118	95.29363618
0.0006	85.26703499
0.0003	53.75485983
0.00015	15.49007571
0.000075	1.984857786

Batch 2

Grain size	Percentage of material that passed
mm	per cent
0.00475	100.00
0.00236	99.90
0.00118	95.99
0.0006	84.33
0.0003	44.73
0.00015	10.78
0.000075	1.65

APPENDIX 5: REBAR CALCULATIONS

Diameter of steel reinforcement on the side of the wooden box:

$$\sigma_{cr} = 80 \times 100 \times 5$$

$$\sigma_{cr} = 40kN$$

$$40 = \sigma_{st} \times \frac{\pi d^2}{4}$$

$$d = 10.6 \text{ mm} \approx 12 \text{ mm}$$

Anchorage:

$$\tau = 2.9 \text{ MPa}$$

$$F = A \times \tau$$

$$40 \times 10^3 = \pi \times d \times l \times \tau$$

$$40 \times 10^3 = \pi \times 12 \times l \times 2.9$$

$$l = 370 \text{ mm}$$

\therefore y12 at 500 mm anchorage

Concrete needed for one box:

$$\text{Area of box} = 0.1 \times 0.08 \times 11$$

$$= 0.088 \text{ m}^3$$

\approx 88l of concrete per box

Sand with 15.5 per cent water content:

$$\text{Volume of sand} = 0.1 \times 0.08 \times 11$$

$$= 0.088 \text{ m}^3$$

= 88 l sand

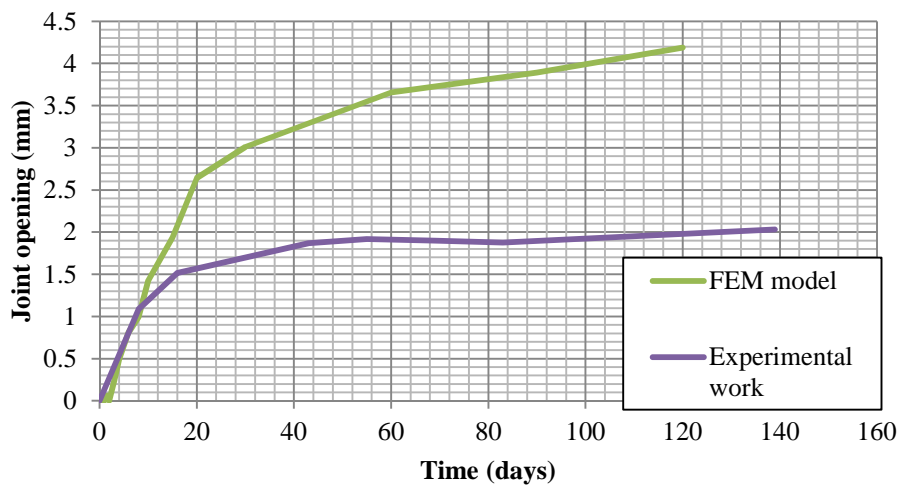
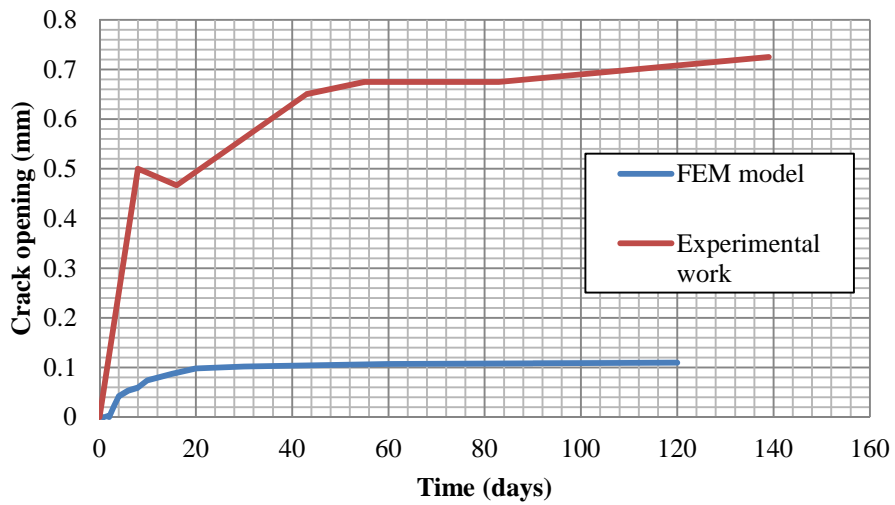
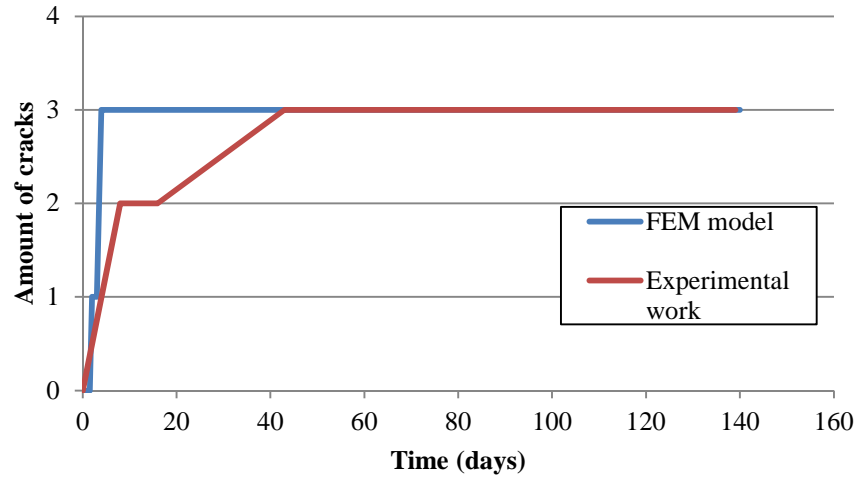
$$= 88 \times 2.6$$

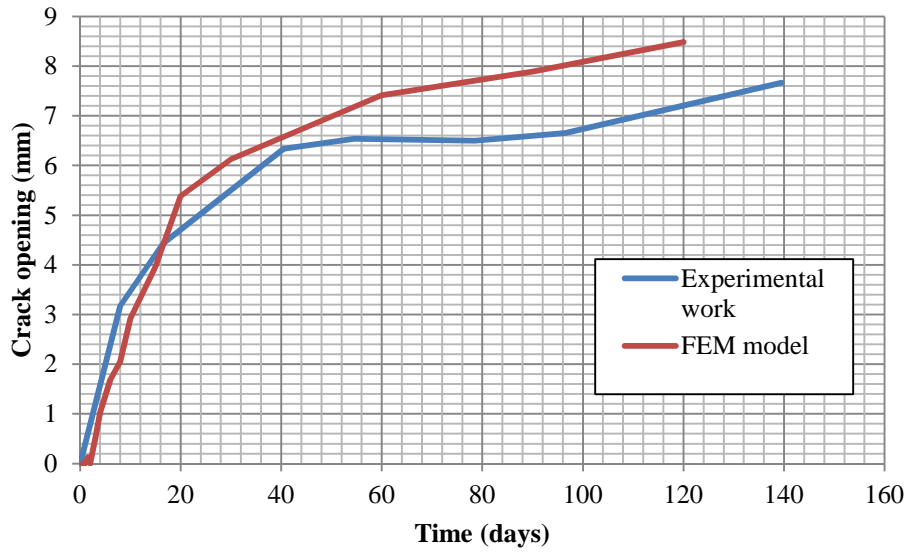
$$= 228.8 \text{ kg sand} \times 0.155$$

$$\text{Water content} = 35.46 \text{ l}$$

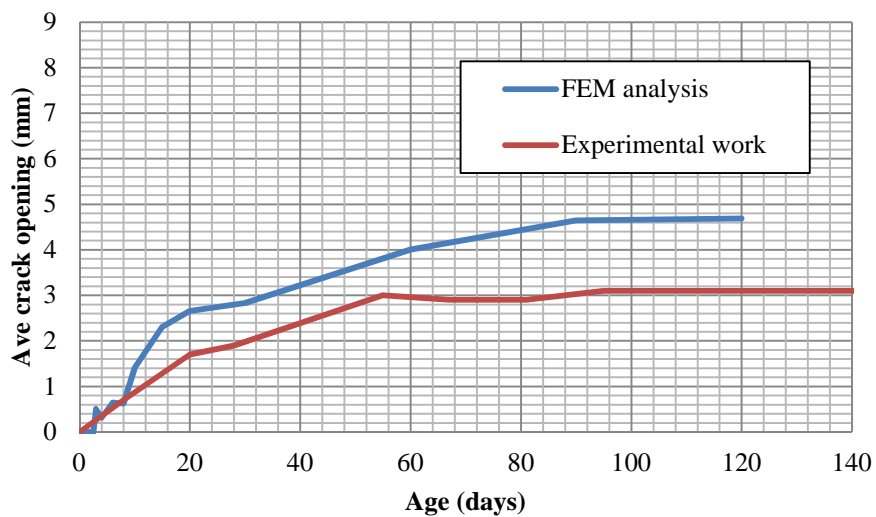
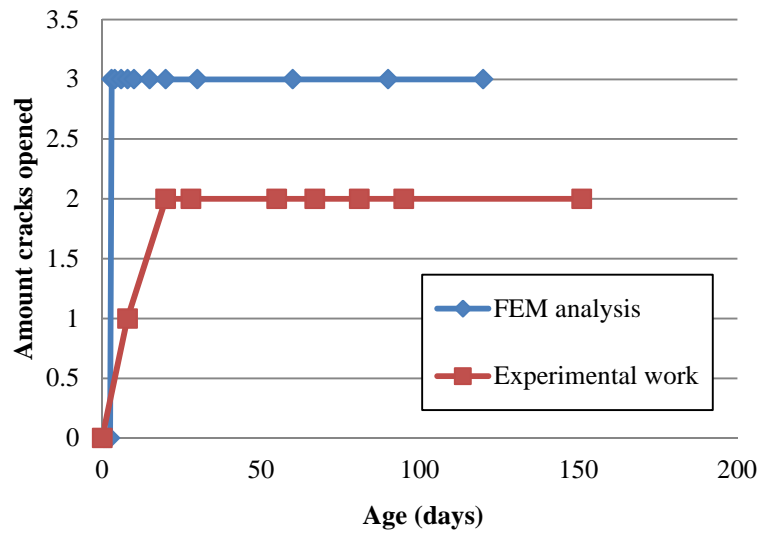
APPENDIX 6: THE RESULTS OF THE EXPERIMENTAL WORK AND FEM ANALYSIS

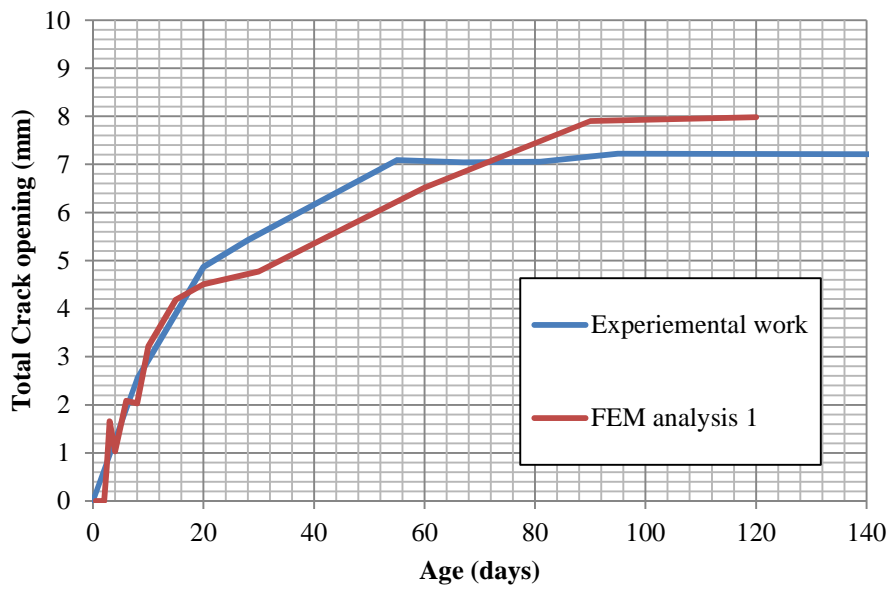
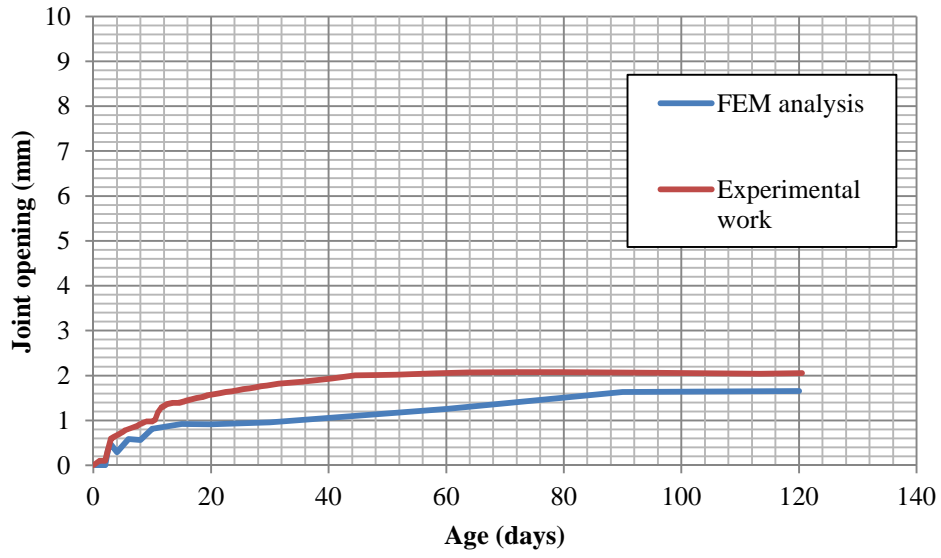
9,8,100,s



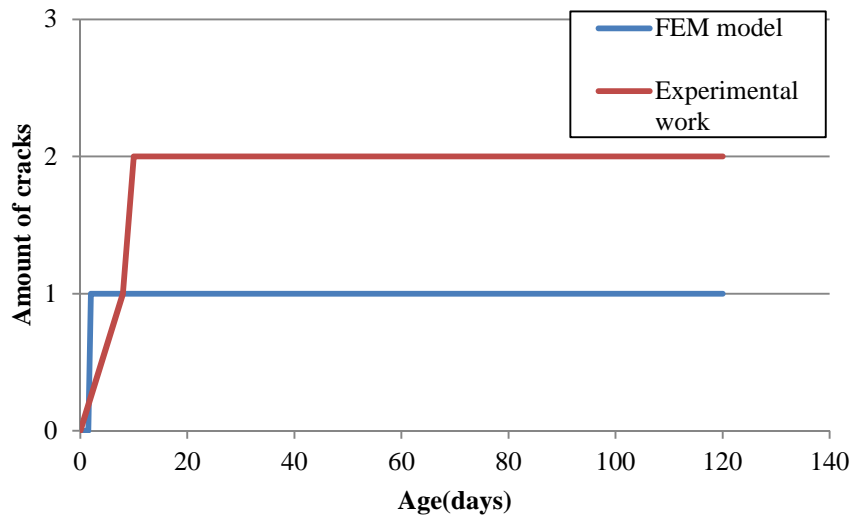


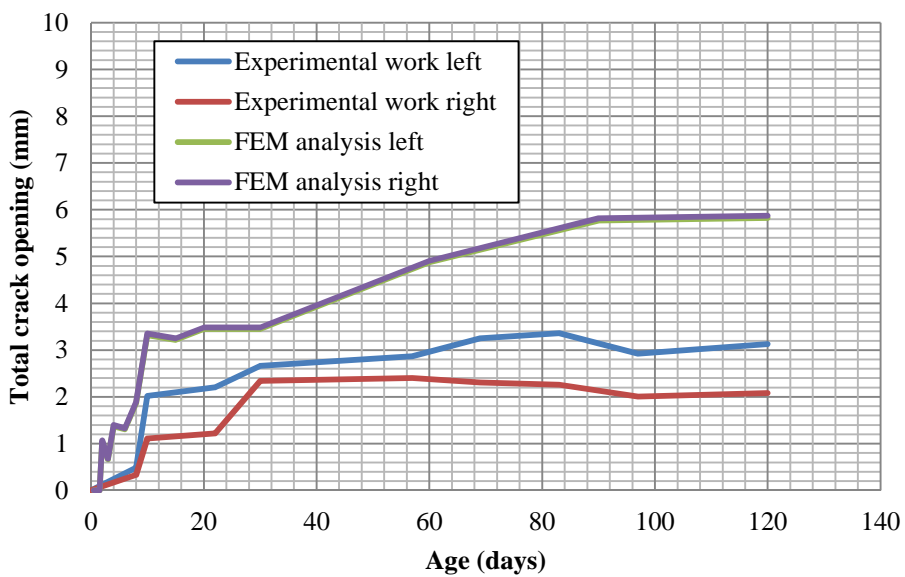
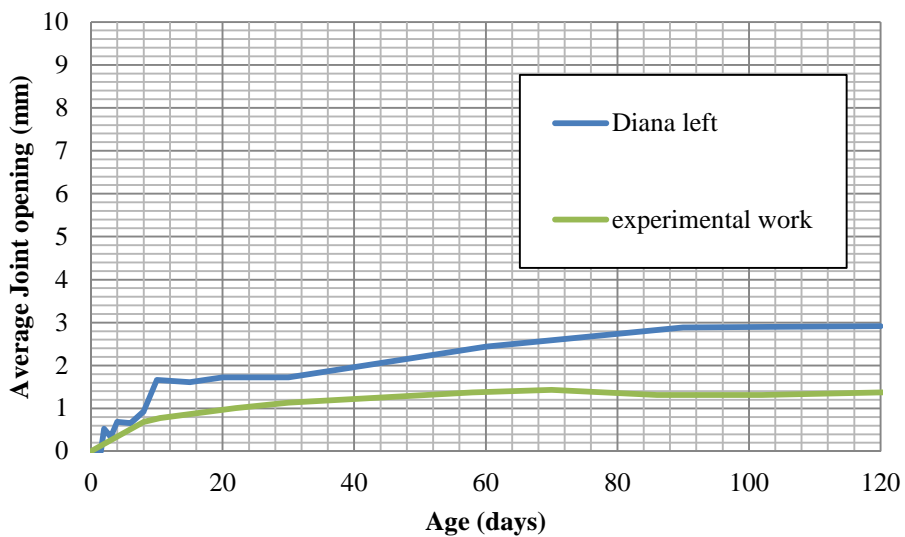
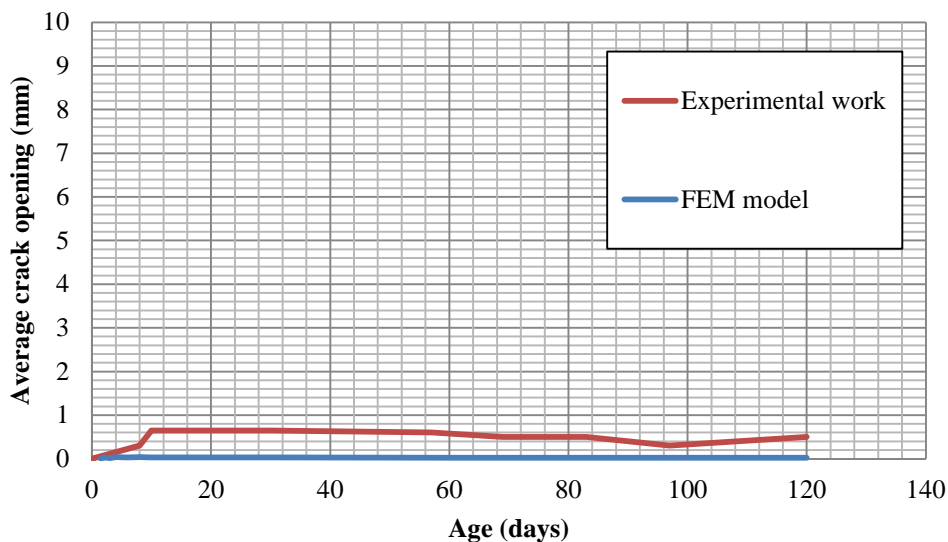
9,5,150,s



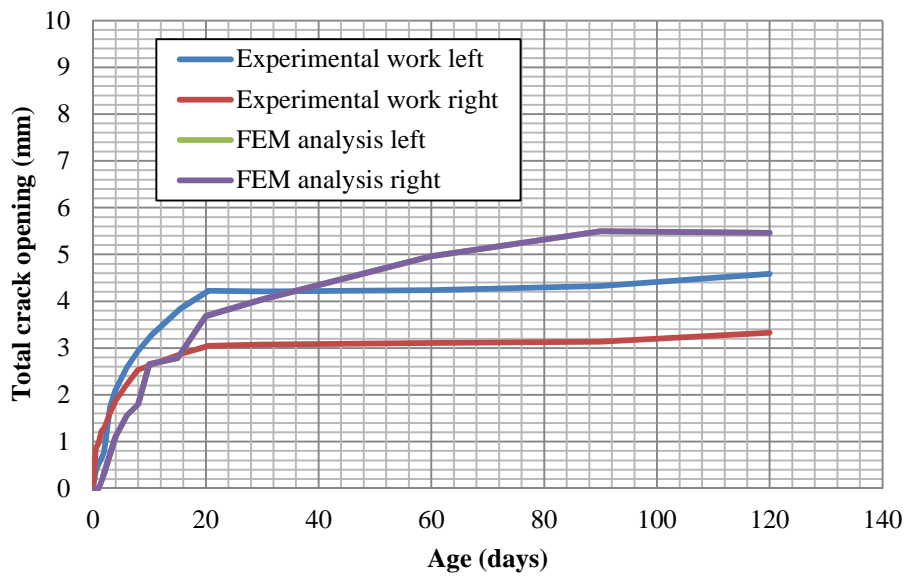
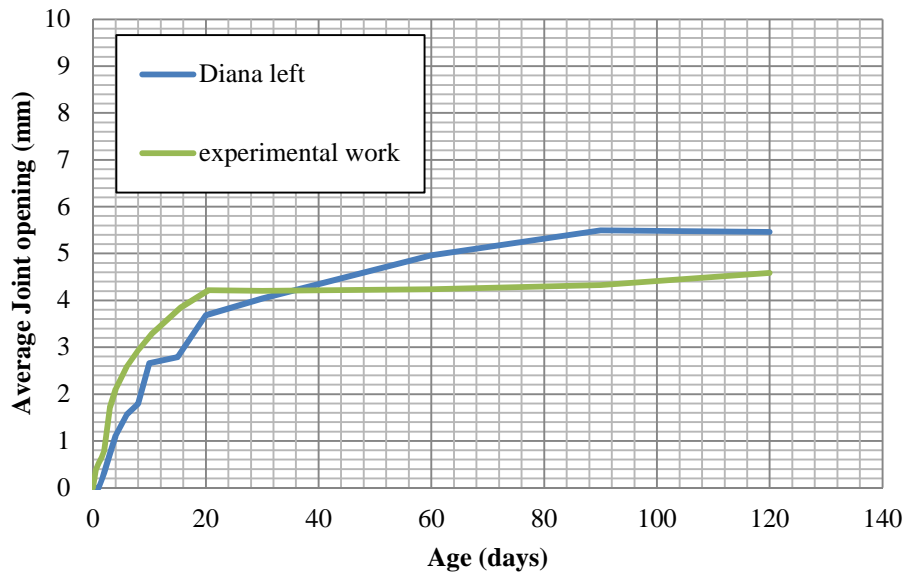


4.5,5,100,s





4.5,0,100.s



APPENDIX 7: DIANA CODE

The DIANA dcf file used to analyse the slab on grade model.

```
*filos
initia
*input
*nonlin

begin execut
  begin load
  steps explic sizes 1.
  loadnr=1
  end load
  begin iterat
    maxite=100
    begin conver
      energy tolcon=1.0e-4
      force off
      displa off
    end conver
  end iterat
  solve pardis
end execut

begin execut
time steps explic size 0.00001 0.0001 0.001 0.00889 0.09 0.1(30) 0.1(65) 0.5(40) 1(40) 1(50) 10(4)
begin iterat
  conver simult
  maxite=1000
  method secant bfgs linear
  linese
  begin conver
    energy off
```

```
force tolcon 0.05 contin  
displa off  
end conver  
end iterat  
solve pardis  
end execut
```

```
begin output femvie  
select steps all  
displa total transl  
stress total cauchy  
strain total green  
strain shrink  
force reacti transl  
stress total tracti global intpnt  
strain total tracti global intpnt  
strain total tracti local intpnt  
maturi total  
end output
```

```
*end
```

The DIANA dat file used to analyse the slab on grade.

```
'UNITS'
```

```
LENGTH M
```

```
TIME DAY
```

```
MASS 7.46496E+9
```

```
TEMPER CELSIU
```

```
FORCE N
```

```
'COORDINATES' DI=2...
```

```
'ELEMENTS'
```

CONNECTIVITY

1 Q8MEM 1 22 23 2

2 Q8MEM 2 23 24 3...

MATERIALS

/ 46222-90231 /3

/ 44021-46221 /1

/ 1-44020 /2

GEOMETRY

/ 46222-90231 /1

/ 44021-46221 /3

/ 1-44020 /2

'MATURI'

EQUAGE

ELEMEN

0 1. 2. 3. 4. 5. 6. 7. 8. 9. 10. 15. 20. 30. 60. 90. 120.

/ 46222-90231 /

0 1. 2. 3. 4. 5. 6. 7. 8. 9. 10. 15. 20. 30. 60. 90. 120.

'MATERIALS'

1 DSTIF 5.038462E+05 9.038462E+8

FRICTI

FRCVAL 3.450000E+04 3.500000E-01 0.000000E+00

GAP

GAPVAL 0.000000E+00

MODE2 1

MO2VAL 1.000000E-02

2 YOUNG 4.700000E+07

POISON 3.000000E-01

DENSIT 1.400000E+03

: ELASTIC PROPERTIES OF CONCRETE

3

YOUNG 3.2E+10

: AMBIENT INFLUENCE ON THE YOUNG MODULUS GIVE MATURITY VALUE THEN YOUNG

MATYOU 0. 0.4E10
 1.0 1.7E10
 2.0 1.77E10
 3.0 2.19E10
 4.0 2.4E10
 5.0 2.55E10
 6.0 2.65E10
 7.0 2.73E10
 8.0 2.79E10
 9.0 2.84E10
 10.0 2.88E10
 15.0 2.92E10
 20.0 3.04E10
 30.0 3.22E10
 60.0 3.34E10
 90.0 3.40E10
 120.0 3.44E10

POISON 0.15

THERMX 10.E-6

DENSIT 2.370000E+03

: CRACK INDEX

: FTMODN

: FTVALU 0. 0.39E6 0.72E6 0.95E6 1.11E6 1.52E6 1.74E6 1.89E6 2.0E6 2.1E6 2.15E6 2.21E6 2.26E6
 2.3E6 :2.44E6 2.54E6 2.65E6 2.76E6 2.8E6 2.82E6

: FTTIME 0. 0.25 0.5 0.75 1. 2. 3. 4. 5. 6. 7. 8. 9. 10. 15. 20. 30. 60. 90. 120.

:BLADSY 127

: SHRINKAGE IN THE CONCRETE

SHRINF 0.0 0.000000 0.000000 0.000000 0.000000 0.000000 0.000000 0.000000 0.000000 0.000000 0.000000
 0.000001 0.000000 0.00016 0.00010 0.00018 0.00020 0.00019 0.00019 0.00023 0.00026 0.00042 0.000405
 0.00043 0.00059 0.000712 0.00072

SHTIME 0 0.125 0.25 0.375 0.4 0.5 0.6 0.7 0.8 0.9 1. 2. 3. 4. 5. 6. 7. 8. 9. 10. 15. 20. 30. 60. 90. 120.

: SHRINN

: H 0.2

: RH 70
: CURAGE 0
: CRACKING
: CRACKING AND TENSILE STRENGTH

CRACK 1

CRKVAL 2.790000E+06

MATCRK 0. 0.004E6

1.0 0.39E6

2.0 0.78E6

3.0 1.08E6

4.0 1.31E6

5.0 1.49E6

6.0 1.64E6

7.0 1.76E6

8.0 1.87E6

9.0 1.96E6

10.0 2.05E6

15.0 2.36E6

20.0 2.56E6

30.0 2.82E6

60.0 3.08E6

90.0 3.20E6

120.0 3.27E6

: TENSION SOFTENING-LINEAR

TENSIO 3

: CRACKB 0.010000E+00

TENVAL 2.79E6

:7.667E2 0.01

GF 7.667000E+02

: SHEAR RETENTION

TAUCRI 0

: BETA 2.000000E-01

'GEOMETRY'

1 THICK 8.000000E-02

2 THICK 8.000000E-02

3 THICK 8.000000E-02

CONFIG MEMBRA

APPENDIX 8: TOTAL CRACK WIDTH OPENING

JOINT SPACING VALUES

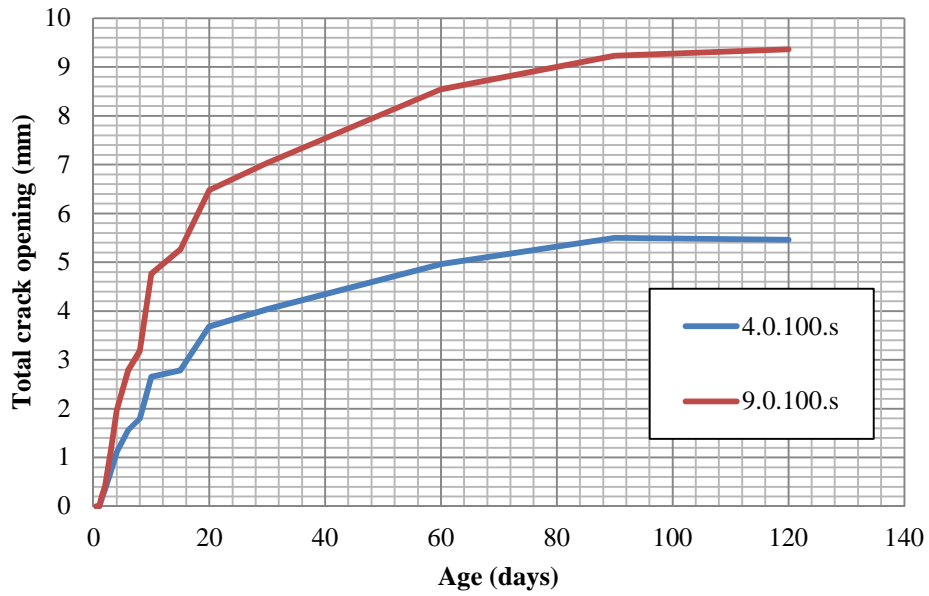


Figure 0.1: The total crack opening of 4m and 9m joint spacings containing no fibres

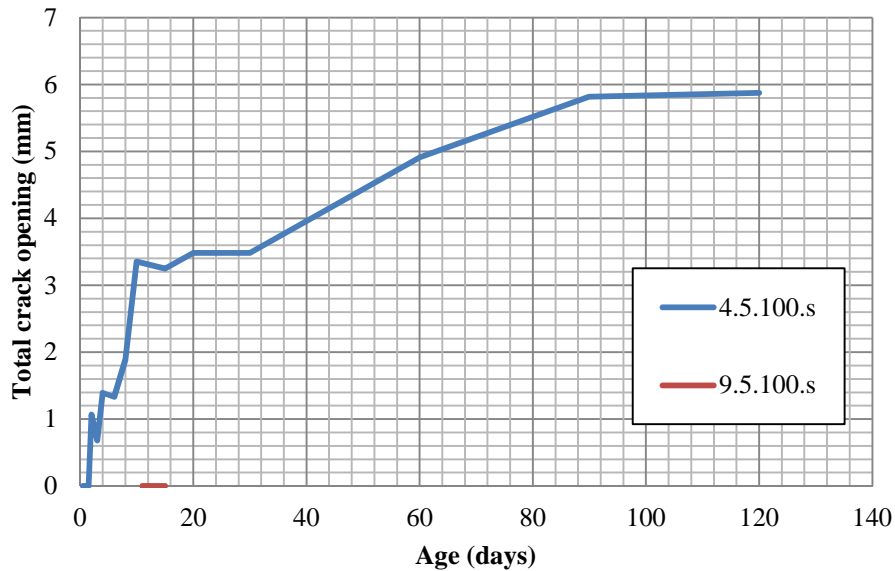


Figure 0.2: The total crack opening of 4m and 9m joint spacings containing 5kg/m³ fibres

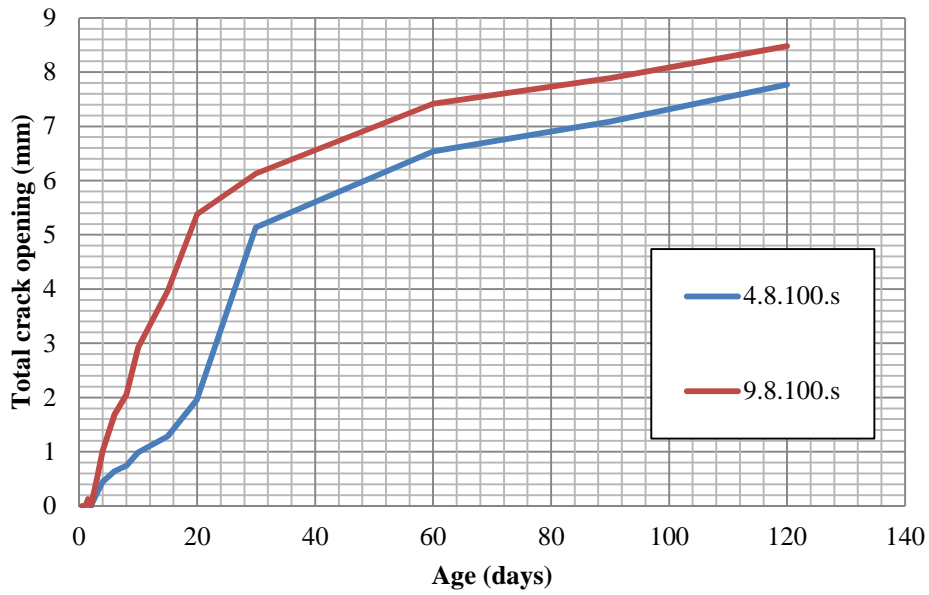


Figure 0.3: The total crack opening of 4m and 9m joint spacings containing 8kg/m³ fibres

FIBRE DOSAGE VALUES

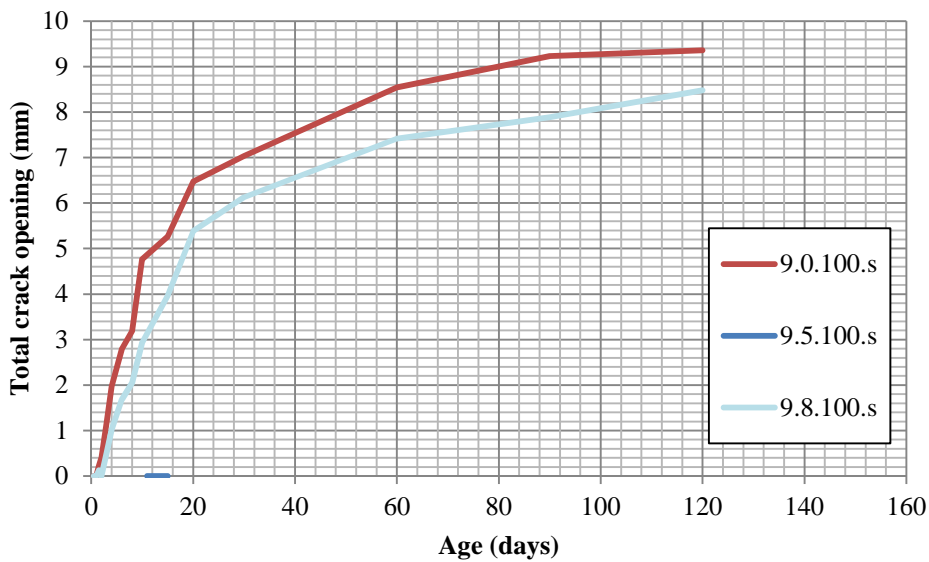


Figure 0.4: The total crack opening of a 9m joint spacing slab containing different fibre dosages

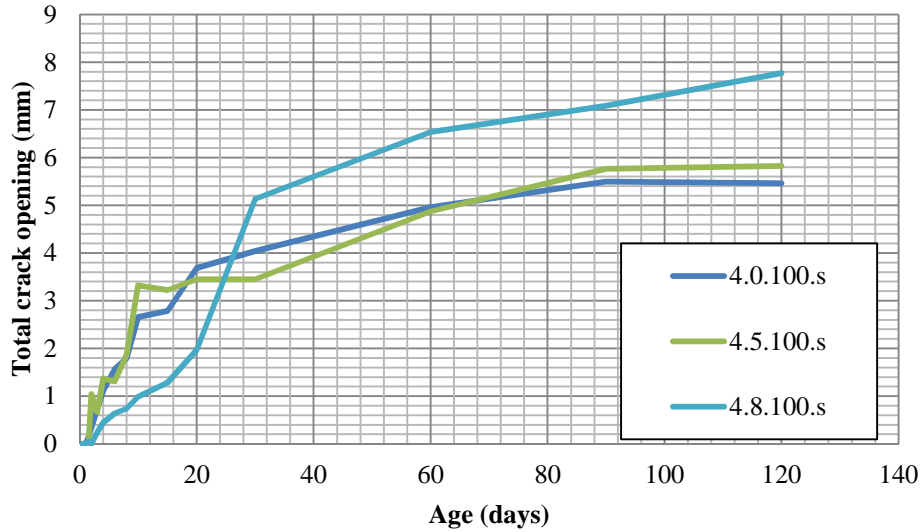


Figure 5: The total crack opening of a 4.5m joint spacing slab containing different fibre dosages

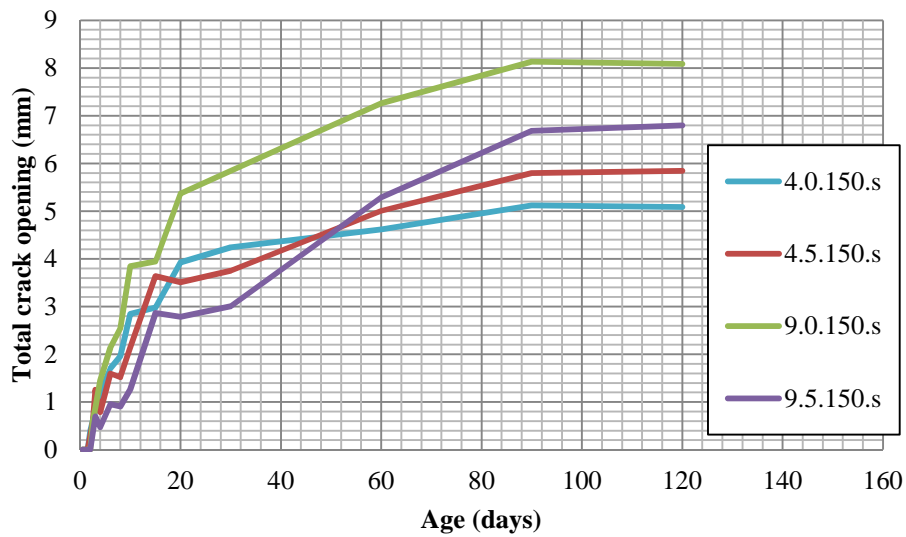


Figure 0.5: A 150mm thick 9m and 4.5m joint spacing slab containing, either 0kg/m³ or 5kg/m³ fibres

DIFFERENT SLAB THICKNESSES

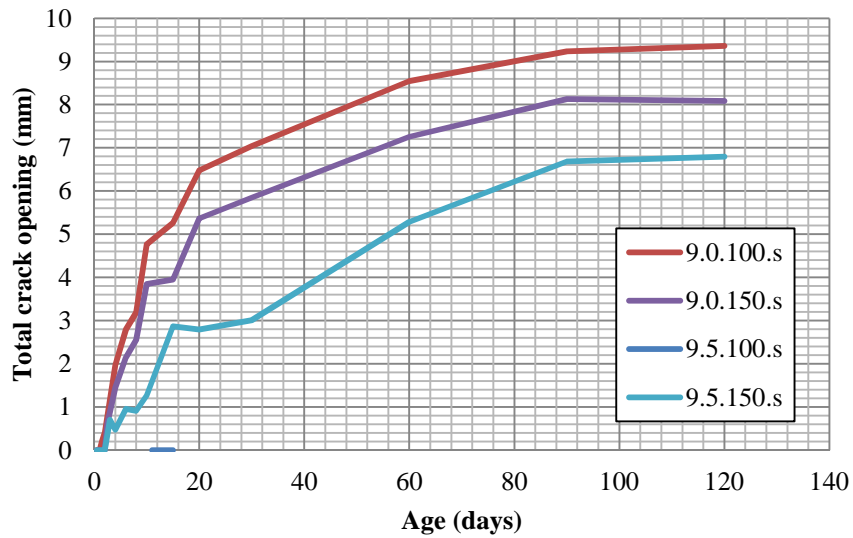


Figure 0.6: A 150mm thick 9m joint spacing slab compared with a 100mm thick 9m slab.

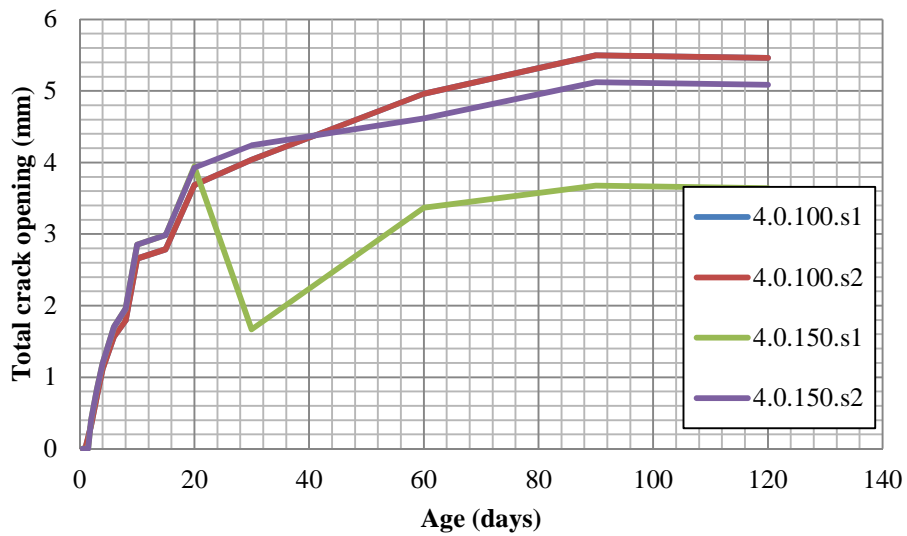


Figure 0.7: A 4.5m joint spacing slab containing no fibres with a thickness of either 100mm or 150mm

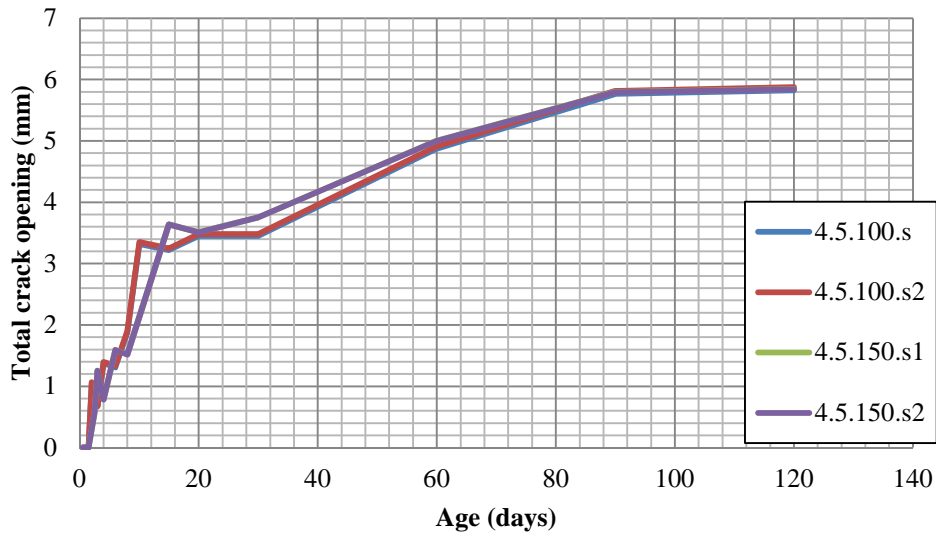


Figure 0.8: A 4.5m joint spacing slab containing 5kg/m³ fibres with a thickness of either 100mm or 150mm

FRICITION BETWEEN SOIL AND CONCRETE VALUES

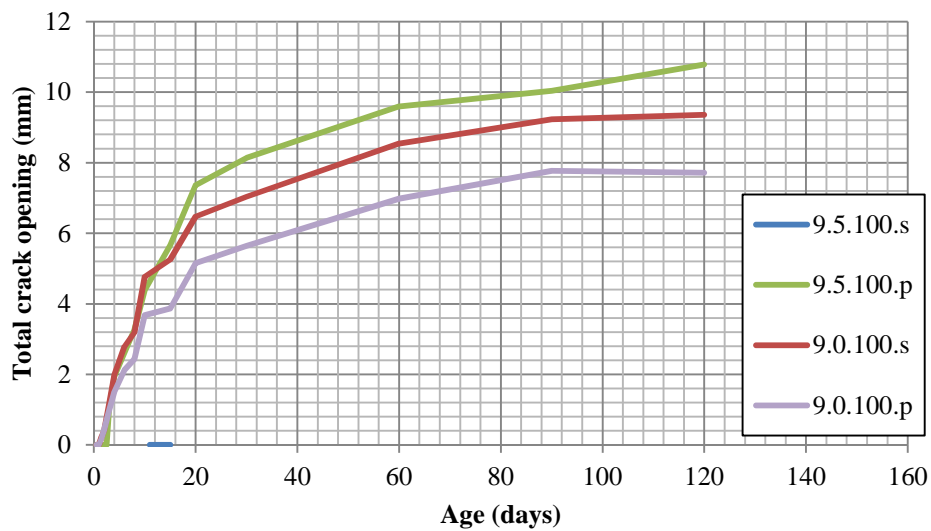


Figure 0.9: The effect of different frictions under a 9m joint spacing slab

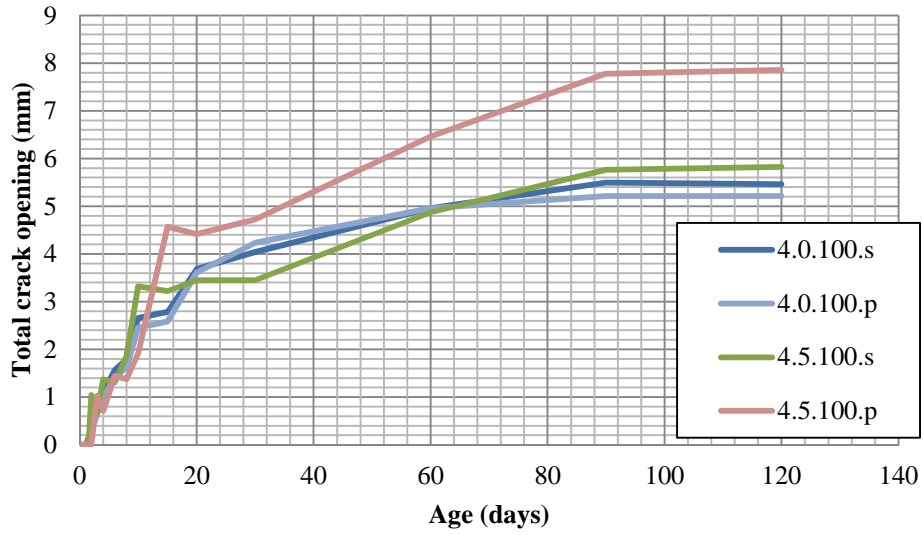


Figure 0.10: The effect of different frictions under a 4.5m joint spacing slab